The Use of Fluorophores for Intraoperative Tumour Detection in Breast Cancer

(Guiding Light Optimising Wide local excisions)



Ms. Martha Kedrzycki MSc, MRCS

This thesis is submitted to Imperial College London in partial fulfilment of the requirements for the degree of Doctor of Philosophy. Except for where indicated, it presents entirely my own work and describes the results of my own research.

Imperial College London

Department of Surgery and Cancer

(14/8/3)

Statement of Originality

I hereby declare that this thesis is my own work, except for where indicated, and has not been submitted in any form for another degree or diploma at any university. Information derived from the published and unpublished work of others has been acknowledged in the text and a list of references is given in the bibliography.

Copyright Declaration

The copyright of this thesis rests with the author. Unless otherwise indicated, its contents are licensed under a Creative Commons Attribution Non-Commercial 4.0 International Licence (CC BY-NC).

Under this licence, you may copy and redistribute the material in any medium or format. You may also create and distribute modified versions of the work. This is on the condition that: you credit the author and do not use it, or any derivative works, for a commercial purpose.

When reusing or sharing this work, ensure you make the licence terms clear to others by naming the licence and linking to the licence text. Where a work has been adapted, you should indicate that the work has been changed and describe those changes.

Please seek permission from the copyright holder for uses of this work that are not included in this licence or permitted under UK Copyright Law.

Abstract

Martha Kedrzycki MSc, MRCS

The Use of Fluorophores for Intraoperative Tumour Detection in Breast Cancer

Breast conserving surgery (BCS) is the crux of treatment for early-stage breast cancer. In BCS, the tumour is resected with a rim of healthy tissue. However, this operation comes with the risk of positive margins, necessitating re-operation to prevent recurrence. Many technologies have been developed to address this issue including localisation, margin assessment, as well as imaging techniques. However, although these decrease the positive margin rate, they do not eliminate it. This thesis explores fluorescence guided surgery as a solution.

In fluorescence guided surgery, the fluorescent properties- often mediated by contrast agents- are used to highlight the tissue of interest. Typically, this uses specific wavelengths of light to activate fluorescent agents, acquiring images in the near-infrared spectrum alongside colour images, followed by software processing, and display of the cancer/healthy tissue border using an overlay on the colour image. It provides a macroscopic view of where the tumour is, its size, and its invasiveness without impeding the view of the surgical field.

The focus of this thesis is to identify breast cancer using fluorescent guidance. Two pilot trials of the GLOW camera system were performed (*in-vitro* and *in-vivo*) to iteratively develop the prototype to incorporate it into surgical workflow. Afterwards, two feasibility trials were performed. The first used indocyanine green (ICG) administered at different timings to assess the vascular structure and permeability of the tumour. The second used aminolevulinic acid (ALA), which targets breast cancer cells via metabolic derangements.

The novelty of this work is that the trial with ICG compares the two different timings. ALA had not been assessed *in-vivo* previously, and thus the efficacy of a novel fluorescent agent in BCS was explored. Both trials included intraoperative and histopathological imaging, processed in a novel manner using pixel-based processing and texture metrics.

Acknowledgements

I would like to thank the NHS for funding my post as a breast clinical translational research fellow, National Institute for Health Research (NIHR) Imperial Bio- medical Research Centre (BRC), the Cancer Research UK (CRUK) Imperial Centre, the Imperial Confidence in Concept (ICiC) Joint Translational Fund, and the Hamlyn Accelerator for Surgical Innovation (HASI) for funding my PhD as well as for believing in my research vision and willpower.

This work would be impossible without the help from my supervisors and colleagues at the Hamlyn Centre. Prof Daniel Elson, Mr Daniel Leff, Ms Maria Leiloglou, Dr Vadzim Chalau, Ms. Dhurka Shanthakumar, and Ms Kelly Gleason. Thank you all for being there when I needed you, I hope our efforts and work to be found useful by the rest of the research community and to contribute towards improved healthcare.

Most importantly, I would like to thank Julia Kedrzycki, Amir Ariyan, and Karlie DeAngelis for their love and support. I would also like to thank the DeAngelis family, Natalie Ashton, Alysha Abid, Steffi Sunny, Rita Wyrebek, Derek and Martyna Gill, Seyi Hong, Rosanna Page, Alysha Shetye, Dylan Roi, and Sam Tukra for their friendship and encouragement during this time.

Table of Contents

1. INTRODUCTION 14

1.1. Breast Conserving Surgery 15
1.1.1. Types of Breast Cancer 15
1.1.2. Positive Margins during Breast Conserving Surgeries 16
1.1.3. Morbidity and Costs of Re-operation 17
1.1.4. Current Techniques 20
1.1.5. Margin Techniques 22
1.1.6. Tumour Identification 25
1.2. Conclusion 26
1.3. The contribution of this work 27

2. FLUORESCENCE GUIDED SURGERY 29

2.1. Introduction to FGS 30
2.2. Components of a NIRF imaging system 30
2.2.1. Commercially Available NIRF Camera Systems 31
2.3. Properties of Light 32
2.3.1. Chromophores 33
2.4. Exogenous Fluorophores for Medical Imaging 35
2.4.1. Passive Targeting 35
2.4.2. Active Targeting 36
2.4.3. Absorption and Emission Spectra 37
2.4.4. Tumour Background Ratio 38
2.4.5. Fluorophores for use in-vivo 38
2.5. Conclusion 43

3. FLUORESCENCE GUIDED SURGERY IN BREAST CANCER 44

3.1. Introduction to FGS in Breast Cancer 45
3.2. Optical Properties of Breast Tissue 45
3.3. Sentinel Node Identification 46
3.4. Lymphatic Mapping 50
3.5. Tumour Identification 53
3.6. Limitations 57
3.7. Conclusion 58

4. CAMERA DEVELOPMENT AND *IN-VITRO* STUDIES USING THE GLOW CAMERA 59

4.1. The GLOW camera system 60
4.2. Identifying optimal camera settings 61
4.3. ICG spectroscopy in bovine serum 62
4.4. Sensitivity of the GLOW camera to multiple fluorophores at varying concentrations in different media 63
4.5. EMI in various media 64
4.6. Filter comparisons with PpIX 65
4.7. Experiment in *ex-vivo* tissue 67
4.8. Comparison to the SPY^{TM} commercial system 69
4.9. Conclusion 70

5. THE *IN-VIVO* PILOT TRIAL WITH ICG 71

5.1. Summary of ICG 72
5.2. Prior studies using ICG 73
5.3. The pilot study 73
5.4. Protocol 74
5.5. Results 75
5.5.1. Patient data 75
5.5.2. Image capturing interface 76

5.5.3. Image processing ... *77*
5.6. Spectroscopy with ICG in breast ... 83
5.7. Conclusion ... 84

6. ICG FEASIBILITY STUDIES USING TEMPORAL VARIATION ... 87

6.1. Methods ... 88
6.2. Results ... 89
6.2.1. Image Processing ... *91*
6.2.2. Ex-vivo: Whole specimens ... *92*
6.2.3. Ex-vivo: Histology cut-up of specimen ... *92*
... *95*
6.2.4. Image analysis and application to patient characteristics ... *96*
6.3. Discussion ... 100
6.4. Conclusion ... 102

7. *IN-VIVO* PILOT TRIAL WITH ALA ... 103

7.1. Summary of ALA ... 104
7.2. Method for ALA Pilot trial ... 108
7.3. Results ... 110
7.4. Discussion ... 119
7.5. Conclusion ... 120

8. COMPARISON OF ALL MODALITIES ... 122

8.1. Methods ... 123
8.2. Results ... 124
8.3. Discussion ... 126

9. CONCLUSION ... 127

9.1. Summary ... 127
9.2. Limitations ... 130
9.3. Future work ... 131

Appendices:

1. **Development of a Fluorescent Probe……..132**
2. **Patient and Public Involvement.……134**
3. **Permission for re-use of materials.……143**

List of Tables

Table 1: Fluorophores Currently Being Investigated in Humans
Table 2: Sentinel Node Studies in Breast Cancer Comparing NIRF to Radioisotope +/- Blue Dye.
Table 3: Lymphatic Mapping Using NIRF.
Table 4: Breast Conserving Surgery using Fluorescent Guidance.
Table 5: T-test for PpIX in bovine calf serum and phosphate buffer solution.
Table 6: Summary of patient demographics and tumour characteristics for ICG.
Table 7: Accuracy of different doses of 5-ALA as per Ottolino-Perry.
Table 8. Summary of patient demographics and tumour characteristics for ALA.
Table 9: TBR results between both filters and *ex-vivo* vs histopathology and NACT vs primary surgery.
Table 10: Advantages and Disadvantages of Various Imaging Modalities, and the contribution of this thesis.

List of Figures

Figure 1: Negative and positive margins.
Figure 2: Consequences of re-operation.
Figure 3: Gold standard margin technique.
Figure 4: Cavity shaves.
Figure 5: Tumour localisation using a wire vs seed.
Figure 6: Intraoperative tumour identification techniques.
Figure 7: Light spectrum.
Figure 8: Properties of light in tissue.
Figure 9: Optical properties of chromophores.
Figure 10: Demonstration of extrinsic fluorophore tumour targeting approaches.
Figure 11: Fluorophores currently in clinical use for cancer imaging.
Figure 12: The GLOW Camera.
Figure 13: Sensitivity results at various distances using concentration and signal to noise ratio.
Figure 14: Calculations to calculate concentrations of drugs in blood of average female.
Figure 15: EMI concentrations in various media.
Figure 16: Absorption and emission spectra of PpIX.
Figure 17: Varying concentrations of PpIX in bovine calf serum using different filters.
Figure 18: *In-vitro* experiment using porcine tissue.
Figure 19: Different Concentrations of ICG as seen via the GLOW camera and commercial system.
Figure 20: Comparing signal noise ratio (SNR) between GLOW camera and commercial system.
Figure 21: Second iteration of software interface.
Figure 22: Marking images of the specimen.
Figure 23: Infrared image of abnormal vasculature in *ex-vivo* specimen.
Figure 24: Expanded ROC calculation.
Figure 25: Texture analysis of images.
Figure 26: Comparison of ICG fluorescence in breast tissue, bovine plasma, and autofluorescence of the breast.
Figure 27: Explanation of how true normal measurements were calculated from pixel value.
Figure 28: XR, unmarked infrared, and marked infrared images.
Figure 29: Cut-up from angiography cohort.
Figure 30: Cut-up from EPR cohort.
Figure 31: Histograms of pixel values between tumour and healthy tissue.
Figure 32: GLOW camera use intraoperatively and during histopathology cut-up.
Figure 33: IR images with green overlay predicting tumour site.
Figure 34: Chemical Structure of ALA.
Figure 35: The metabolism of ALA to PpIX.
Figure 36: Absorption and Emission Spectra of PpIX.
Figure 37: ALA *ex-vivo* specimen images.
Figure 38: ALA histopathology cut-up images.
Figure 39: Comparison of primary interventions and filters on histopathology cut-up images.
Figure 40: Histograms of pixel values between tumour and healthy tissue.
Figure 41: Examples of green overlay on colour images.
Figure 42: Histogram of TBR values between studies in *ex-vivo* and histopathology results.
Figure 43: Summary of study results for ALA and ICG trials.
Figure 44: ANOVA analysis on *ex-vivo* TBR.
Figure 45: Flowchart of enzyme activated probe development.

List of Abbreviations (in alphabetical order)

ABS: Association of Breast Surgeons

(5-)ALA: (5-)aminolevulinic acid

ALAD: ALA dehydratase

ANOVA: analysis of variance

ASBRS: American Society of Breast Surgeons

BCS: breast conserving surgery

BMI: body mass index

CEA: carcinoembryonic antigen

C-met: mesecnhymal epithelial transition factor

CT: computed tomography

DCIS: ductal carcinoma *in-situ*

EGFR: epidermal growth factor receptor

EPR: enhanced permeability and retention effect

ER: oestrogen Receptor

FAD: flavin adenosine dinucleotide

FDA: Food and Drug Administration

FECH: ferrochelatase

FGS: fluorescence guided surgery

FOV: field of view

FSA: frozen section analysis

GLOW: Guiding Light Optimising Wide local excisions

HER2: herceptin receptor

HyCoSuL: hybrid combinatrial substrate library

ICG: indocyanine green

ID: identification

IDC: invasive ductal carcinoma

i-KNIFE: intelligent-knife

ILC: invasive lobular carcinoma

IMC: inflammatory mammary carcinoma

IMPC: invasive micropapillary carcinoma

iMRI: intraoperative magnetic resonance imaging

IOUS: intraoperative ultrasound

IR: infrared

LCIS: lobular carcinoma *in-situ*

LOOCV: leave-one-out-cross-validation

LR: logistic regression

MB: methylene blue

NADH: nicotinamide adenine dinucleotide

NIRF: near infrared fluorescence

OCT: optical coherence tomography

PpIX: protoporphyrin IX

PBGD: porphobilinogen deaminase

PBS: phosphate buffered solution

PR: progesterone receptor

REC: research ethics committee

RI: radioisotope

ROI: region of interest

ROLL: radioguided occult lesion localisation

RSL: radioactive seed localisation

SD: standard deviation

SNR: signal noise ratio

SSO-ASTRO: Society of Surgical Oncology and the American Society of Radiation Oncology

SVM: support vector machine

TBR: tumour background ratio

UK: United Kingdom

UROD: uroporphyrinogen decarboxylase

US/USA: United States of America

UV: ultraviolet

VEGF: vascular endothelial growth factor

WGL: wire guided localisation

Contribution

Publications

1. Kedrzycki MS, Leiloglou M, Ashrafian H, Jiwa N, Thiruchelvam PTR, Elson DS, Leff DR. 2021, Meta-analysis comparing fluorescence imaging with radioisotope and blue dye-guided sentinel node identification for breast cancer surgery., *Annals of Surgical Oncology*, Vol: 28, Pages: 3738-3748, ISSN: 1068-9265. https://doi.org/10.1245/s10434-020-09288-7
2. Kedrzycki MS, Elson DS, Leff DR. 2020, ASO author reflections: fluorescence-guided sentinel node biopsy for breast cancer, *Annals of Surgical Oncology*, Vol: 28, Pages: 3749-3750, ISSN: 1068-9265. https://doi.org/10.1245/s10434-020-09344-2
3. Leiloglou M, Chalau V, Kedrzycki MS, Thiruchelvam P, Darzi A, Leff DR, Elson DS. 2021, Tissue texture extraction in indocyanine green fluorescence imaging for breast-conserving surgery, *Journal of Physics D: Applied Physics*, Vol: 54, ISSN: 0022-3727. https://doi.org/10.1088/1361-6463/abe571
4. Leiloglou M*, Kedrzycki M*, Chalau V, Thiruchelvam P, Darzi A, Elson D, Leff D. 2021, Versatility in Fluorescence Guided Surgery with the GLOW Camera System, *Surgical Life: The Journal of the Association of Surgeons of Great Britain and Ireland*
5. Kedrzycki MS*, Leiloglou M*, Chalau V, Chiarini N, Thiruchelvam PTR, Hadjiminas DJ, Hogben KR, Rashid F, Ramakrishnan R, Darzi AW, Elson DS, Leff DR. 2021, The impact of temporal variation in indocyanine green administration on tumor identification during fluorescence guided breast surgery., *Annals of Surgical Oncology*, Vol: 28, Pages: 5617-5625, ISSN: 1068-9265. https://doi.org/10.1245/s10434-021-10503-2
6. Leiloglou M*, Kedrzycki MS*, Elson DS, Leff DR. 2021, ASO author reflections: Towards fluorescence guided tumor identification for precision breast conserving surgery., *Annals of Surgical Oncology*, ISSN: 1068-9265. https://doi.org/10.1245/s10434-021-10626-6
7. Leiloglou M*, Kedrzycki MS*, Chalau V, Chiarini N, Thiruchelvam PTR, Hadjiminas DJ, Hogben KR, Rashid F, Ramakrishnan R, Darzi AW, Leff DR, Elson DS. Indocyanine Green Fluorescence Image Processing Techniques for Breast Cancer Macroscopic Demarcation. *Sci Rep* **12,** 8607 (2022). https://doi.org/10.1038/s41598-022-12504-x
8. Kedrzycki MS, Elson DS, Leff DR. 2023. Future Guidance in Breast Conserving Surgery: Tumor Localization versus Tumor Identification. *British Journal of Surgery*. 110(8), 920-922. https://doi.org/10.1093/bjs/znac409.
   Kedrzycki M*, Chon HTW*, Leiloglou M, Chalau V, Leff DR, Elson DS. Fluorescence guided surgery imaging systems for breast cancer identification: a systematic review, *J. Biomed. Opt.* **29**(3), 030901 (2024), doi: 10.1117/1.JBO.29.3.030901.
   *joint first authorship

Presentations:

1. Kedrzycki M, Leiloglou M, Chalau V, J. Qi, P. Martin-Gonzalez, G. Hanna, A. Darzi, D.R. Leff, D.S Elson. Poster Presentation: Fluorescence Image Guided Surgery in Breast Cancer using the Imperial Camera System. Imperial Confidence in Launch & Corporate Speed Dating. 19.02.19. London, UK.

2. .Leiloglou, M. Kedrzycki, V. Chalau, F. Avila-Rencoret, Q. Li, J. Lin, G. Hanna, A. Darzi, D.R. Leff, D. S. Elson. Oral & poster presentation: Snapshot Fluorescence Hyperspectral System for Breast Cancer Surgery Guidance. Image Guided Therapies Network+ Tri-Annual Meeting, 06.03.19. London, UK.
3. M. Leiloglou , V. Chalau, M. Kedrzycki, J. Qi, P. Martin-Gonzalez, G. Hanna, A. Darzi, D.R. Leff, D. S. Elson. Oral and Poster presentation: Fluorescence Intensity Image Guided Breast Conserving Surgery. 14th European Molecular Imaging Meeting. 19-22.03.19. Glasgow, UK.
4. M.Leiloglou, M. Kedrzycki, V. Chalau, F. Avila-Rencoret, Q. Li, J. Lin, G. Hanna, A. Darzi, D.R. Leff, D. S. Elson. Poster presentation: Snapshot Fluorescence Hyperspectral System for Breast Cancer Surgery Guidance. Hamlyn Symposium Advcanced Biophotonics Workshop. 26.06.19. London, UK.
5. Leiloglou, M. Kedrzycki, V. Chalau, Q. Li, G. Hanna, A. Darzi, D.R. Leff, D.S. Elson. Poster Presentation: Visualising the Invisible: A Fluorescence Imaging System for Cancer Surgery Guidance. Imperial Graduate School PhD Summer Showcase. 12.07.19. London, UK.
6. Chalau, V., Kedrzycki, M., Leiloglou, M., Thiruchelvam, P., Leff, D.R., Elson, D.S. Poster Presentation: Variability of indocyanine green (ICG) near-infrared maximum emission wavelength in breast tissues. European Molecular Imaging Meeting. 24-27.08.21. Geottingen, Germany.
7. M. Kedrzycki, M. Leiloglou, V. Chalau, D.R. Leff, D.S. Elson. Poster Presentation: GLOW: Guiding Light to Optimise Wide Local Excisions. London Surgical Symposium. 16.10.19. London, UK.
8. M. Kedrzycki, M. Leiloglou, V. Chalau, P. T. R. Thiruchelvam, J. Lin, D. Elson, D.R Leff. Oral Presentation: First in Human Study Using the 'GLOW' Near Infrared Camera System in Breast Cancer. Imperial Surgery & Cancer Department Afternoon. 12.12.19. London, UK.
9. M. Kedrzycki, M. Leiloglou, H.Ashrafian, N. Jiwa, P.T.R. Thiruchelvam, D. Elson, D.R. Leff. Poster Presentation: Meta-analysis of Sentinel Node Mapping Techniques Comparing Near Infrared Fluorescence Imaging to Blue Dye and Radioisotope. Imperial Surgery & Cancer Department Afternoon. 12.12.19. London, UK.
10. Kedrzycki M, Leiloglou M, Chalau V, Leff D, Elson. Poster Presentation: Guiding Light Optimising Wide Local Excisions. London Surgery Symposium. 16.10.2019. London, UK.
11. Leiloglou, M., Gkouzionis, I., Basilio Avial-Rencoret, F., Chalau, V., Kedrzycki, M., Darzi, A., Leff, D.R., Elson, D.S. Oral Presentation: Snapshot Hyperspectral System for Breast-Conserving Surgery Guidance. Optical Society Biophotonics Congress: Biomedical Optics. 22.04.2020. Miami, US. https://doi.org/10.1364/TRANSLATIONAL.2020.TW2B.3
12. Kedrzycki, M.S., Leiloglou, M., Ashrafian, H., Jiwa, N., Thiruchelvam, P.T.R., Elson, D.S., Leff, D.R. Poster Presentation: Meta-analysis of Sentinel Node Mapping Techniques Comparing Near Infrared Fluorescence Imaging to Blue Dye and Radioisotope. American Society of Breast Surgeons Symposium. 29.04-03.05.2020. Las Vegas, US. https://doi.org/10.1245/s10434-020-08630-3
13. Kedrzycki, M.S., Leiloglou, Chalau, V., Thiruchelvam, P.T.R., M., Lin, J., Elson, D.S., Leff, D.R. Poster Presentation: First in Human Study Using the 'GLOW' Near Infrared Camera System in Breast Cancer. American Society of Breast Surgeons Symposium. 29.04-03.05.2020. Las Vegas, US. https://doi.org/10.1245/s10434-020-08630-3

14. Kedrzycki, M., Leiloglou, M., Leff, D.R., Elson, D.S. Poster Presentation: Illuminating Cancer: A Systematic Review of Fluorophores available for Fluorescence Guided Surgery in Humans. European Molecular Imaging Meeting. 24-28.08.2020. London, UK.
15. Kedrzycki, M., Leiloglou, M., Chalau, V., Lin, J., Thiruchelvam, P.T.R., Leff, D.R., Elson D.S. Poster Presentation: Fluorescence Guided Surgery Using Indocyanine Green to Demarcate Vasculature in Breast Cancer. London Surgical Symposium. 22.09.2020. London, UK.
16. M. Kedrzycki, M. Leiloglou, V. Chalau, P. T. R. Thiruchelvam, D.R Leff, D.S. Elson. Oral Presentation: Guiding Light Optimising Wide local excisions. Surgery & Cancer Department Afternoon. 9.12.2020. Virtual, UK.
17. Kedrzycki MS, Leiloglou M, Chalau V, Lin J, Thiruchelvam PTR, Elson DS, Leff DR. 2021, Guiding light to optimize wide local excisions: the "GLOW" study, Volume XXII 2021 American Association of Breast Surgeons. Publisher: Springer, Pages: S199-S200, ISSN: 1068-9265
18. Jiwa N, Kedrzycki M, Kumar S, Gandhewar R, Chauhan H, Wright C, Takats Z, Ashrafian H, Leff DR et al., 2021, Diagnostic Accuracy of Nipple Discharge Fluid Cytology: A Meta-Analysis and Systematic Review of the Literature, Publisher: SPRINGER, Pages: S346-S347, ISSN: 1068-9265
19. D. Shanthakumar, M. Leiloglou, V. Chalau, M.S. Kedrzycki, A. Darzi, D.R. Leff, D.S. Elson. 2022, Multispectral imaging for intraoperative tumour visualisation in breast conserving surgery. London Surgical Symposium. 19.10.2022. London, UK.
20. M. Kedrzycki, M. Leiloglou, V. Chalau, D. Shanthakumar, P. T. R. Thiruchelvam, D. S. Elson, D.R. Leff. 2023, 5-ALA induced fluorescence for tumor visualization in breast-conserving surgery: Part 2 of the "GLOW" study. American Association of Breast Surgeons
21. M. Kedrzycki, M. Leiloglou, V. Chalau, D. Shanthakumar, P. T. R. Thiruchelvam, D. S. Elson, D.R. Leff. 2023, Fluorescence and Multispectral Imaging in Breast Conserving Surgery – Proof of Concept Trial. American Association of Breast Surgeons
22. D. Shanthakumar, M. Leiloglou, V. Chalau, M.S. Kedrzycki, A. Darzi, D.S. Elson, D.R. Leff. 2023, Intra-operative multispectral imaging for precision in breast conserving surgery, Volume 49 2023 Association of Breast Surgeons. Publisher: European Journal of Surgical Oncology. https://doi.org/10.1016/j.ejso.2023.03.012
23. H. Chon, M. Kedrzycki, M. Leiloglou, P. Kirupanathan, D. S. Elson, D.R. Leff. 2023. Fluorescence guided surgery imaging systems for breast cancer identification: A systematic review, Volume 49 2023 Association of Breast Surgeons. Publisher: European Journal of Surgical Oncology. https://doi.org/10.1016/j.ejso.2023.03.148
24. Kedrzycki M., The JJ., Cai W., Ezzat A., Thiruchelvam P., Elson DS., Leff, DR. Poster Presentation: Prospective single-centre qualitative service evaluation on magseed for wide local excision. Association of Breast Surgeons. 29.4-05.02.2021. Virtual, UK. https://doi.org/10.1016/j.ejso.2021.03.057
25. The JJ, Cai W, Kedrzycki M, Thiruchelvam PTR, Elson DS, Leff DR. Magseed-Guided Wide Local Excision During the COVID-19 Pandemic: A Tenable Solution to Barriers in Accessing Elective Breast Cancer Surgery. Association of Surgeons in Training. 03-05.2021. Birmingham, UK. https://doi.org/10.1093/bjs/znab259.205

Grants Awarded

Imperial Confidence in Concept Grant for Research (£59 975) June 2019

Hamlyn Accelerator SI grant (£48 000) March 2021

Other Achievements

1. 2nd place poster prize: Imperial Confidence in Concept Launch & Corporate Speed Dating. 19.02.19. London, UK.
2. 1st place prize: Graduate School Summer Showcase Research as Art Competition, 12.07.19. London, UK.
3. People's choice award: Graduate School Summer Showcase Research as Art Competition, 12.07.19. London, UK.
4. Honourable mention at Surgery & Cancer Departmental Christmas Showcase, 09.12.20. London, UK.
5. Mention of our research article on commercial website: https://diagnosticgreen.com/row/news/indocyanine-green-fluorescence-image-processing-techniques-for-breast-cancer-macroscopic-demarcation/

Patient and Public Involvement

1. Imperial CRUK Patient and Public Involvement group meeting. 14.03.19. Charing Cross Hospital, UK.
2. Research as Art Competition/PhD Summer Showcase, Graduate School. 12.7.19. Imperial College London, UK
3. 'GLOW camera for breast-conserving surgery' Hamlyn Centre Christmas showcase, 18.12.19.
4. 'Fluorescence Imaging System for Breast-Conserving Surgery Guidance-First In-Human Trial' at Breast Breakfast. 13.3.20. Charing Cross Hospital, London.
5. 'GLOW: Shining a light on breast cancer through fluorescence-guided surgery', interview with Nikita Rathod published on Imperial blogs. 2.4.20. Imperial College London, UK
6. 'Better Breast Cancer Surgery', Imperial College Podcast, 27.1.21. London, UK
7. Open age talk, Virtual. 24.2.21. London, UK.
8. 'Lighting the way to better breast cancer surgery?', Imperial Science café talk, 10.3.21. London, UK.
9. Gdansk University of Medicine, Virtual. 17.03.21. Gdansk, Poland.
10. Royal Society of Medicine. 27.3.21. Cambridge University, UK.
11. Women in Surgery. 24.11.21. University of Portsmouth, UK.
12. Cancer Revolution: Science, Innovation and Hope. 25.5.22. Science Museum, UK.

Ethical Approval:

REC approval 19/LO/0927, obtained on 19/7/2019 IRAS ID: 260633

1. Introduction

In early-stage breast cancer, breast conserving surgery (BCS) combined with radiotherapy is the treatment of choice. However, BCS comes with the risk of tumour being left behind and the need for re-operation.

This work addresses the high rate of positive margins in breast conserving surgery (BCS). This chapter introduces the prevalent issue of positive margins during breast conserving surgery (BCS). It provides a state-of-the-art evaluation of innovations arising to tackle incomplete resection during BCS. This first chapter goes into detail about the challenge of breast conserving surgery and the consequences of this problem for all parties involved. It describes the current technologies developed to address the problem of incomplete resection and their limitations. Fluorescence guided surgery has the potential to overcome those limitations.

The work in this chapter is my own, apart from the Magseed work which was done in collaboration with Jhia The and Wenyi Cai.

This work was presented at the *European Molecular Imaging Meeting* (2021) 'Illuminating Cancer: A Systematic Review of Fluorophores available for Fluorescence Guided Surgery in Humans', the *Association of Breast Surgeons* (2023) 'Fluorescence guided surgery imaging systems for breast cancer identification: A systematic review', the *Association of Breast Surgeons* (2021) 'Prospective single-centre qualitative service evaluation on Magseed for Wide Local Excision', and the *Association of Surgeons in Training* (2021) 'Magseed-Guided Wide Local Excision During the COVID-19 Pandemic: A Tenable Solution to Barriers in Accessing Elective Breast Cancer Surgery'.

1.1. Breast Conserving Surgery

According to Cancer Research UK there were 55,122 new cases of breast cancer in 2018 in the United Kingdom (1), and 2.3 million cases globally (2). Of those, 90% receive surgery (1), where the options are either mastectomy or breast conserving surgery (BCS) with adjuvant treatment. In appropriately selected patients, BCS in combination with radiotherapy has been shown to be superior to mastectomy with regards to oncological outcomes (3, 4), with the added benefits of fewer complications and improved quality of life (5). Therefore, BCS has quickly become the predominant treatment for breast cancer surgery, with an uptake rate of 70% (6). However, BCS comes with the risk of incomplete resection.

1.1.1. Types of Breast Cancer

Breast cancer is heterogeneous with regards to genotype and phenotype. The most common histological subtypes are:

- invasive ductal carcinoma (IDC),
- invasive lobular carcinoma (ILC),
- ductal carcinoma in situ (DCIS),
- lobular carcinoma in situ (LCIS),
- inflammatory breast cancer

Furthermore, there is also phenotypical variation in receptor expression, namely oestrogen (ER), progesterone (PR), and Herceptin (Her2). Approximately 80% of breast cancers are IDC, which are ER+, PR+ and Her2- (7). Therefore, each tumour is unique in how it behaves, what investigations need to be done, the treatments required (as well as the order of said treatments), and how it responds to treatment.

1.1.2. Positive Margins during Breast Conserving Surgeries

The challenge is that there is a significant risk of failing to remove the tumour in its entirety during index BCS. This is due to the blind nature of the procedure, as the only tools at a surgeon's disposal are the size estimate from pre-operative imaging, approximate tumour geo-location from guidance systems (wires, seeds), and where possible tactile palpation of the tumour. Margins are determined post-operatively via histology, and if the cancer crosses the cut edge of the specimen it is classified as a positive margin (demonstrated in **Figure 1**).

There is no international standard as to what constitutes a positive margin. According to the Association of Breast Surgery (ABS), a clear margin is defined as 1mm for both IDC and DCIS (8). Conversely, according to the Society of Surgical Oncology-American Society for Radiation Oncology (SSO-ASTRO), a clear margin is defined as no ink on tumour for IDC and 2 mm for DCIS (8). As positive margins are associated with a two-fold higher risk of ipsilateral recurrence, those patients with positive margins require another operation to remove the residual tumour (9). This affects up to 27% of women undergoing BCS (10). In our institution (Imperial College London), a recent audit confirmed a positive margin rate of 27% (244/909) according to ABS and 31% (281/909) according to SSO-ASTRO in women without neoadjuvant chemotherapy (NACT). (11)

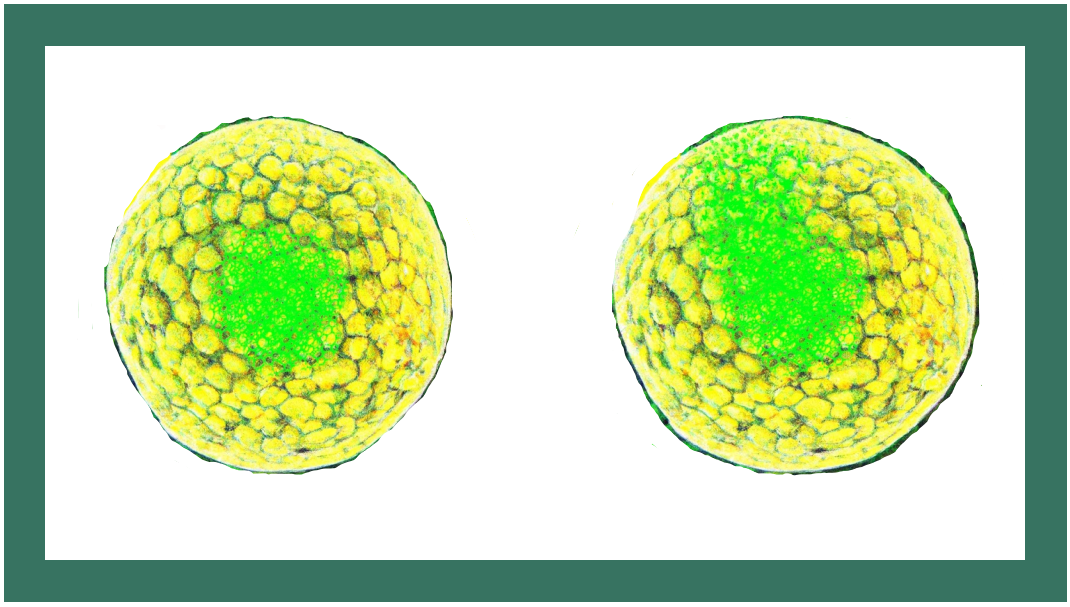


Figure 1: **Negative and positive margins.**
The image on the left depicts negative margins whereby the tumour (green) is encircled by a rim of healthy (yellow) tissue. Conversely, the image on the right demonstrates a positive margin, whereby the tumour broaches the healthy rim.

1.1.3. Morbidity and Costs of Re-operation

Positive margins affect as many as 27% of women undergoing BCS (10). In view of the high rate of local cancer recurrence in women with positive margins, these patients need to undergo a second surgery. This accounts for approximately 11000 women annually in the UK (10). However, these repeat surgeries do not guarantee success and a further 12% of women need to undergo re-operation for a second time (12).

Reoperation causes a significant emotional and psychological burden such as:

- Increased patient stress (10)
- Poor cosmetic outcome (less breast tissue, increased scarring) (13)
- Repeated anaesthetic and surgical risks
- Delays to adjuvant therapy (10)
- Delays in return to work (10)

These consequences are demonstrated in **Figure 2.**

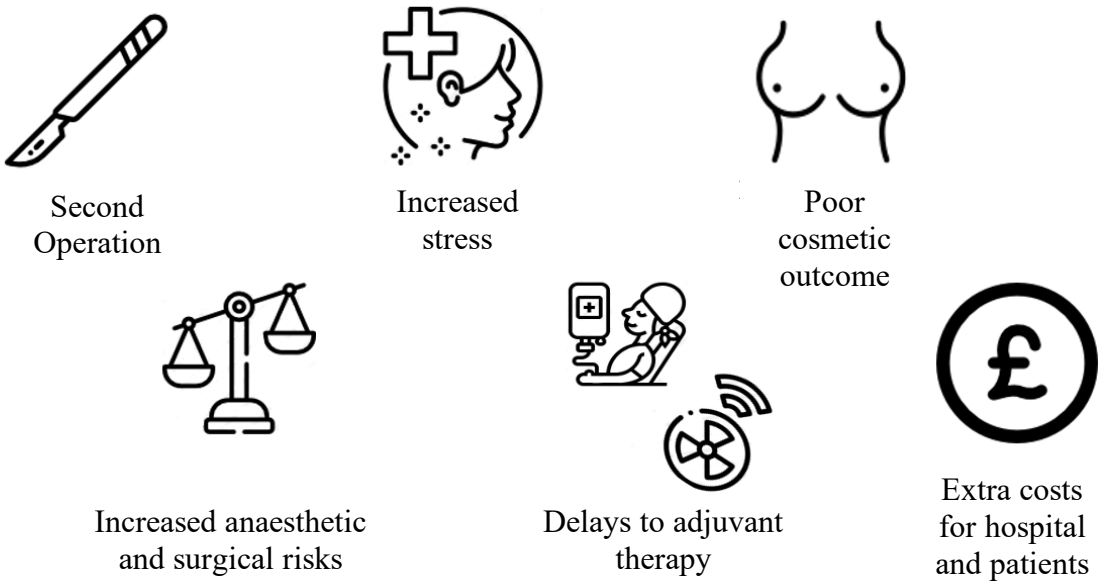


Figure 2: Consequences of re-operation.
A second operation (top row left) negatively impacts both the patient and hospital. There is an associated increase in stress (top row middle), worse cosmetic outcome secondary to less breast volume in and scarring (top row right). It also increases the anaesthetic and surgical risks such as bleeding, infection, and blood clots (bottom row left) and delays adjuvant radiotherapy and/or chemotherapy (bottom row middle). Lastly, it is costly to both the patient and the hospital (bottom right). The patient is unable to return to work due to the additional treatment time. The hospital loses cost as it needs pay for the resources involved (staff, theatre space, post-operative care, etc.).

Not only would FGS benefit patients but also hospital resources. First and foremost are the costs involved with a reoperation such as those associated with readmission, staff, theatre space, medication, and post-operative care. Furthermore, there would be a decreased workload from the repeat operation which affects multiple stakeholders such as those involved with the operation itself (surgeons, anaesthetists, nurses) and those involved in processing the specimen afterwards (histopathologists). Lastly, the operation time would be reduced, thus enabling an increase in patient turnover resulting in optimised theatre usage.

Reoperative intervention for failed BCS costs £4511 per patient and the NHS £22 million triannually (14). Although the cost effectiveness of FGS in BCS has not been studied, FGS has proven to be cost-effective in pancreatic, gastroesophageal, and hepatic surgery (15).

Breast conserving surgery historically relied on preoperative imaging combined with intraoperative tactile and visual perception of the surgeon. However, given that palpation only BCS is associated with positive margin rates (PMR) of up to 42% (16), there is an obvious clinical need for augmenting surgical outcomes. The solution to eliminating positive margin rates has not yet been found, however various methods and technologies have attempted to address this issue.

1.1.4. Current Techniques

Gold standard histopathology can be intraoperatively mimicked by frozen section analysis (FSA) or imprint cytology. However, both require a skilled pathologist to be readily available, delay surgery by about 30 minutes, and have high associated costs (**Figure 3**) (17).



Figure 3: Gold standard margin technique.
Left image is histopathologist looking through a microscope, right image is view of normal (non-cancerous) tissue.

Other centres capitalise on routine cavity shaves to address PMR. According to the Randomized Clinical Trial by Chapgar et al., routine cavity shaves reduced positive margins by half (18). However, this comes at the risk of taking more healthy tissue and decreasing breast volume, subsequently impairing cosmetic outcome (**Figure 4**) (19).



Figure 4: **Cavity shaves.**
Image of the initially resected specimen (central). Following this initial resection, further tissue is removed by performing cavity shaves in all directions. Clockwise, they are superior, medial, inferior, and lateral cavity shaves.

Alternatively, various methods/technologies have been explored for tumour localisation, wherein they pinpoint the core of the tumour (19, 20):

- **Wire guidance localisation (WGL)** is the gold standard for small impalpable tumours (21). This includes multiple tumours in close proximity. Wires can also give an approximation to the size of the tumour. However, the resection is crude, wires often displace, they have an associated risk of sharps injuries, and they still have high positive margin rates (**Figure 5, left**) (21).
- **Seeds (radioactive, magnetic, radar)** are similar to wires but require a probe to detect the location of the seeds, providing the surgeon with auditory feedback. Unlike wires, seeds have a lower risk of displacement or sharps injuries but have the disadvantage that some (e.g, magnetic seeds) are not MRI compatible and require plastic instruments to be used in the operating room. (**Figure 5, right**)

According to a Cochrane review (21), wire guidance and radioactive seeds/colloid are equivalent in their positive margin rates. The meta-analysis by Davey et al. (22) concluded that

radioactive seeds, radioactive colloid as well as Magseed® (Endomag, Cambridge, UK) were all comparable in terms of PMR, but superior to wire guidance. However, a recent paper I published highlights that these technologies only localise the tumour core, thus they fail to identify the tumour in its entirety (23). It identified that a major flaw for guidance technologies (wires or seeds) was that they are unable to provide information on the size and invasiveness of the tumour itself. This was why identification techniques which highlight the tumour in its entirety could improve PMR during BCS (section 1.1.6). My thesis will focus on fluorescence guidance during surgery, an identification technique providing real-time visual intraoperative feedback of the whole tumour (Chapter 2).

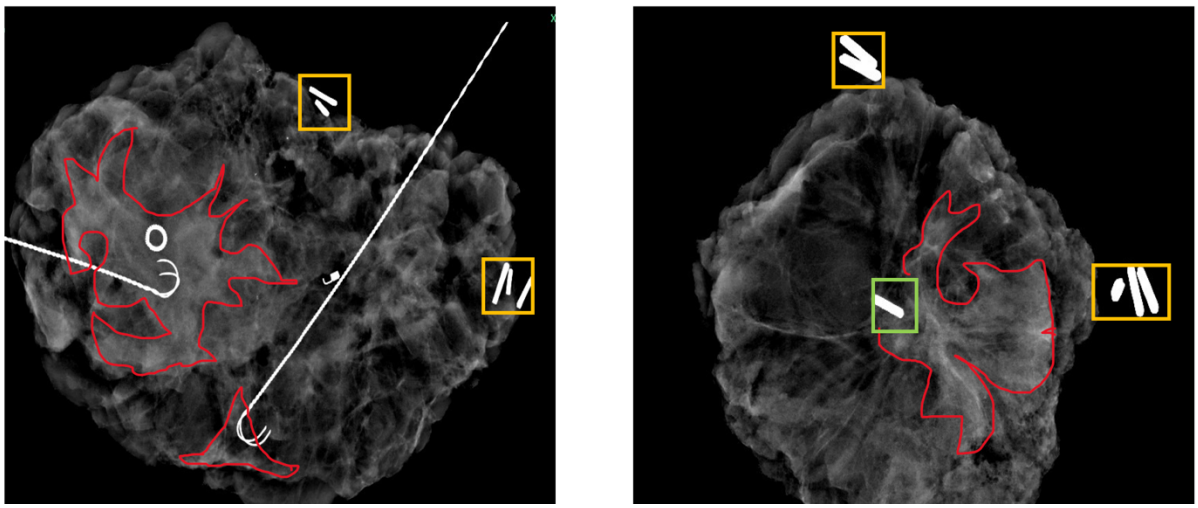


Figure 5: Tumour localisation using a wire vs seed.
Anterior-posterior specimen XRays. The orientation of the specimen is marked by 2 staples superior and 3 staples laterally (orange squares). Tumour is marked in red. The image on the left is an example of wires bring used to localise different sites of breast cancer. The image on the right is an example of a seed technology (green square), requiring a probe to identify location. Both only provide an approximation of the tumour core.

1.1.5. Margin Techniques

A variety of alternate techniques have been developed to assess the margins. Although they are unable to localise the tumour itself, they can assess the outermost aspects of the resected specimen and the cavity. Many of these technologies use a probe (confocal microscopy,

bioimpedance, etc.) which is time consuming as it depends on the surface area of the probe and specimen.

Optical (high resolution imaging):

- **MicroCT** (Bruker) is a high resolution CT image providing an image based on tissue density. It provides a 3D image with high spatial resolution (<1um) which can differentiate between breast cancers or benign tissues (including DCIS) (24). It images the ex-vivo specimen up to 15cm in size (25) with a sensitivity of 83.3% and 94.7% specificity (24).
- **Confocal Microscopy** uses a probe to detect the properties of reflected light (from a laser) to visualize tissue on a cellular level (26). Despite high resolution, it is unable to assess a depth more than tens of micrometers. The probe can be used both *in-vivo* (invasive) and *ex-vivo* (which is used after the specimen is fixed and stained (26).
- **Optical Coherence Tomography (OCT)** (Leica Envisu R-Class) (19) differs from microCT in that it provides micron-level resolution at a larger depth (up to several mm) of the specimen (27). It can provide high-resolution images of the tissue microstructure, 1cm2 at a time, with a sensitivity of 81.7% and 81.9% (24, 27).
- **Fluorescence Molecular Imaging** (i.e. Spectropen/STS) (19) uses a probe which uses light at a specific wavelength to activate fluorescent probes at a different wavelength and collects those emission signals to differentiate between tumour and healthy tissue (28). It can be used both intraoperatively and postoperatively on the specimen. It has a lower spatial resolution than confocal microscopy but has a larger field of view and increased depth capacity (28).

***N.B. Intraoperative ultrasound (IOUS), intraoperative MRI (iMRI),and Cherenkov luminescence** visualise the entire tumour (not just tumour margins) thus are considered identification techniques and are discussed in section 1.1.6.

Bioimpedence (electrical properties of tissues):

- **Radiofrequency Spectroscopy** (i.e. MarginProbe) assesses the electrical properties of the tissue (including conductivity and permittivity) to identify structural and compositional changes (cellularity, fluid content, etc.) (17, 19, 29, 30). However, it lacks in sensitivity (70.4%) and specificity (58.5%) .
- **Bioimpedance Spectroscopy** (i.e. ClearEdge), also uses electrical properties of tissue but instead measures the bioimpedance (resistance) of tissue. It is also used to infer molecular composition and physiological properties of tissue (19, 31).

Spectroscopy:

- **Raman microspectroscopy** uses light to induce molecular vibrations which result in light scattering. It can provide information on molecular composition and structure of tissue. In the study by Kong et al., Raman achieved 95.6% Sn and 96.2% Sp based on changes in concentrations of nucleic acids, collagen, fat (32).
- **Rapid Evaporative Ionization Mass Spectrometry (REIMS)** (19) examines surgical smoke (vaporised tissue) produced from intraoperative electrocautery and performs mass spectrometry (33). This determines molecular composition using lipids, which according to St John et al was able to provide a sensitivity of 90.9% and specificity of 98.8% in invasive breast cancers (33).

Due to the limitations of the above listed methods/technologies, none have been able to replace the current gold standard which remains formal histopathology. Furthermore, these techniques can only localise the tumour, and not identify the full size, extent, or invasiveness of it. The ideal technology would enable the visualisation of macroscopic tumour margins in real time, without impeding the field of view of the surgeon (23).

1.1.6. Tumour Identification

Intraoperative modalities to visualise tumour may have an advantage to help guide BCS and reduce positive margin rates. Given that all of these enable visualise the tumour in its entirety rather than pinpoint the centre, it is more likely that these techniques will improve the PMR. These systems include the following:

- **Intraoperative ultrasound (IOUS)** emits sound waves and captures the reflected signal (**Figure 6**). Not only can it guide specimen resection, but it can also confirm complete resection by analysing the cavity. Despite halving the PMR, limitations include dependency on the skill of the operator, requires additional training, lacks in sensitivity (55.7%) (but has a specificity of 84.4%) (24), and is incapability of identifying DCIS (17, 34).
- **Intraoperative MRI (iMRI)** capitalises on creating a magnetic field which stimulates protons into unpredictable movement. It then captures the time for protons to realign with the magnetic field, and creates an image reflecting the difference in timings. Shortcomings include that it is dependent on the patients intraoperative position matching the position during the pre-operative scan (30, 35).
- **Cherenkov luminescence imaging (CLI)** uses radioactive tracers which polarise atoms and emit light when they return to their ground state. Emitted gamma rays are

detected via a special camera system, which then can reconstruct an image. A major limitation however is that this technique exposes the patient to ionizing radiation (36).

- **Fluorescence Guided Surgery (FGS)** is capable of real-time intraoperative visualisation of tumour, thus providing surgical guidance for complete resection of the tumour without delay (**Figure 6**) (19, 23). Like IOUS, it can both guide and confirm complete resection by analysing the cavity, thus potentially surpassing other imaging techniques in PMR rates. Unlike IOUS or iMRI, FGS is not dependant on the operator or patient position, nor is there a delay while it scans. Furthermore, it does not expose the patient to ionising radiation as is the case with CLI. However, it exposes patients to the side effects of drugs used to enhance tissue fluorescence.

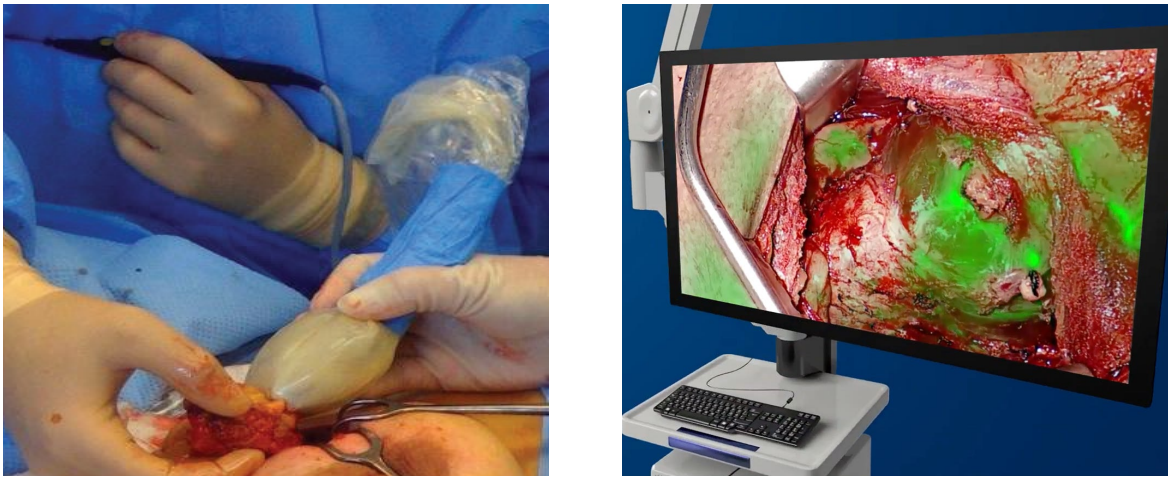


Figure 6: Intraoperative tumour identification techniques.
Left image is of intraoperative ultrasound. Right image is fluorescence imaging with a screen displaying green overlay where tumour is suspected.

1.2. Conclusion

In summary, this chapter summarises the issues of positive margins during breast conserving surgery. It goes through the current technologies attempting to address it, as well as their limitations. Thus, it highlights the need for further improvement. It also introduces the reader to the hypothesis of this thesis- that fluorescent guidance during breast conserving surgery

has the potential to improve a surgeon's ability to identify the tumour, thus reducing positive margins.

1.3. The contribution of this work

This thesis will explore the potential of near infrared fluorescence (NIRF) imaging with regards to BCS. The fluorescence guided surgery system that was used throughout this thesis was constructed in-house and named 'GLOW' (Guiding Light Optimising Wide local excisions).

The main hypothesis being assessed is whether the signal from fluorescent light can differentiate between tumour and healthy tissue in the breast.

The following chapter will explain the concept of fluorescence guided surgery (FGS), and the third chapter will describe how it is being investigated in breast conserving surgery.

Subsequent chapters will assess the camera system *in-vitro*, followed on by 3 *in-vivo* feasibility trials.

- The *in-vitro* trial will assess the prototype camera specifications. This will include optimal distances and corresponding field of view, minimal detectable fluorophore concentration, and depth of signal penetration in porcine tissue. It will also compare the prototype to a commercial system.
- The first *in-vivo* feasibility trial will focus on testing the safety, useability, and integration of the camera into clinical workflow through rapid prototyping. This will use the nonspecific fluorophore indocyanine green (ICG) and will be used to power the following trial.

- The second feasibility trial will explore the effect of timing of administration of ICG, and whether pre-operative or intraoperative administration results in a difference in results of signal strength and accuracy.
- The third feasibility trial will actively target breast cancer cells via an accumulation of fluorescent Protoporphyrin IX (upon administration of its metabolic precursor 5-Aminolevulinic acid).

The penultimate chapter will compare the previous trials in view of determining which technique is the most accurate. Finally, the conclusion will go through a brief summary of the findings from each of the chapters, the limitations of these studies, and what the future holds for fluorescence guided surgery.

2. Fluorescence Guided Surgery

This chapter explores the concept of fluorescence guided surgery. It explains the technology itself and compares the various camera systems available. It goes into detail about how light interacts with tissue, and how the properties of light are distinct in different tissues. Furthermore, it provides examples of how fluorescence can be used to distinguish cancer from healthy tissues. These signals are mediated by different fluorescent agents, some of which may be targeted to a particular receptor or enzyme. It also explains how these targeted fluorescent agents work as well as their advantages and disadvantages. Lastly, it explores the way in which the difference in light signal can be measured and compared.

This chapter is entirely my work apart from Figures 8, 9, 10. Figures 8 and 10 were created by Maria Leiloglou, and Figure 9 is reproduced with permission from IntechOpen. Permissions for re-use of images are provided in Appendix 3.

This work was presented at the *European Molecular Imaging Meeting* (2020) 'Illuminating Cancer: A Systematic Review of Fluorophores available for Fluorescence Guided Surgery in Humans.

2.1. Introduction to FGS

FGS uses near infrared fluorescence (NIRF) to identify targeted tissue (**Figure 7**) (37). It achieves this by capitalising on an imaging system sensitive to fluorescent molecules found in tissues. FGS can be used in a variety of settings including cancer surgery. Through the provision of real-time intraoperative feedback, FGS can guide the surgeon regarding whether a more extensive cancer resection is required.

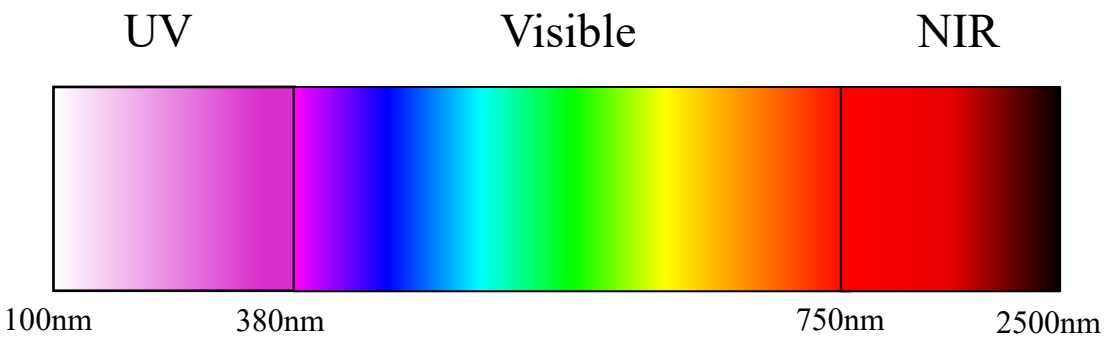


Figure 7: Light spectrum.
UV= ultraviolet. NIR= near infrared. Image of a part of the electromagnetic spectrum and the associated wavelengths for ultraviolet (100-400nm), visible (380-750nm), NIR (750-2500nm). NIR is further subdivided into NIR1 (750- 1400nm), and NIR2 (1400-2500nm) wavelengths. Most innate fluorophores are found in the 280-700nm region. In the main, fluorophore probes lie close to or within the NIR range.

2.2. Components of a NIRF imaging system

NIRF systems comprise a:

- **light source** - a filtered broadband light source incorporating the specific wavelength to excite fluorescent molecules (fluorophores)
- **cameras** – a system of 2 cameras for simultaneous registration of the fluorescence image (high sensitivity NIR camera with built-in filter to capture the emitting wavelength of said fluorophore) and a white-light image (conventional colour camera)

- **processing software** - to integrate and analyse the 2 video streams and overlay the information (38). NIRF is non-ionising, safe, yields high image resolution, and has good sensitivity to fluorophores. It capitalizes on fluorescent signals from the near infrared spectrum (>650nm), where interference from endogenous fluorophores (280-800mm) is minimal (39).

At present NIRF is used primarily for perfusion studies, functional studies (of hepatic and renal systems), and identification of some tumours(40). NIRF could potentially demonstrate enhanced visualisation of the tumour in real-time, which could prove invaluable intraoperatively. In view of its potential to enhance precision of cancer surgery, it is currently being investigated with regards to a variety of solid organ tumours (40).

2.2.1. Commercially Available NIRF Camera Systems

Eleven camera systems have been identified within the remit of breast conserving surgery, only 5 of which are Food and Drug Administration (FDA) approved (41, 42, 43, 44, 45, 46, 47, 48, 49). These include the Photodynamic Eye™ (PDE; Hamamatsu Photonics, Shizuoka, Japan) (42, 43), Fluobeam 800™ (Fluoptics, Grenoble, France) (44), Artemis™ (Quest Medical Imaging, Middenmeer, Netherlands) (45, 46), mini-FLARE™ (Beth Israel Deaconess Medical Center, Boston, MA, USA) (47, 48) and the Visual Navigator™ (SH System, Gwangju, Korea) (49). All of these cameras act within the remit of the infrared spectrum.

2.3. Properties of Light

When light comes into contact with tissue, a variety of things can occur, as demonstrated in **Figure 8**. The excitation light (1) can either be reflected (2, 3), absorbed (4), or after absorption later emitted as fluorescence (5,6). One type of reflection is specular (2) meaning it mirrors the incoming light and reflects it at the same angle of impact. The remainder of the light enters the tissue, where it either comes back out in the form of diffuse reflection (3), gets absorbed (4), or is partially absorbed and then emitted as light at a lower energy level in a phenomenon known as fluorescence. The fluorescent light can go on to be absorbed (5) or come back out of the tissue (6).

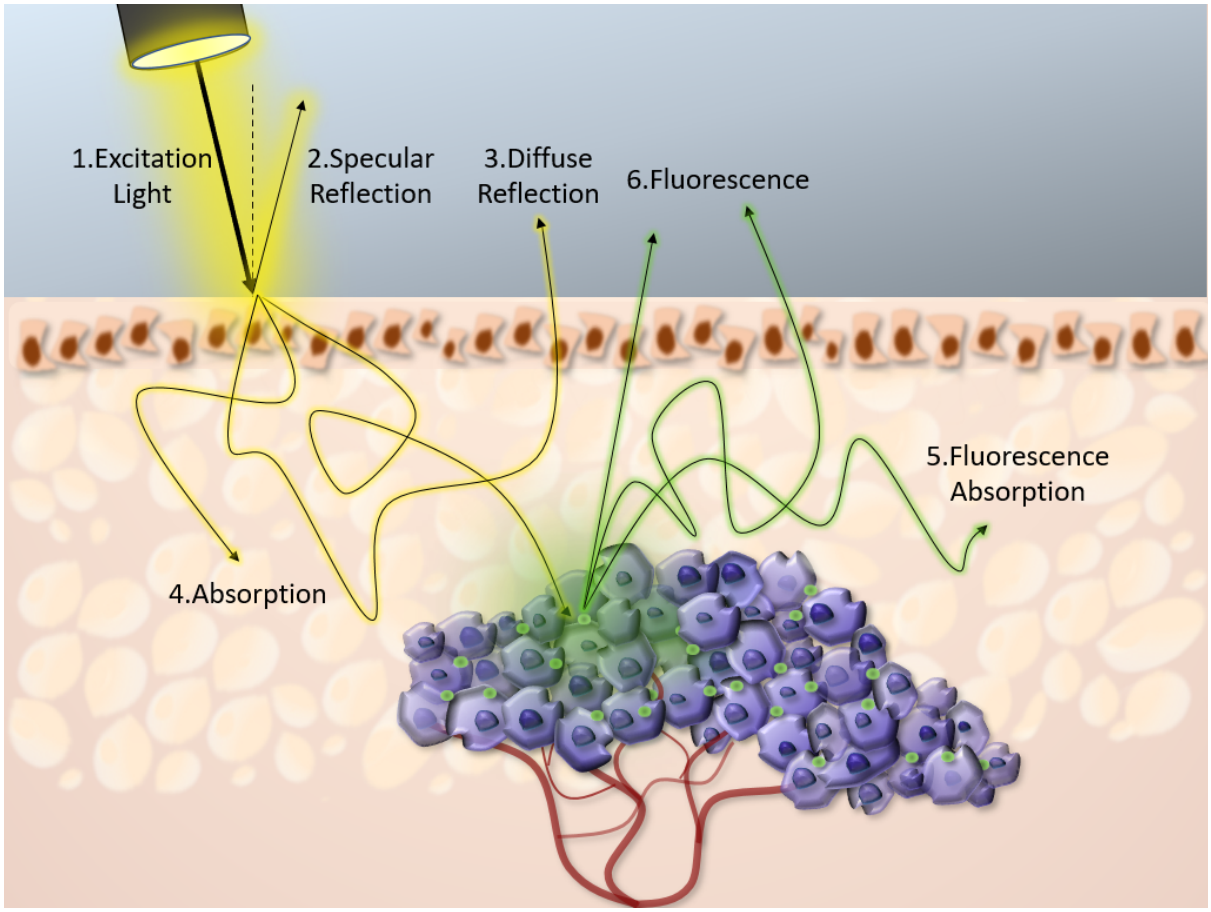


Figure 8: Properties of light in tissue.

Illustration of light-tissue interactions. Upon illumination of the tissue, part of the incident light (i) is reflected from the tissue surface without changing its initial properties (spectral shape or polarization state). This reflection is called "specular reflection" (ii), whereby both incident and reflected light are coplanar and at the same angle to the surface normal (perpendicular to the surface direction). Part of incident light can also be scattered (iii) in the tissue and re-emerge from the surface. This light is called "diffuse reflection" (iv) and its direction/spectral shape and polarization state are altered compared to the incident light. Finally, part of the incident light can be absorbed by a fluorophore (v), whereby part of the initial energy will be emitted as fluorescence (vi), or absorbed by a chromophore (viii), whereby no subsequent fluorescence emission occurs. Fluorescence light can be absorbed or scattered as well prior to its emergence from surface.

Image reproduced with the permission of publisher (50).

2.3.1. Chromophores

There are many molecules within the human body which upon illumination alter their spectral shape and emit light at a longer wavelength. These are called chromophores, as they are responsible for the colour properties of compounds. Occasionally, the light is absorbed, resulting in the transformation of light energy into heat. Some examples of chromophores

include: tryptophan, flavins, NADH, pyridoxine, collagen lipo-pigments, porphyrins, elastin, oxygenated/deoxygenated haemoglobin, fat, melanin, bilirubin and β-carotene. The spectral properties of some chromophores are demonstrated in **Figure 9.** A subset of chromophores exhibit fluorescent properties, thus are called endogenous fluorophores.

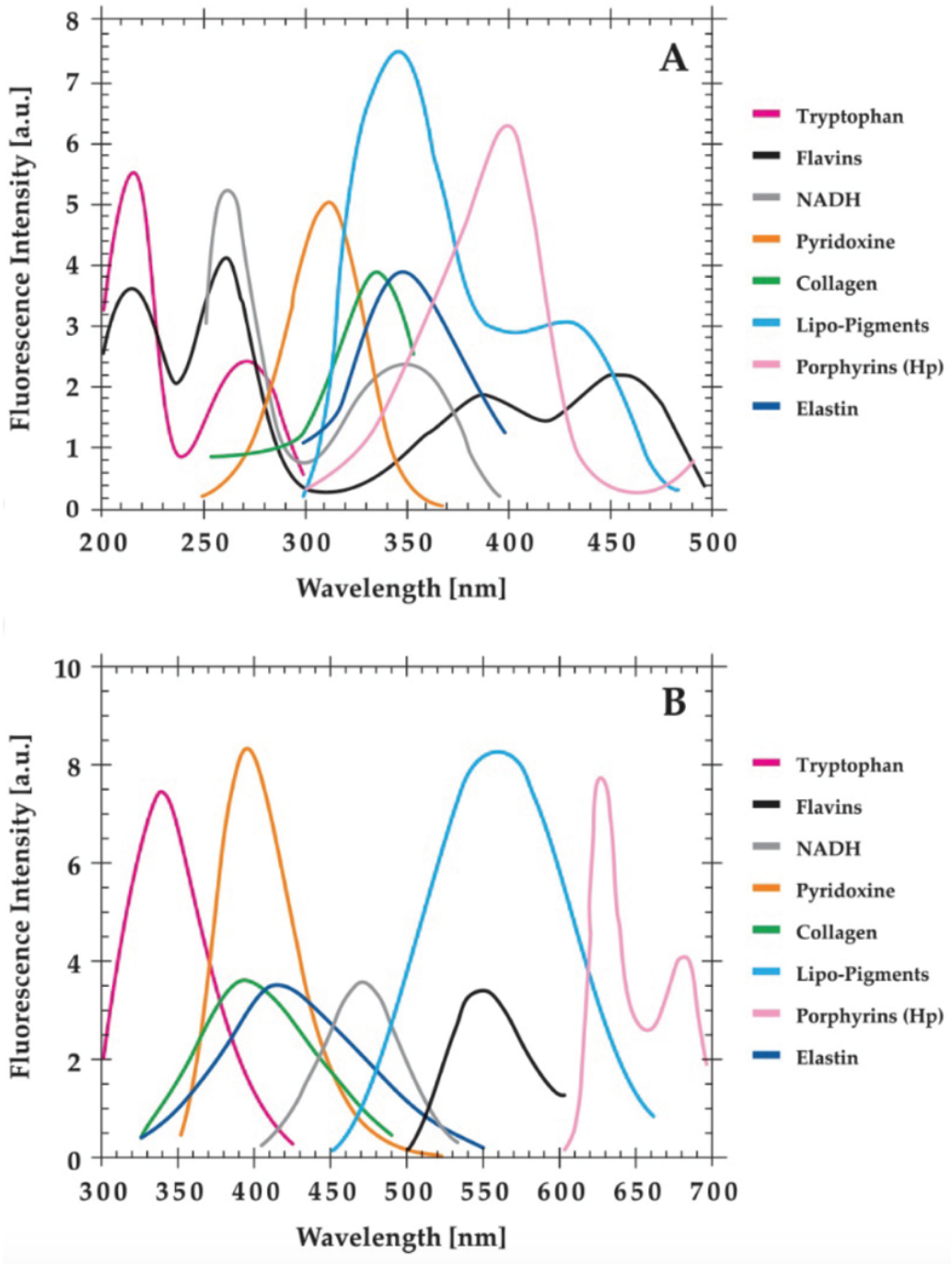


Figure 9: Optical properties of chromophores.
A) Absorption spectra, B) Emission spectra
Note. Image reproduced with the permission of publisher (51).

2.4. Exogenous Fluorophores for Medical Imaging

Fluorophores can be sub-categorised into 2 groups: namely “passive” and “active targeting”. Passive fluorophores target systemic circulation. They accumulate in the desired tissue most often due to the enhanced permeability & retention (EPR) effect (52, 53). Active targeting implies that the fluorophore is designed to specifically accumulate in certain tissues/ cells/ organelles and not others (see Figure 10) (52, 54).

2.4.1. Passive Targeting

There are 4 fluorophores capitalising on EPR passive targeting which are clinically approved by the European Medical Association (EMA) for clinical use in humans. These include fluorescein, aminolevulinic acid (ALA), indocyanine green (ICG), and methylene blue (MB). Fluorescein, ICG and MB are presumed to non-specifically target cancer via the enhanced permeability and retention (EPR) effect. This occurs due to the dysregulated angiogenesis which causes the vasculature to be inherently more permeable in combination with impaired lymphatic outflow of tumours. This is demonstrated in **Figure 10A.** ALA also passively targets cancerous tissues; however, this occurs via deranged haeme metabolism resulting in the accumulation of protoporphyrin IX (PpIX), an endogenous fluorophore (55).

Fluorescein was the first to be used in gliomas, however, this has been superseded by ALA in light of its improved sensitivity and specificity (56). This is due to fluorescein using the EPR effect whereas ALA targets faulty metabolism specific to breast cancer cells, resulting in a more precise resection (55, 56). Furthermore, ALA is safer as it already exists within the body, whereas fluorescein is a foreign agent that risks anaphylaxis (57). ALA is approved for use in

tumour margin delineation intraoperatively in brain, bladder, and skin cancers, and is currently being investigated in breast cancer (58, 59). ICG is approved for its use in angiography, cardiac function, and liver function studies (60). Methylene blue on the other hand is approved for uses outside of fluorescent imaging as a treatment for: methemoglobinemia, malaria, sepsis, and vasoplegia (61). Although these 4 fluorophores tend to accumulate in cancers, as it is via a nonspecific mechanism, they are considered to be passive. However, apart from ALA, any studies aiming to provide evidence of tumour delineation outside of their approved uses (listed above) are considered 'off-licence'.

2.4.2. Active Targeting

The majority of medical fluorophores are designed to actively target molecules present in certain tissues (**Table 1**). They can directly target a specific protein such as a receptor or enzyme. Receptors are targeted via tailored antibodies with a fluorescent component attached(52), as demonstrated in **Figure 10B**. Alternately, fluorophores can be dependent on activation by a certain enzyme present only in the targeted tissue, whereby the quencher molecule (which blocks fluorescence) is cleaved off, only then permitting fluorescence to occur as illustrated in **Figure 10C**. The majority of these fluorophores are not specific to a certain type of cancer or ER/PR/Her2 status, as they target receptors which tend to be overexpressed in a multitude of cancers. Potential targets include epidermal growth factor (EGFR), carbonic anhydrase IX (CAIX), and carcinoembryonic antigen (CEA) (62, 63, 64, 65, 66).

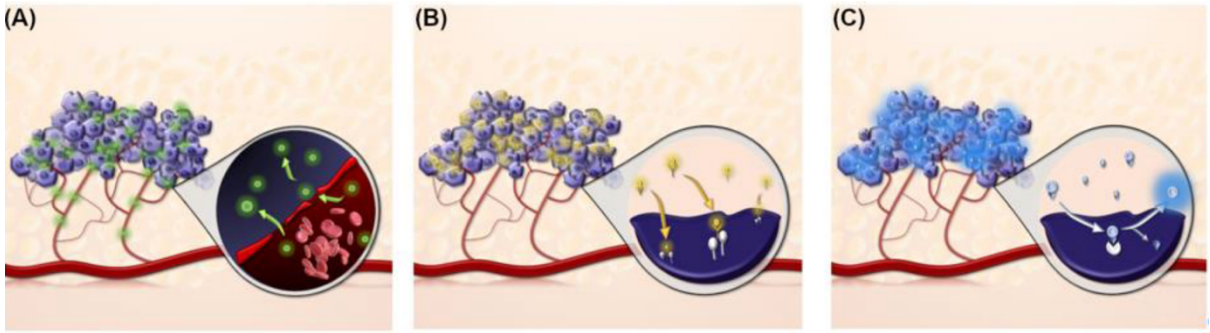


Figure 10: Demonstration of extrinsic fluorophore tumour targeting approaches.

(A) Passive targeting, whereby the contrast agent leaks into the tumour through porous vasculature.
(B) Active targeting whereby the fluorophore is conjugated with agents that have a high affinity towards targets that are overexpressed in cancer cells.
(C) Active targeting whereby the contrast agent is optically silent until its cleavage by enzymes specific to the tumour microenvironment.

Note. Image reproduced with the permission of publisher (50).

2.4.3. Absorption and Emission Spectra

The majority of these fluorophores have absorption and emission spectra approaching or within the infrared spectrum (>700λ). Since the fluorescence is outside the human visual spectrum, the fluorophores do not disturb the operator's visual field. Additionally, infrared fluorophores are able to penetrate tissues deeper than fluorophores within the visual spectrum (which are limited to superficial detection) (67). However, for those fluorophores which are within the visual spectrum, this can be problematic in view of increased background noise (from endogenous fluorophores) and decreased tissue penetration. For example, EC17 has a similar emission spectrum to breast tissue autofluorescence (520-530nm), and thus failed to distinguish tumour from background during BCS (46). However, EC17 was much more efficacious when it came to ovarian tissue as per the study done by Tummers et al. (46). This is due to the difference emission spectra wherein the background autofluorescence of ovarian tissue peaks between 390 and 440nm (68).

2.4.4. Tumour Background Ratio

Tumour Background Ratio (TBR) is a value determined by the fluorescence of cancerous tissue compared to normal tissue. TBR quantifies the contrast between the targeted tissue and the surrounding tissues. This value is dependent on the fluorophore being examined, the sensitivity of the camera system being used, as well as the background fluorescence of the normal tissue. Background signal originates from a variety of sources such as ambient light, reflected light from the light source, camera noise, or autofluorescence of the normal tissue. There is no set value for a minimum TBR threshold as cameras can be capable of detecting very subtle changes. However, the higher the TBR value, the better it is for the surgeon to be able to differentiate between tissues. Historically, most studies aimed for an *in-vivo* TBR >2.5 for tumour identification. However, as this was seldom achievable, the study by Tummers et al. has deemed >1.5 to be sufficient *in-vivo* (but >3.0 in pre-clinical studies) (69). The TBR calculation is as follows:

$$\text{TBR} = \frac{\text{intensity of tumour fluorescence}}{\text{intensity of healthy region fluorescence}}$$

2.4.5. Fluorophores for use *in-vivo*

To identify the key fluorophores used in surgery, a literature review was conducted using the databases Medline, Embase, Scopus, and Web of Science in March 2020. The following Medical Subject headings were used in combination with AND/ OR operators: '*Surgery*' AND '*Fluorophore*' AND '*Near-infrared*'. 14 fluorophores were identified (**Figure 11**).

Articles describing *in-vivo* clinical trials using fluorescence guided surgery were included. Studies were excluded if they were: a) animal, cell line, phantom, or in vitro studies, b) camera,

photoacoustic, photothermal, or photodynamic, Raman spectroscopy studies, c) not published in the English language. Covidence (Veritas Health Innovation, Melbourne, Australia) systematic review software was used to deduplicate, screen studies, and extract data. Data extracted included mechanism of action of the fluorophore, fluorescent properties, clinical uses, and safety profile.

4271 articles were identified, of which 1407 were duplicates. 2867 abstracts were screened, resulting in 64 full texts to be assessed. Of those, only 24 articles were included.

From those articles, 14 fluorophores were identified.

*Of note, fluorescein which previously used angiography (of the heart and liver) as well as glioma identification has not been included as it has been replaced with fluorophores with a better safety profile (ICG and ALA respectively).

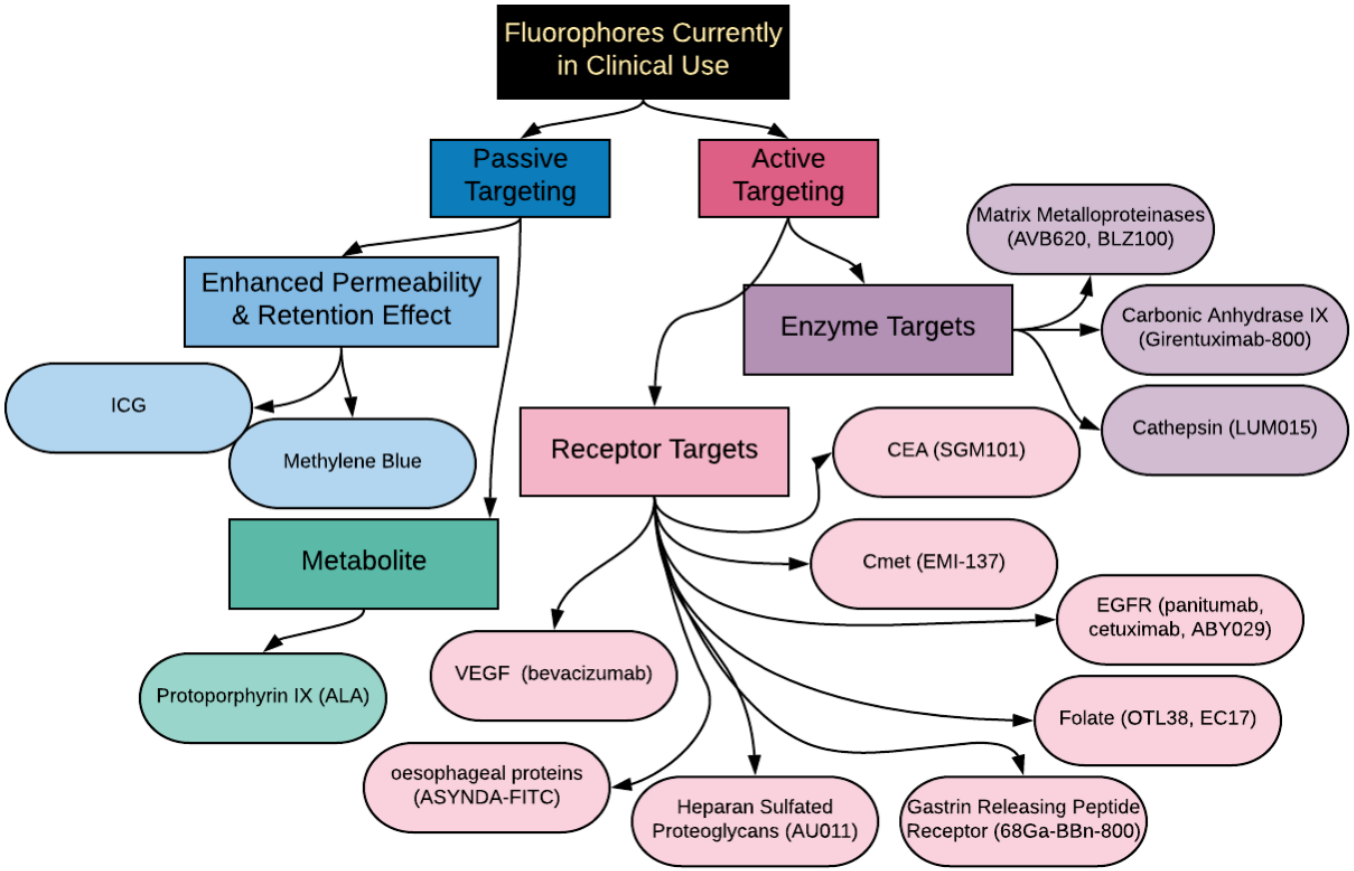


Figure 11: Fluorophores currently in clinical use for cancer imaging.
They are separated into 2 categories: passive and active targeting. Passive targeting is further subcategorized into fluorophores which capitalize on the enhanced permeability and retention effect (ICG and methylene blue) and as a metabolite of enzymatic processing (Protoporphyrin IX). Active Targeting is subcategorized into targeting receptors (VEGF, oesophageal proteins, heaparan sulphated proteoglycans, gastrin releasing peptide receptor, 2 targeting folate, 3 targeting EGFR, CMET, and CEA) or requiring activation using enzymes (matrix metalloproteinase, carbonic anhydrase IX, cathepsin).
*ICG= indocyanine green, ALA= aminolevulinic acid, VEGF= vascular endothelial growth factor, EGFR= epithelial growth factor receptor, CEA= carcinoembryonic antigen
*fluorescein was excluded as it has been superseded by other drugs (ICG, methylene blue, ALA)
N.B. This image was presented at the European Molecular Imaging Meeting (not published).

Dye	Target	Cancers trialled	Presence in breast cancer	Absorption λ	Emission λ	Formulation	Dose	Time between administration & Imaging	Tumour-to-Background Ratio	References
68Ga-BBN-IRDye800CW	gastrin-releasing peptide receptor (GRPR)	Glioblastoma	No	775nm	850nm	Intravenous	1mg	2h	4.9	(70)
ABY-029 (IRDye800CW)	Epidermal Growth Factor Receptor (EGFR)	Sarcoma, Glioma	45% (14-91%)	775nm	850nm	Intravenous	N/A (30-180nm. Safety up to 30000nm)	1-3h pre-op	N/A	(62, 63)
Aminolevulinic Acid (ALA)/ Protoporphyrin IX (PpIX)	Passive (deranged haem metabolism)	Glioma, Bladder, Skin, Breast	Yes	405nm - 635nm	635nm - 705nm	Oral (topical)	20mg/kg	2-4 hours pre-op	3.6 +/- 1.1	(57, 71, 72)
ASYNDA-FITC	Unknown oesophageal proteins	Oesophagus	No	471nm	519nm	topical	100um	0-5 minutes	4.2	(73)
AVB620 (-Cy5 + Cy7)	Activated by matrix metalloproteinases (MMPs)	Breast	Yes	620nm	670nm	intravenous	8mg	12-20h pre-op	Not reported	(74, 75, 76)
AU-011 (+IR700)	heparan-sulfated proteoglycans (expressed by ocular melanoma cells)	Ocular, Choroidal, Uveal, Melanoma	No	Not reported	Not reported	intravitreous	N/A	N/A	N/A	(77)
Bevacizumab-800CW	Vascular Endothelial Growth Factor- Alpha (VEGF-A)	Breast, Oesophageal, Pancreas	Yes	774nm	791nm	Intravenous	4.5mg	3 days pre-op	1.8-9	(78, 79, 80)
BLZ 100/ Tozuleristide (-ICG) (81, 82, 83)	Matrix metalloproteinase 2 (MMP2) + transmembrane inhibitor (TIMP2), MMP1, ClC-3 Cl ion channel,	CNS, Breast, Sarcoma, Glioma, Skin	>75% infiltrative breast cancers	Not reported	Not reported	Intravenous	3-30mg, 6-12 mg	1h pre-op	2.5	(81, 82, 83, 84)
Cetuximab-IRDye800	Epidermal Growth Factor Receptor (EGFR)	Pancreas, Glioma	45% (14-91%) 13-76% in TNBC	778-785nm 774nm	820nm 789nm	Intravenous	50-100mg	2-5 days pre-op	3.7	(62, 85, 86)
EC17	Folate receptor	Ovarian, Breast, Kidney, Lung	86% in TNBC 30% overall	465-590	520-530nm Overlaps breast autofluore scence	Intravenous	0.1mg/kg	2-3h pre-op	7.0 in ovarian ca, 2.3 in breas cat	(46, 87)
EMI-137	C-met (tyrosine kinase receptor)	Colorectal	5-70%	653nm	675nm	Intravenous (topical)	0.13mg/kg	3h pre-op	5.5 +/- 0.5	(88, 89)
Indium-111-DOTA-Girentuximab-IRDye800CW	carbonic anhydrase IX	Renal Cell Carcinoma	Overexpressed in all BC cell lines	775nm	850nm	Intravenous	5/10/30/50mg *highest TBR in 10mg group (3pts only tho)	4 days pre-op	2.5 +/-0.8	(64)
Indocyanine Green	Passive (Enhanced Permeability and Retention effect)	Angiography, Lymphography, Breast	30-90% Sn and 30-73% Sp	800nm	830nm	Intravenous/ Intratumoral	0.25mg/kg	2-3 minutes if IV	Variable (perfusion dependent)	(44, 60, 90)
LUM015 (-Cy5)	Cathepsin K/L/S activated	Breast, Sarcoma, Pancreas, Colon	Yes	650nm	675nm	intravenous	0.5-1mg/kg	2-6h pre-op	4.22-4.7	(91, 92, 93, 94)
Methylene Blue	Passive (Enhanced Permeability and Retention effect)	Breast,	Yes	609nm - 668nm	675nm	Intravenous/ Intratumoral	1mg/kg	3 hours pre-op	Variable (perfusion dependent)	(48)

OTL-38 (-ICG)	Folate receptor	Ovarian, lung, breast	86% in TNBC 30% overall	776nm	796nm	Intravenous	0.0125mg/kg in 250ml 5% dextrose	2-3 hours pre-op	4.4	(87, 95, 96, 97, 98)
Panitumab-IRDye800	Epidermal Growth Factor Receptor (EGFR)	Colorectal, lung, glioma, head and neck	45% (14-91%)	775nm	850nm	Intravenous	0.5-1mg/kg	2-5 days pre-op	8.85-9.96	(62, 99)
SGM-101 (-BM104)	Carcinoembryonic Antigen (CEA)	Pancreas, colorectal	17.4%	685nm (670-700nm)	705nm	Intravenous	5-7.5-10mg	2 days pre-op	1.6	(65, 66, 100)

Table 1: **Fluorophores Currently Being Investigated in Humans.**
These fluorophores have been assessed in terms of target, cancers which they had been trialled in, target presence in breast cancer, absorption and emission spectra, formulation, dose, time between administration and imaging, and tumour to background ratio.[1,2]

[1] Fluorescein was not included as it has been superseded by aminolevulinic acid in gliomas.
[2] Decisions about which agents would be used in the feasibility studies presented in chapters 5-7 was based off of the information found in Table 1.

As per **Table 1** there are a variety of drug formulations available. These include oral, topical, intravenous, intravitreous, and intratumoral. Furthermore, the administration to visualisation time is variable as there is variation in the absorption rate, need for enzymatic activation or metabolism, pharmacokinetics, and pharmacodynamics. The timing between administration and visualisation ranges from immediately before surgery through to as long as 5 days pre-operatively depending on the drug.

Since the time of this search, Nagaya et al. identified 2 new fluorophores being investigated in clinical trials for cancers (40). These are chlorotoxin (in breast cancer) and BBN[7-14] NH2 (in glioma) (40). Furthermore, they found additional cancers being targeted using panitumab (skin) and bevacizumab (colorectal and gastric cancers) (40).

2.5. Conclusion

In summary, this chapter has reviewed the current state of FGS. FGS has proven to be safe, easy to use, comes without radiation nor impediment to the surgeons' view of the operating field, and can be used in real-time. However, it requires a suitable targeted contrast agent. It provided an in-depth review of the current state of camera systems and fluorescent agents which can be exploited in various operations.

This thesis will explore the current status of FGS in breast cancer. The next chapter will describe what fluorophores have been trialled in breast cancer, and how they can be deployed to aid in BCS.

3. Fluorescence Guided Surgery in Breast Cancer

This chapter presents the optical properties in breast cancer, and the many ways in which FGS has been used in treatment. It includes the inherent fluorescent molecules which exist, their optical properties, and highlights which ones can be used to differentiate breast cancer from normal tissue. It goes on to describe the various probes which have been trialled in augmenting the difference in light properties between breast cancer and normal tissue. It also compares gold-standard identification of axillary sentinel lymph nodes and how they compare to fluorescent guidance using indocyanine green. Lastly it describes how FGS is used to map lymphatic pathways.

The work presented in this chapter was carried out jointly with Maria Leiloglou. I performed the systematic reviews and extracted data. Maria Leiloglou performed a meta-analysis on the sentinel nodes. We co-wrote the article on the 'Meta-analysis comparing fluorescence imaging with radioisotope and blue dye-guided sentinel node identification for breast cancer surgery' and I wrote the accompanying reflection to that article.

The work in this chapter was published in the journal of *Annals of Surgical Oncology* (2021) 'Meta-analysis comparing fluorescence imaging with radioisotope and blue dye-guided sentinel node identification for breast cancer surgery' and 'ASO author reflections: fluorescence-guided sentinel node biopsy for breast cancer'. It was also presented at the at the *American Society of Breast Surgeons Symposium* (2020) and at the *Imperial Surgery & Cancer Department* (2019) 'Meta-analysis of Sentinel Node Mapping Techniques Comparing Near Infrared Fluorescence Imaging to Blue Dye and Radioisotope.'

3.1. Introduction to FGS in Breast Cancer

There have been various trials exploring fluorescence imaging for different aspects of breast surgery. Following a systematic review, these areas include tumour identification (i.e. gliomas) (101), discerning sentinel nodes (to assess cancer spread) (102), lymphatic mapping (for lymphatic reconstruction in oedema) (103), as well as determining perfusion during reconstructive surgeries (i.e. muscle flap perfusion in breast reconstruction) (104).

3.2. Optical Properties of Breast Tissue

Optical imaging of the breast is incapable of visualising morphological characteristics of the breast in the way that mammography or MRI can; however, it is able to classify physiological properties. Breast tissue is composed of adipose and connective tissue, mammary glands (and their associated ducts), as well as blood vessels and lymphatics (105). It possesses a low absorption of light in the infrared spectrum, meaning that it is ideal for NIRF (105). However, light is highly scattered, reflected, refracted, and only a portion of it fluoresces. According to Chorfi et al., all malignant tissue demonstrates an increase in scattering in comparison to normal healthy tissue due to variations in nuclear size within the cells(106).

Physiologically, there are multiple differences between tumour and normal tissue. There is an increase in water content due to increased inflow from angiogenesis and limited lymphatic outflow (107). There is also an increase in energy molecules NAD/FADH due to the cancer cells' rapid proliferation and resulting energy requirement (108). However, oxy- and deoxyhaemoglobin (which are related to blood oxygen saturation) cannot be used to differentiate between tumour and normal tissue. This is because in growing tumours with high

metabolic activity, there is an increase in the demand for oxygen (109). Contrarily, tumours may outgrow their blood supply and become necrotic, thus having a decreased oxygen content (110). Furthermore, collagen is decreased from enzymatic protease breakdown required for tumour growth (108). However, as these endogenous fluorophores overlap within the visible spectrum, it is extremely difficult to identify a specific peak as demonstrated in the previous chapter (**Figure 9**).

3.3. Sentinel Node Identification

I performed a meta-analysis to investigate the accuracy of fluorescence imaging of sentinel nodes compared it to the gold standard of radioisotope (RI) and blue dye (BD), as well as RI or BD individually (111). 1748 studies were reviewed, of which only 10 studies met the inclusion criteria (primary breast intervention, ICG was compared and the results were expressed as number of sentinel nodes identified) (111). 1 lower quality study was added to enable the meta-analysis of ICG vs dual technique. In total, these studies compared the data accrued from 976 patients (**Table 2**) (111).

Various camera systems were used to capture the data. Most commonly the photodynamic eye (PDE) camera system and Mini-Flare camera system were used, in 5 and 3 studies respectively. 3 studies compared ICG and RI and BD (2 of which compared ICG to ICG-albumin). These formed a part of the 8 studies which compared ICG to RI and 5 studies which compared ICG to BD. The dyes were injected either peri-areolar or in the skin overlying the tumour.

Paper	Method	Patients	Camera	Dyes	avg SLN/pt	SLN ID rate
Ballardini 2013 (102)	cohort	134	PDE	ICG + RI	ICG 1.83	245/246
					RI 1.74	231/246
He 2016 (112)	cohort MC	99	FIRE	ICG + BD	2.90 (both)	284/289
					ICG 2.80	276/289
					BD 2.00	202/289
Mieog 2011 (113)	NRCT	24	Mini-Flare	ICG + RI + BD	ICG 1.46	I35/35
					RI 1.25	35/35
					BD 1.46	30/35
Pitsinis 2015 (114)	cohort	50	PDE	ICG + BD	ICG 1.8	87/87
					BD 1.7	84/87
Polom 2012 (115)	cohort	28	PDE	RI + ICG	ICG 2.4	68/72
					RI 2.1	58/72
		21	PDE	RI +- ICG(albumin)	ICG 2.1	45/45
					RI 2 .0	42/45
Samorani 2015 (116)	cohort	301	PDE	ICG + RI	ICG 1.9	583/589
					RI 1.6	458/589
Schaafsma 2013* (117)	CT	16	Mini-FLARE	0.5 ICG + RI + BD	ICG 1.31	21/21
					RI 1.31	21/21
					BD 1.1	17/21
		16	Mini-FLARE	ICG + RI + BD	ICG 1.69	27/27
					RI 1.69	27/27
					BD 1.6	22/27
Somashekhar 2020 (118)	NRCT	100	Iryllic.nm	ICG + RI + BD	ICG 2.80	280/290
					2.40 (RI+/- BD)	246/290
Sorrentino 2018 (119)	cohort	70	HD laparoscopic system	ICG	ICG 1.14	76/82
		194		RI	RI 1.01	78/82
		71		ICG + RI	1.16 (combo)	
Valente 2019 (120)	cohort	92	PDE	ICG + IR	ICG 2.40	124/235
					RI 2.20	202/235
Van der Vorst 2012 (121)	RCT	12	Mini-FLARE	ICG + RI	1.5 (combo)	ICG 18/18
						RI 18/18
		12	Mini-Flare	ICG + RI + BD	1.6 (combo)	ICG 19/19
						RI 17/19
						BD 16/19

Table 2: Sentinel Node Studies in Breast Cancer Comparing NIRF to Radioisotope +/- Blue Dye.
pts= patients, avg SLN/pt= average sentinel lymph node per patient, SLN ID rate= sentinel lymph node ID rate, CT= clinical trial, RCT= randomised CT, NRCT= nonrandomised CT, ICG= indocyanine green, RI= radioisotope, BD= blue dye, *low quality study included in order to analyse ICG vs dual technique.
Note. Table reproduced with the permission of publisher (111).

A range of 1.0-5.5 lymph nodes were found per patient. Each lymph node resected was assessed using the various identification modalities- visible blue colour in BD, radioactivity using a gamma probe in RI, or whether fluorescence was visible upon using NIRF imaging. ICG identified the highest number of lymph nodes (82.6%), closely followed by radioisotope (77.7%) (111). Blue dye identified the least number of lymph nodes per patient (77.6%) (111). Sensitivity regarding the ability of ICG/ BD/ RI to accumulate in only tumour positive lymph nodes was seldom reported. However, according to Meric-Bernstam et al. neither ICG, RI, nor BD demonstrated preferential accumulation in metastatic lymph nodes (122).

Few studies commented on the fluorescent intensity of the lymph node as compared to normal tissue, known as the signal background noise (SBR) ratio. However, of the studies which did offer this data the SBR for ICG ranged from 2.5-11.3, all whilst using the Mini-Flare camera. That being said, most camera systems are equipped to differentiate SBR's less than 2.

Data meta-analysis was performed on the total number of lymph nodes identified by each technique divided by the total number of lymph nodes. A heterogeneity test (using Cochran's Q) determined the use of fixed or random effects models for pooled odds ratios, both of which were reported with 95% confidence intervals.

We observed the following with regards to sentinel node identification:

- ICG was superior to BD alone (OR 9.07, 95% CI 6.73-12.23, $p<0.05$) (111)
- ICG was equivalent to RI alone (OR 2.58, 95% CI 0.35-19.08, $p<0.5$) (111)
- ICG was superior to the gold standard combination of blue dye [BD] and radioisotope technique [RI] (OR 4.22, 95% Confidence Interval [CI] 2.17-2.8, $p<0.001$) (111)

Therefore, ICG is significantly superior to BD and equivalent to RI. However, the comparison of ICG to the dual technique is unlikely to reflect a true comparison as one would expect it to be at least equivalent to RI, if not superior with the addition of BD. This result is likely an artefact of the metanalysis as there were only 3 studies where a comparison of all 3 modalities was reported, 1 of which was poor quality.

ICG has the potential to revolutionize the gold standard (RI and BD) for sentinel node biopsy during breast conserving surgery in centres which are unable to use RI and are thus dependent on BD alone. Furthermore, it removes the risks associated with blue dye such as skin tattooing and hypersensitivity (111).

When compared with RI, ICG removes the risks associated with ionizing radiation. It also removes the need for an injection the day prior to surgery (thus eliminating both hospital and patient inconvenience), the need for hospitals to be appropriately built to limit external radiation, comes at a decreased cost, and is safer (111). Furthermore, it eliminates the difficulty of limited sources providing radioisotopes and the associated rapid decay (rapid transport is required as it cannot be stored) (123).

According to the systematic review by Sanidas et al., sentinel node biopsy using BD is much more difficult than with RI (124). However, with ICG, it has the potential to be even easier as one may be able to directly visualise the superficial lymphatics and sentinel node(s) through the skin (125), enabling planning for the incision. However, a possible downside is that if the lymphatics are damaged intraoperatively, ICG might pool in the cavity thus giving a false positive reading.

3.4. Lymphatic Mapping

Lymphoedema is a condition in which there is impaired outflow of the protein rich fluid found in the interstitial space into systemic circulation (126). In the case of breast cancer, it is often caused by the resection of the lymph nodes, but it can also be caused by radiation to the axilla (126, 127). It is most commonly associated with 19.9% axillary clearance procedures but can also occur in 5.6% of sentinel node resections (127). Clinical symptoms include progressive swelling (with accompanying redness or skin thickening) and sometimes pain (127). Current treatments are mostly non-operative (multi-layered bandages, compression sleeves, etc.), however there are some operative options (microvascular surgery, excisional procedures, drainage, etc.) (128). In microsurgery, one such option is the LYmphatic Microsurgical Preventive Healing Approach (LYMPHA), whereby a lymphatic-venous bypass is created in blocked lymphatic vasculature (129). However, in order to formally diagnose and attempt to treat lymphoedema, surgeons need to visualise the lymphatic system.

6 studies reported on lymphatic mapping **(Table 3)** (115, 122, 130, 131, 132, 133). All used ICG, however 1 study combined it with radioactive tracer (115) and 2 studies combined it with radiotracer tracer and/or blue dye (132, 133). 5 studies injected ICG intraoperatively (122, 130, 131, 132, 133), only Polom et al. administered it pre-operatively (115). However, success of this technique was not reported consistently thus comparison between studies was not possible. In the 5 studies where detectability was reported, it ranged from 73-100% (115, 122, 131, 133, 134). 3 studies compared whether there were single or multiple lymphatic pathways with detection rates varying from 21-86% and 42-93% respectively (131, 132, 133). Interestingly, Ogasawara reported that in 21/37 cases there was no lymphatic drainage from the tumour (133). Lastly, 2 studies compared the configuration of the lymphatic vessels themselves, either

describing the individual lymphatic vessels (as tortuous or normal) or the overall configuration (as single or multiple channels) (122, 132).

In conclusion, visualisation of lymphatic pathways with ICG is possible, thus making microsurgery such as LYMPHA a prospect.

Paper	Method	Number of Patients	Dyes	Time Dye Administered	Injection Site	Detectability	Single Path	Multiple Paths
Guo 2014 (131)	RCT	36	ICG	start of operation	sub-areolar	35/36 (97%)	31/36 (86%)	15/36 (42%)
Hirche 2011 (134)	Feasibility study	46	ICG	start of operation	sub-areoalar	45/46 (98%)	N/A	N/A
Hojo 2010 (132)	NRCT	113 + 28	ICG + BD or RI	start of operation	sub-areolar and tumour skin	N/A	29/141 (21%)	131/141 (93%)
Meric-Bernstam 2014 (122)	NRCT	20	ICG	start of operation	4x intraparenchymal, 1 sub-areolar, 7 arm	20/20 (100%)	N/A*	N/A*
Ogasawara 2008 (133)	NRCT	37	ICG + BD +/- RI	start of operation	peri-areolar and tumour skin	27/37 (73%)	25/37 (68%)	20/37 (54%)
Polom 2012 (115)	NRCT	21 + 28 49	RI+ICG/ICG-albumin	pre-operatively	tumour skin	47/49 (96%)	N/A	N/A

Table 3: Lymphatic Mapping Using NIRF.
*configuration of lymphatics were: 12 normal, 6 sternal, 2 tortuous, and 1 dense network

3.5. Tumour Identification

As per **Table 4**, 17 studies were published regarding the use of fluorophores in identifying breast cancer intraoperatively. These studies were used to determine which fluorophores would be assessed in this work.

2 studies assessed endogenous fluorophores potentially related to tumorigenesis, namely NADH, flavin, and collagen. NADH and flavin tend to be increased in malignancy due to the increased metabolic rate, whereas collagen tends to be decreased due to tumour enzymes degrading the matrix encouraging invasion (108, 135). These demonstrated a sensitivity and specificity of 70-85% and 84-92% respectively (108, 135).

3 studies assessed ICG in breast cancer (44, 90, 136). However, 2 of these studies had too few patients, Intes with 3 (136), and Veys with 9 (44). In the study by Pop et al., (90) which looked at a cohort of 52 patients, the sensitivity and specificity of ICG for breast tumour tissue was low (33% and 74% respectively).

It could be presumed that MB would have a similar profile to ICG given their similar mechanism of action (EPR effect). Whilst there are 2 studies that evaluated MB (48, 137), they did not report sensitivity nor specificity for breast cancer tissue.

3 studies assessed bevacizumab800, 1 of which trialled various doses of the agent (78, 79, 80). Overall, this fluorophore which targets vascular endothelial growth factor (VEGF) receptors has relatively high sensitivity and specificity (88-98% and 79-89% respectively) (78, 79, 80).

2 studies investigated LUM015. The first study by Smith et al. assessed varying doses of LUM015 (which is cathepsin activated) and found that there was a signal in the 10 patients who received the drug (93). However, 50% of patients had positive margins on specimen processing (50% sensitivity, 50% specificity). Following on, the team's recent RCT included 406 patients, margin analysis reported a sensitivity of 49% and specificity of 85% , with a negative predictive value of 98% (138).

There were a further 2 small scale studies looking at targeted fluorophores. The study by Park et al. used PM700 and PM800 which target calcium deposits (a hallmark of DCIS) and was performed on 10 *ex-vivo* specimen and did not report sensitivity and specificity (47). Lastly, the study by Tummers et al. explored EC17 which targets folate receptors (46). These receptors are overexpressed in 30% of BC but 86% of triple negative breast cancer (TNBC) (87, 139). Although sensitive in all 3 patients, it did not provide an adequate TBR as it emits at the same wavelength (520-530nm) as breast tissue autofluorescence (46). As per **Table 1**, OTL38 also targets folate but works at a higher wavelength (776-796nm) (97, 98). It has not yet been trialled in breast cancer, however as it does not have any overlap with breast tissue autofluorescence, it could potentially permit an adequate contrast between tumour and normal tissue.

Fluorophores suche as ABY-029 (62, 63), cetuximab-IRdye800 (62, 85, 86), and panitumab-IRdye800 (62, 99) could prove useful as they target EGFR, a receptor commonly overexpressed in solid tumours. EGFR has been reported to be overexpressed in up to half of triple negative breast cancers (TNBC) and inflammatory breast cancers (140).

Paper	Method	Patients	Camera	Contrast Agent	Target	Excitation	Emission	Timing	Formula	TBR	ID	Sn (%)	Sp (%)	FNR (%)
Breslin 2004 (135)	cohort	56 (tissue)	Skinscan	N/A	endogenous	300nm-460nm	300-600nm	N/A	N/A	N/A	N/A	70	91.70	30.0
Dintzis 20 (82)	CT (phase 1)	11	SIRIS	6mg BLZ-100	N/A	750nm	>800nm	1-26 pre-op	IV	N/A	N/A	N/A	N/A	N/A
	CT (phase 1)	12	SIRIS	12mg BLZ-100	N/A	750nm	>800nm	1-26 pre-op	IV	N/A	N/A	N/A	N/A	N/A
Intes 2003 (136)	cohort	3	custom made	0.25mg/kg ICG	EPR effect	805nm	830nm	0-10 min	IV	N/A	N/A	.2/2	N/A	0
Lamberts 2016 (80)	CT (phase 1)	20	custom made	4.5mg bevacizumab800	VEGF receptors	778nm	795nm	3d pre-op	IV	N/A	N/A	N/A	N/A	N/A
Koch 2017 (78)	pilot cohort	19	EagleRay-V3	4.5mg bevacizumab800	VEGF receptors	N/A	investigated	3d pre-op	IV	1.8-9	?100%	98	79	2
Koller 2018 (79)	CT	3/26	SurgVision	4.5mg bevacizumab800	VEGF receptors	N/A	800nm	?>1h pre-op	IV	N/A	N/A	88	89	12.5
	CT	10/26	SurgVision	10mg bevacizumab800	VEGF receptors	N/A	800nm	N/A	IV	1.8	N/A	88	89	12.5
	CT	10/26	SurgVision	25mg bevacizumab800	VEGF receptors	N/A	800nm	N/A	IV	3.1	N/A	88	89	12.5
	CT	3/26	SurgVision	50mg bevacizumab800	VEGF receptors	N/A	800nm	N/A	IV	N/A	N/A	88	89	12.5
Park 2018 (47)	retro NR SC	10 (tissue)	mini-FLARE	PM700 + PM800	Calcium	514nm, 785nm	700nm, 800nm	N/A	N/A	N/A	N/A	N/A	N/A	N/A
Ottolino-Perry 2021(101)*	CT (phase. 2)	15	PRODIGI	15mg/kg 5-ALA	Haeme metabolism	405nm	N/A	2-4h pre-op	oral	NA	N/A	N/A	N/A	N/A
	CT (phase 2)	15	PRODIGI	30mg/kg 5-ALA	Haeme metabolism	405nm	N/A	2-4h pre-op	oral	NA	N/A	N/A	N/A	N/A
Pop 2019 (90)	cohort	52	N/A	0.25mg/kg ICG	EPR effect		700nm, 800nm		IV	1.4 +/- 0.6	N/A	33	73.90	N/A
Pu 2013 (108)	retro NR SC	38 (tissue)	Perkin-Elmser	N/A	endogenous	340nm	342-525nm	N/A	N/A	NA	N/A	*collagen vs NADH 85% Sn, 85% Sp		
Smith 2018 (93)*	CT	5	LUM imaging system	*control	cathepsin activate	630nm	700nm	N/A	N/A	2.1	N/A	N/A	N/A	N/A
	CT	5	LUM imaging system	0.5mg/kg LUM015	cathepsin activate	630nm	700nm	2-6h pre-op	IV	4.7 +/- 1.2	.5/5	100	N/A	0
	CT	5	LUM imaging system	1mg/kg LUM015	cathepsin activate	630nm	700nm	2-6h pre-op	IV	4.2 +/- 1.0	.5/5	100	N/A	0
Smith 2023 (138)	RCT	406	LUM imaging system	1mg/kg LUM015	cathepsin activate	N/A	N/A	N/A	IV	N/A	N/A	85	49	N/A
Tummers 2014 (48)	CT	2	mini-FLARE	1.0 mg/kg MB	EPR effect	670nm	700nm	3h pre-op	IV	2.5 +/- 0.9	83%	N/A	N/A	17.0
Tummers 2016 (46)	cohort	3	Artemis	0.1mg/kg EC17	folate receptor	490nm	500nm	N/A	IV	.2/3	.3/3	100	N/A	N/A
Veys 2018 (44)	cohort	9	N/A	0.25 mg/kg ICG	EPR effect	N/A	N/A	N/A	IV	3.3 +/- 1.7	NA	NA	31.70	5.8

Unkart 2017 (76)	CT (phase 1)	6 (27)	not specified	AVB620**	matrix metalloproteinases	NA	NA	2-20h pre-op	IV	0.7	NA	NA	N/A	N/A
Zhang 2019 (137)	cohort	3	not specified	0.5mg/kg MB	EPR effect	668nm	N/A	3h pre-op	IV	N/A	failed	NA	N/A	N/A
		9	not specified	1mg/kg MB	EPR effect	668nm	N/A	3h pre-op	IV	0.5	1.58+/-0.36	NA	N/A	N/A

Table 4: Breast Conserving Surgery using Fluorescent Guidance.
*These studies were identified after the initial systematic review on which the feasibility trials were based. However, for the purpose of this thesis they have been included.
**1, 2, 4, 8, 16mg of AVB-620 trialled in 15 patients (3 patients per dose) for safety, expansion cohort of 12 patients used 8mg dose split into 2 groups based on timing of administration, 1 group was administered AVB-620 the day before surgery and the other group was given it on the day of surgery. (141)

However, as none of the above fluorophores have proven themselves sufficiently accurate to identify breast cancer, they are not yet able to be adopted into clinical practice. Perhaps a solution will be to administer a combination of multiple fluorophores which will target multiple enzymes or receptors, thereby potentially enabling the tumour to fluoresce in its entirety.

3.6. Limitations

Signal strength often varies and it can be attributed to a many factors such as:

1. Microscopic tumour fragments may provide an insufficient fluorophore concentration to provide an adequate signal.
2. There is great variety in the genotype and phenotype variety of breast cancer (e.g., mucinous adenocarcinoma and mucoepidermoid carcinoma did not fluoresce as well as DCIS or adenocarcinoma) (17, 48).
3. Variety in phenotype makes it unlikely that one receptor/enzyme is present in all types of breast cancer. Furthermore, the expression of said receptors/enzymes is variable.
4. Necrotic tumours may lack the blood supply impeding delivery of the fluorescent agent.
5. Autofluorescence spectra of breast tissue may overlap with that of exogenous fluorophores, thus preventing distinction between tumour and healthy tissue (as was the case with EC17) (46).

This thesis will aim to tackle points 1 through 5. The inadequate signal will be trialled with the sensitivity of our GLOW camera system in Chapter 4. Studying aberrant vasculature with a near infrared fluorophore will address points 2 through 4 in Chapters 5 and 6. A metabolite which is overexpressed within the visible spectrum in all breast cancer cells be investigated in Chapter 7 and address points 2 to 5. This thesis will also address how an increase in intracellular

concentration of that metabolite in combination with camera filter modifications can overcome point 5 in Chapter 8.

3.7. Conclusion

This chapter provided an overview of fluorescent properties in breast cancer. It explained how the autofluorescence provided through the metabolic or structural properties of endogenous fluorophores can be used to distinguish between healthy and cancerous tissue. It went on to explore the various near infrared probes and how they have been trialled in tumour, sentinel node, and lymphatic pathway identification. Although all these applications are 'off-licence', ICG is being increasingly used in sentinel node mapping in centres which are unable to facilitate the sourcing and safety of radioisotopes. Furthermore, ICG is capable of mapping lymphatic pathways after sentinel node resection, thus enabling reconstruction and preventing lymphoedema. This thesis aims to progress FGS integration with BCS through experimenting with novel ideas to improve the accuracy of this technique.

4. Camera Development and *in-vitro* studies using the GLOW camera

In this work, the GLOW camera was trialled *in-vitro* to determine the optimal camera settings. In a controlled laboratory study, we experimented with 3 fluorophores, namely EMI-137, PpIX, and ICG. We assessed the sensitivity of the GLOW camera to the strength of the signal provided at the expected concentration in blood, $1/10^{th}$, and $1/100^{th}$ in various media (phosphate buffer solution, methanol, bovine serum, olive oil, milk). We also compared the efficacy of 2 different camera excitation filters and how it affects the strength of signal of PpIX and EMI-137. Lastly, we compared the GLOW camera to the commercial SPY system.

Maria Leiloglou and Vadzim Chalau built the camera system being assessed. They performed initial experiments with ICG and determined initial camera hardware and software settings. The experiments performed in this chapter performed collaboratively.

The work in this chapter was published in the journal of *Surgical Life: The Journal of the Association of Surgeons of Great Britain and Ireland* (2021) 'Versatility in Fluorescence Guided Surgery with the GLOW Camera System'. It was presented at the *European Molecular Imaging Meeting* (2019) 'Fluorescence Intensity Image Guided Breast Conserving Surgery.'

4.1. The GLOW camera system

The GLOW camera is composed of a xenon light source, dual colour and fluorescent cameras, a beam splitter, and interchangeable lenses and emission filters (**Figure 12**) (38). The light source is modifiable for activating wavelengths customisable for each fluorophore. In the camera system itself, the lens system (A) collects light, and the beam of light is split into 2 (B). Fluorescent light is transmitted through a band-pass filter (C) to the monochrome camera (D). Colour images are captured in the RGB camera (E). The interchangeable lens enables a wide range in working distance and field of view, whereas the interchangeable filters permit customisation of the apparatus for various fluorophores (38). The camera was assessed *in-vitro* to determine optimal camera settings, sensitivity to 3 fluorophores at various concentrations in different media, the maximum depth of signal in tissue, and finally it was compared against a commercially approved system.

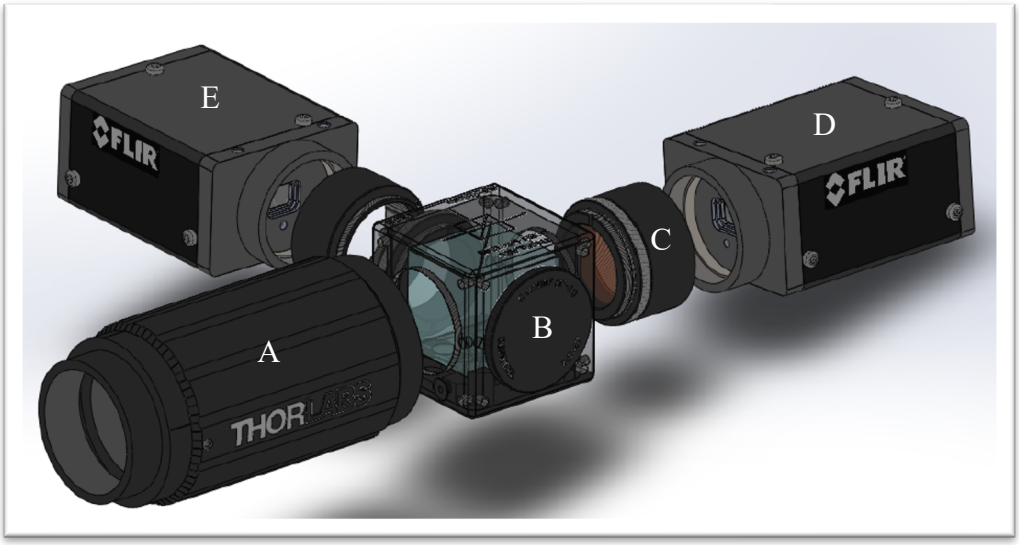


Figure 12: The GLOW Camera.
A) The lens system collects visible and fluorescent light.. B) A beam splitter separates the light into 2 beams. C) Fluorescence is transmitted through a band-pass filter to the D) monochrome camera. E) Colour images are captured in the RGB camera.

4.2. Identifying optimal camera settings

Optimal excitation and emission spectra for ICG is 500-700nm and 775-875nm respectively as identified in the literature (142). This was confirmed through spectroscopic measurements which were obtained *in-vitro* and *ex-vivo* (38). The device was initially studied using aqueous ICG solution (in the range of 1-100 10^{-9} mol) to evaluate the aperture size, focal length, and object distance. With these results, the working distance/ field of view (FOV) was determined and signal to background ratio was calculated (**Figure 13**).

Camera working distances ranged from a minimum of 10cm (with FOV of 3.1x 2.2cm with 40um resolution) up to 56cm (FOV 8.4 x 6.3 cm with 80um resolution) (38). The optimal setting was 30cm working distance (with FOV 6.1 x 4.4) when the system was able to detect features as small as 50um (38).

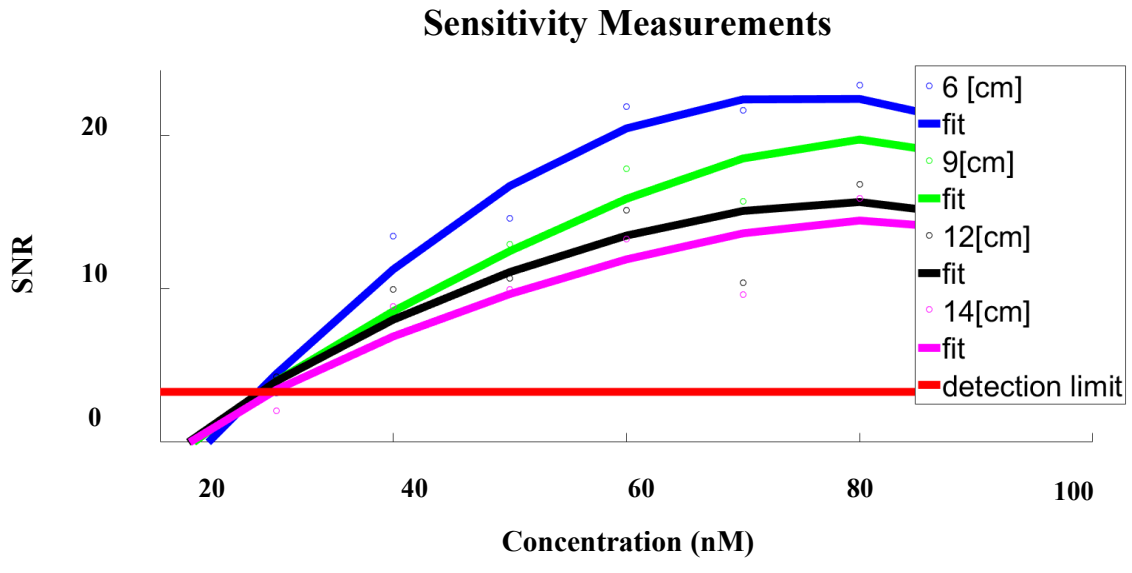


Figure 13: Sensitivity results at various distances using concentration and signal to noise ratio.
This experiment was performed with a lens of 35 mm focal length and f/2.8 aperture. An SNR of 3.28 is the detection limit. Concentrations down to 30 nM can be detected at a frame rate of 40 frames per second [fps].
Note: Image reproduced with the permission of publisher (38).

In this chapter and the following *in-vivo* pilot study, we rapidly prototyped the camera intraoperatively in order to achieve the good quality images with regards to exposure, sharpness, shutter, frame rate, and acquisition time with minimal gain applied.

4.3. ICG spectroscopy in bovine serum

The spectral properties of ICG were assessed using a laboratory spectrofluorometer. ICG was reconstituted to levels expected in blood within bovine plasma. Excitation was measured to be in the range of 400-820nm, with maximum emission at 820nm (143). This falls within optimal spectra as identified in the literature (142).

4.4. Sensitivity of the GLOW camera to multiple fluorophores at varying concentrations in different media

Various concentrations of EMI-137 and PpIX were assessed using 5 different base solutions (methanol, serum, phosphate buffered saline [PBS]) (38). I calculated the expected amount of each solution in the blood of a 70kg female (making the assumption that all ALA was converted to PpIX). I then compared a control sample (of just the base solution) to the intensity of the fluorophore solution expected in blood, $1/10^{th}$, and $1/100^{th}$ of that solution (**Figure 14**).

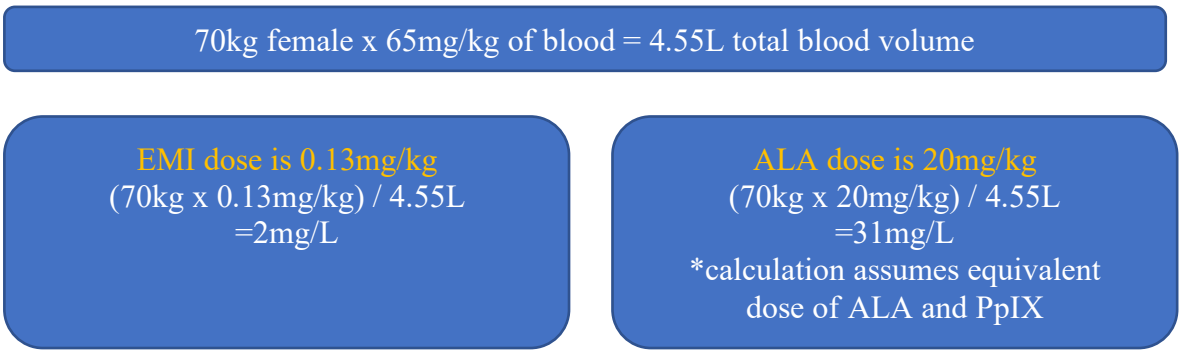


Figure 14: Calculations to calculate concentrations of drugs in blood of average female.
The top calculation is for the amount of blood within the average female body (4.55L). The left is a calculation for how much EMI we can expect in the blood (2mg/L) and the right is for ALA (31mg/L).

4.5. EMI in various media

There was an obvious difference between the signal strength of different concentrations of EMI and PpIX. However, even at the lowest concentration (1/100th of what was expected in the blood) there remained a marked difference between that and the control. This can be observed in **Figure 15**.

Images using milk and olive oil were hyperfluorescent at all concentrations. This is likely due to the high concentrations of endogenous fluorophores present within those media.

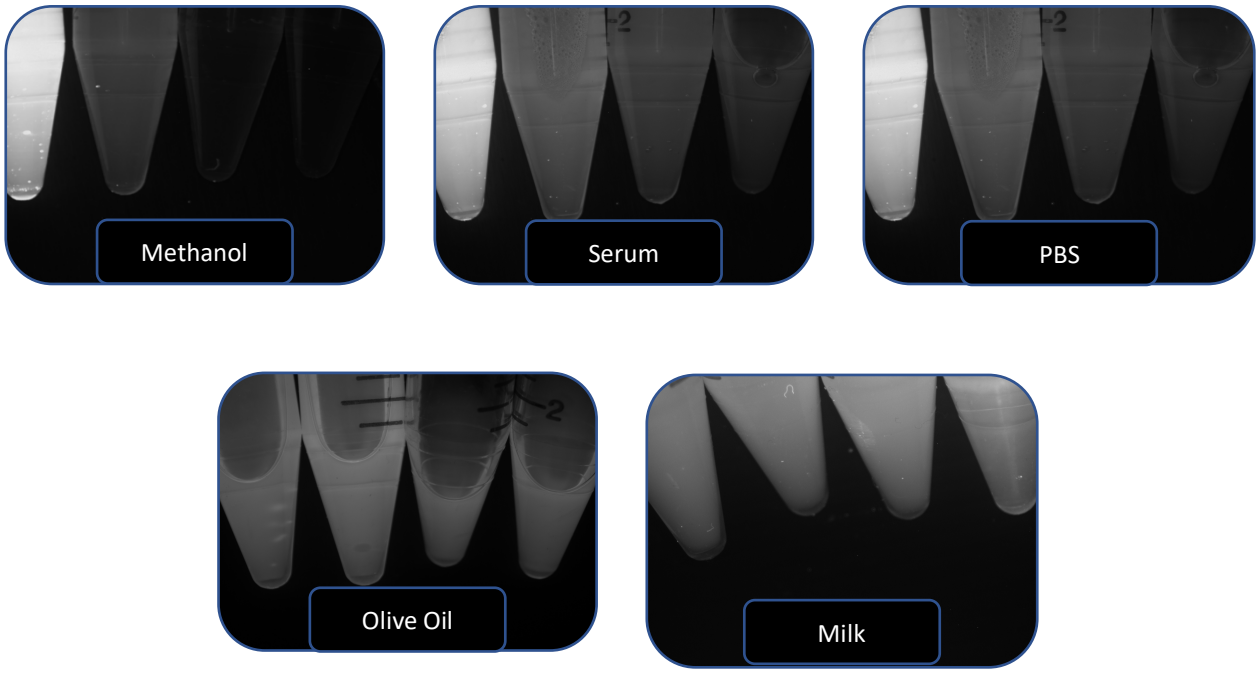


Figure 15: EMI concentrations in various media.
Clockwise from the top left is EMI in methanol, serum, PBS, milk, and olive oil. Within each image, from left to right is the concentration expected in blood, 1/10th of that, 1/100th of that, and a control. Images taken were using the 500-625nm filter (which includes endogenous fluorophores) (38).

4.6. Filter comparisons with PpIX

PpIX has dual excitation wavelengths, 405nm and 635nm, and thus also has 2 respective emission peaks at 635nm and 705nm (144) (**Figure 16**). The excitation wavelength in the violet spectrum offers the highest peak known as the Soret band (400- 450nm) which emits at 635nm (55). This wavelength is highly absorbed by blood (145) and also activates FAD (72). However, there is minimal autofluorescence in breast tissue, as it is composed of mostly fat and connective tissues (71).

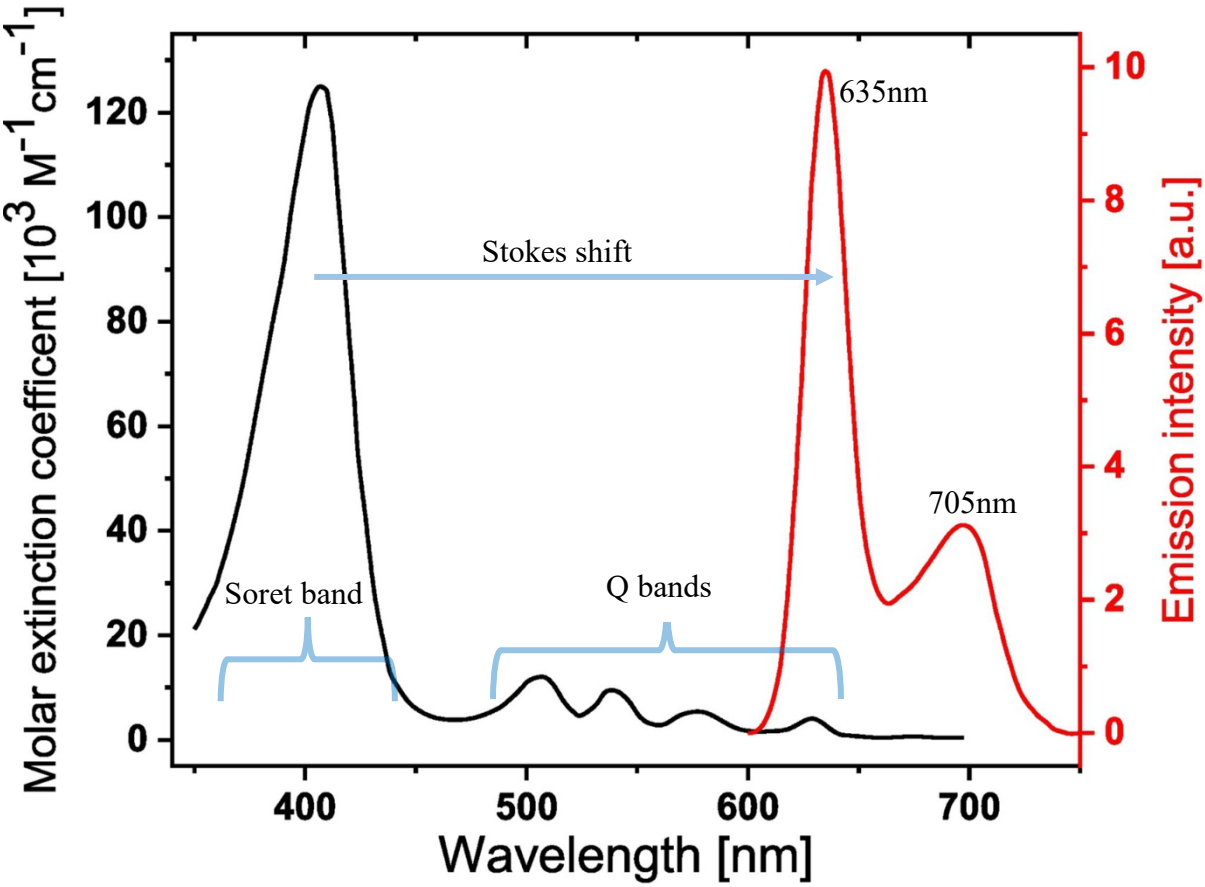


Figure 16: Absorption and emission spectra of PpIX.
PpIX has dual excitation wavelengths, 405nm (also known as the Soret band) and 635nm. It therefore also has 2 emission peaks at 635nm and 705nm respectively.
This image was reproduced and modified with the permission of the publisher. (146)

We examined the signal strength of PpIX using 2 filters (400-625nm and 500-625nm). A single set of images were obtained using varying concentrations of PpIX (concentration in blood, 1/10, and 1/100) dissolved in phosphate buffer solution and bovine calf serum. **Figure 17** displays images from the bovine calf serum experiment.

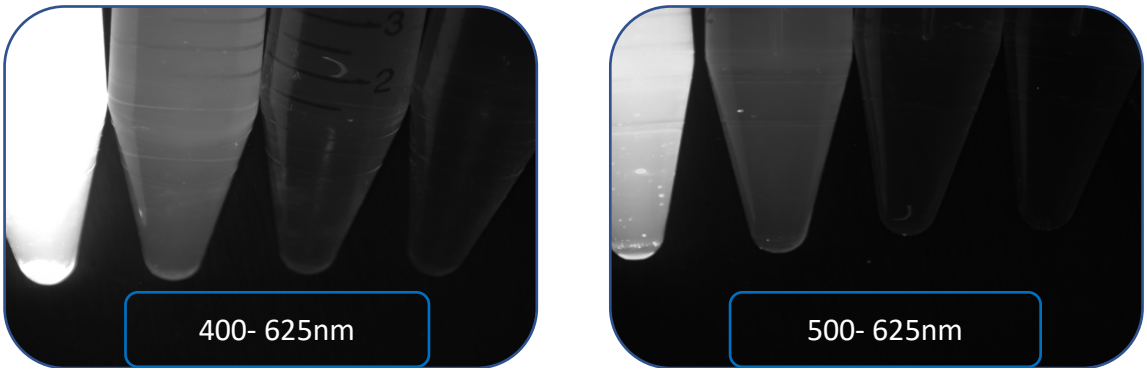


Figure 17: Varying concentrations of PpIX in bovine calf serum with different filters.
From the left to the right of each image is the concentration expected in blood, 1/10th of that, 1/100th of that, and a control. The first column uses an emission filter of 450-625nm, second column uses 500-625nm filter.

The mean of multiple pixels from a region of interest (using the same image taken on the same solution on 1 day) were compared using paired samples t-test. The calculations were performed in Matlab (MATLAB, R2017b, The MathWorks, Inc.). When dissolved in bovine calf serum, paired T-test results demonstrated that there was no significant difference at *in-vivo* concentrations of PpIX between the two filters (38). However, the 400-625nm filter was superior at the 0.1gr/L (p=0.038) and 0.01gr/L (p=0.007) concentrations (38). When dissolved in phosphate buffer solution the 450-625nm filter was superior both the in-vivo concentration (p= <0.0001)and at 0.01gr/L (p=0.018) (38). The calculations and results are demonstrated below in **Table 5**.

Bovine Calf Serum

	Concentration in blood (gr/L)		
Filter	1	0.1	0.01
450- 625nm SBR	109 +/- 7.2	132 +/- 32.8	70 +/- 13.4
500- 625nm SBR	120 +/- 14.4	99 +/- 20.7	48 +/- 7.5
Comparison Statistics			
StD	4.04	1.32	3.21
Pooled StD	11.38	22.278	10.83
T experimental	-1.6	2.31	3.17
T critical (for 0.05 significance)	1.86	1.86	1.86
***p-value* of t-test**	**0.074**	**0.038***	**0.007***

Phosphate Buffer Solution

Filter	Concentration in blood (gr/L) in Phosphate Buffer Solution		
	1	0.1	0.01
450- 625nm SBR	119 +/- 2.4	27 +/- 3.5	5 +/- 0.7
500- 625nm SBR	76 +/- 5.3	22 +/- 5.6	3 +/- 1.5
Comparison Statistics			
StD	2.38	2.56	4.30
Pooled StD	6.84	4.68	1.21
T experimental	10	1.74	1.86
T critical (for 0.05 significance)	1.86	1.86	1.86
***p-value* of t-test**	**<0.0001***	**0.06**	**0.018***

Table 5: T-test for PpIX in bovine calf serum and phosphate buffer solution.
SBR= signal background ratio, StD= standard deviation. SNR +/- StD for the two different filtrations combinations and corresponding p-values of the t-test comparisons for different solvent and PpIX concentrations. All *p*-values <0.05 indicated with a * are of statistical significance, showing that parts of the Soret band could be potentially useful for excitation despite overlap with autoflluorescence.

4.7. Experiment in *ex-vivo* tissue

The depth at which PpIX could be detected was interrogated by injecting 0.1mL of PpIX (at the expected blood concentration) at increasing 1mm intervals until it could no longer be detected. The maximum depth which could be detected was 5mm from the surface (38), as demonstrated in **Figure 18**.

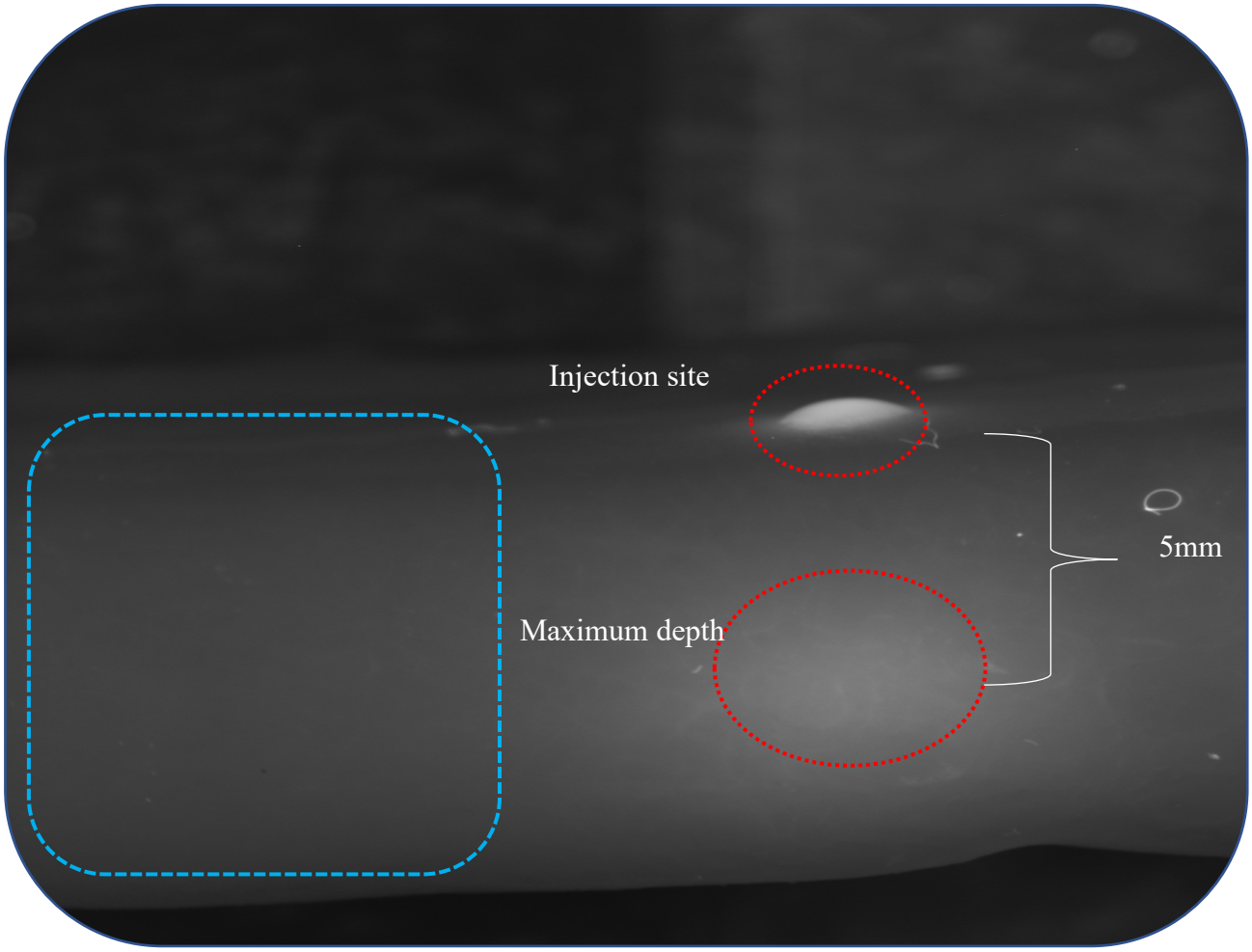


Figure 18: Infrared image of an *in-vitro* experiment using porcine tissue.
In this experiment, PpIX was injected into the tissue in 1mm increments. The red dotted ellipse on the top right is at the injection site where the concentration was highest thus brightest. The red dotted ellipse on the bottom right is at 5mm depth and is exhibits a dimmer signal that could still be differentiated from the normal tissue within the blue dotted square. We were unable to obtain signal past 5mm depth.

4.8. Comparison to the SPY™ commercial system

The GLOW camera then underwent comparative testing with the commercial SPY™ (Novadaq Technologies, Toronto, Canada) to evaluate whether it was ready to be used in *in-vivo* feasibility trials. Varying concentrations of ICG were assessed for fluorescence intensity as seen by the 2 different camera systems (**Figure 19**).

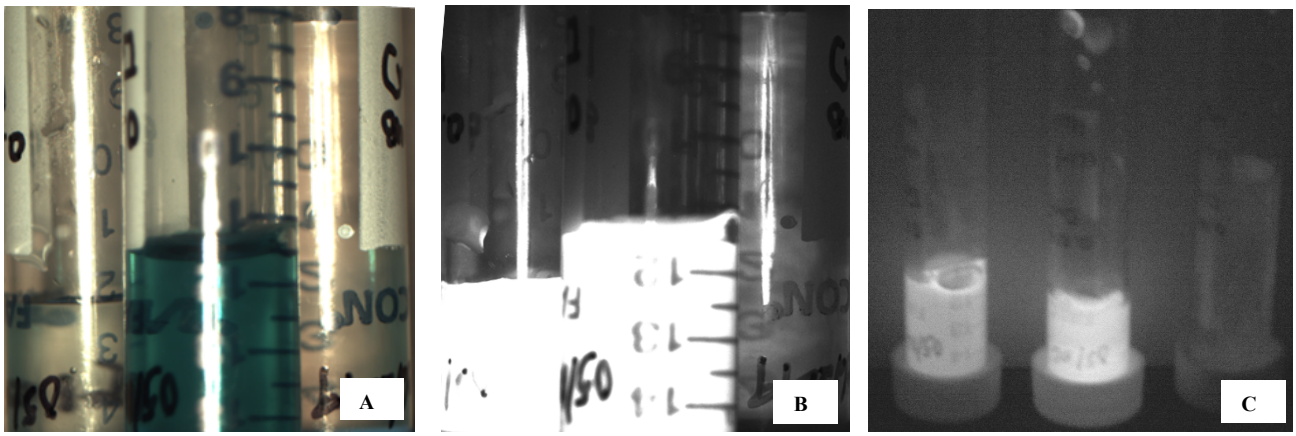


Figure 19: Different Concentrations of ICG as seen via the GLOW camera and commercial system.
A) The Red Green Blue Camera visualisation of the 3 different concentrations of ICG. B) Those vials as seen using the Fluorescence Imaging Camera as compared to C) SpyPhi camera. The middle vial has a concentration equivalent to what we would expect to find in blood during *in-vivo* testing (0.00645 mM). The left vial has been diluted to a concentration of 1/10th of what we would expect to have *in-vivo* (0.000645mM). The right vial has been diluted to a concentration of 1/100th of what we would expect to have *in-vivo* (0.0000645). The far-right vial shows some fluorescence in image B, but none in C.

Compared to the GLOW camera system (Imperial College London, London, United Kingdom), the SPY™ camera proved easier to use, accommodated for various working distances, and already had the image overlay algorithms built into the display system. Contrarily, the GLOW camera system worked best at approximately 20cm from the sample, and only displayed raw image data (38). However, the GLOW camera was more sensitive to lower concentrations of ICG (**Figure 20)** (38). That being said, the sensitivity to ICG is clinically irrelevant given that both are capable of detecting it at expected blood levels.

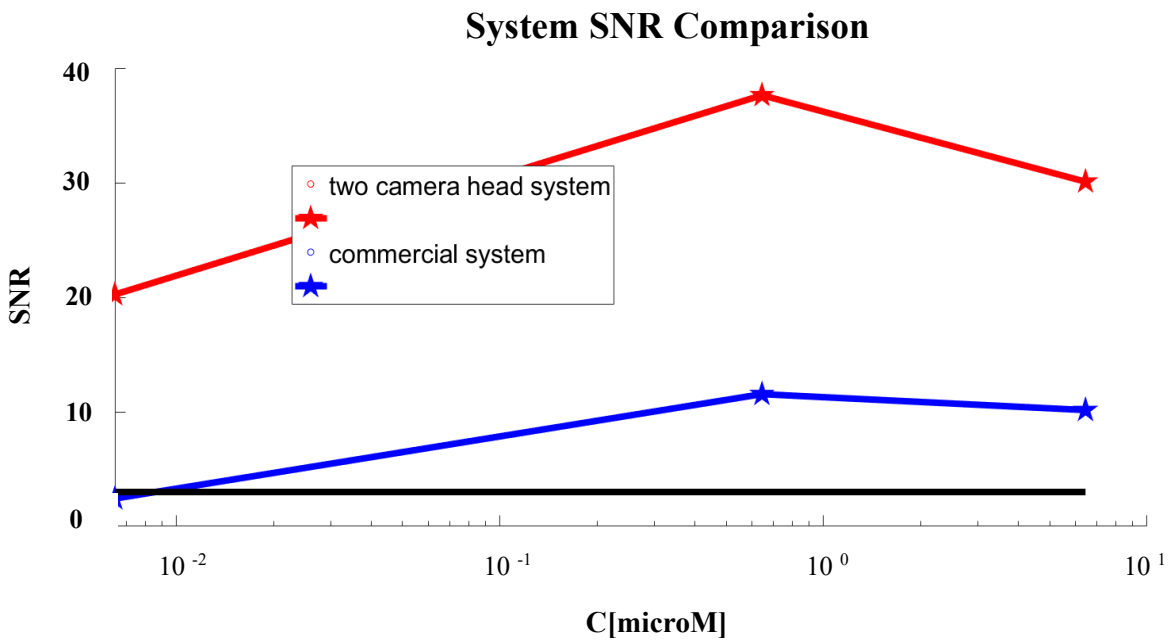


Figure 20: Comparing signal noise ratio (SNR) between the GLOW camera and commercial system. Images of excised lumpectomy specimen as seen through RGB and NIRF camera, as well as overlay image provided as feedback after software processing with LabView.

Through this comparative testing, we determined that our prototype was not inferior to the SPY^{TM} system with regards to sensitivity, and ready for trials *in-vivo*. However, rapid prototyping would be required in order to improve user friendliness, limit intraoperative disturbance, and develop software for real-time intraoperative feedback.

4.9. Conclusion

In this work, the GLOW camera was trialled *in-vitro* in various controlled laboratory studies. We determined that the GLOW camera was capable of detecting concentrations as low as 1/100th of blood in methanol, phosphate buffered solution, and bovine serum. We also identified that the 400-625nm camera filter was superior to the 500-625nm filter, which will be further explored in chapter 6 of this thesis. Lastly, we found that although the GLOW camera was inferior in useability, the sensitivity was comparable to that of the commercial SPY system.

5. The *in-vivo* pilot trial with ICG

This chapter involves trialling the GLOW camera *in-vivo*. In this feasibility study, we used indocyanine green (ICG), which was previously used in the *in-vitro* camera studies, to determine camera function *in-vivo*. ICG is a fluorophore which is clinically approved in other applications, and capitalising on the passive targeting of tumour tissue.

We investigated whether:

a) the camera functioned *in-vivo*

b) whether it could be incorporated into the workflow of the operation, and

c) if there was anything worth investigating further with this fluorophore.

Maria Leiloglou was responsible for creating the protocol and gaining ethical approval. I was responsible for recruitment and gathering of metadata. Maria Leiloglou and Vadzim Chalau assisted with intraoperative camera usage. I marked the images for tumour or healthy tissue, after which Maria Leiloglou compared them against clinicopathological data. Using this, Maria Leiloglou performed a power calculation to determine the number of patients needed for the subsequent study. All of us contributed equally to the research paper 'Tissue texture extraction in indocyanine green fluorescence imaging for breast-conserving surgery'.

The work in this chapter was published in the *Journal of Physics D: Applied Physics* in (2021) 'Tissue texture extraction in indocyanine green fluorescence imaging for breast-conserving surgery'. It was presented at the *American Society of Breast Surgeons Symposium* (2020) and the *Imperial Surgery & Cancer Department Afternoon* (2019) 'First in Human Study Using the 'GLOW' Near Infrared Camera System in Breast Cancer', the *London Surgical Symposium*

(2019) ‘GLOW: Guiding Light to Optimise Wide Local Excisions’ and in (2020) ‘Fluorescence Guided Surgery Using Indocyanine Green to Demarcate Vasculature in Breast Cancer’, the *Imperial Confidence in Concept* (2019) ‘Fluorescence Image Guided Surgery in Breast Cancer using the Imperial Camera System’, and at the *Imperial Graduate School PhD Summer Showcase* (2019). ‘Visualising the Invisible: A Fluorescence Imaging System for Cancer Surgery Guidance’.

5.1. Summary of ICG

ICG is a clinically approved fluorophore utilised to assess (147):

- Cardiac function (cardiac output, stroke volume)
- Circulating blood volume
- Cerebral perfusion
- Liver function (blood flow, excretory function)
- Perfusion of choroid (in the eye)

Anything outside of these uses is experimental. We attempted to use it in breast tumours.

As described in chapter 1, ICG is a passive fluorophore which is presumed to target cancerous tissue via the enhanced permeability and retention effect. This means that it targets cancerous tissue due to the compromised vascular architecture and impaired lymphatic outflow present in tumours. This therefore allows the ICG to passively ‘leak’ into the tumour, thus causing the tumour to fluoresce. It behaves in the infrared spectrum, with an absorption of 800nm and emission peak at 830nm *in-vivo* (147).

5.2. Prior studies using ICG

There were three studies previously undertaken using ICG, summarised as follows:

- Pop et al., 2019 (abstract only) (90):
    - Fluorescence imaging *in-situ* and of fresh specimen
    - 15 classified as hyperfluorescent + 40 nonfluorescent, resulting in:

        Sensitivity (Sn) 33.3% (3/9), Specificity (Sp) 73.9 % (34/46),

        Negative Predictive Ratio (NPR) 85 % (34/40)
- Veys et al., 2018 (44):
    - Fluorescence imaging of patients with neoadjuvant chemotherapy (NACT)
    - Only 9 specimens from which acquired 172 samples. 52 malignant + 120 benign.
    - Sn 94.2%, Sp 31.7%, NPR 92.7%, False Negative Ratio (FNR) 5.8%, False Positive Ratio (FPR) 68.3%
- Poellinger et al., 2011 (148):
    - Optical tomography (not FGS) of 13 malignant cases
    - subjective analysis of specimen processed as whole
    - Angiography timing (vascular imaging immediately prior to resection) Sn=50-67% + Sp 75-80%
    - EPR (delayed imaging of 'leak' into tumour) Sn= 75- 85% + Sp 62-92%

5.3. The pilot study

The pilot study undertaken was entitled 'Development and validation of an optical imaging system for Intraoperative Near Infrared Fluorescence guidance in breast cancer tumour

resection and reconstructive surgery (50, 143). This preliminary work by Maria Leiloglou (in partnership with myself and Vadzim Chalau) combined the Imperial camera with indocyanine green (ICG) and assessed the protocol, hardware, software, and clinical feasibility for integration of the camera system within the operating room (50, 143).

5.4. Protocol

In this research ethics committee (REC) approved single site feasibility trial (REC 18/LO/0218), 10 patients were included. Each patient was administered 12.5mg of ICG, which corresponds to the dose given to a 50kg woman (using 0.25mg/kg ICG). ICG was given intravenously just before resection of the tumour, illuminating the vasculature (angiography phase) (143). It is worth noting that ICG is effective and has a sied effect profile at doses between 0.1-0.5 mg/kg (147).

During the operation, images were captured of the tumour *in-situ* once skin flaps were raised. After tumour resection, images of the *in-vivo* cavity were acquired. Following this, whist the operation continued, images of the anterior and posterior aspects of the *ex-vivo* specimen were obtained concurrently. In the first 3 patients, rather than acquire *in-situ* and cavity images, instead a video was used to record the site of the operation from the time of injection and for the following 2 minutes (i.e. the half-life of ICG). The remainder of the surgery and patient care was as per standard (143).

Metadata gathered for analysis included**:**

- Patient Demographics (age, BMI, ethnicity)

- Surgery Performed (BCS +/- SNL +/- ANC)
- Cancer details (type, hormonal status, stage, size)
- Operation and Imaging details (type of operation, time of knife to skin, time of injection, time of imaging, etc.)
- Positive margin rate and reoperation rate

Images captured were of all sides of the specimen (anterior, posterior, medial, lateral, superior, inferior).

Effectiveness of camera incorporation into surgical workflow was assessed. This included: ease of use, camera manoeuvrability, ability to identify the target lesion, and the software with regards to capturing and storing the images.

Images were marked using specimen mammography to determine tumour site, and histopathology was used to mark healthy tissue. Lastly, the marked images underwent pixel-based processing to calculate TBR using texture metrics.

5.5. Results

5.5.1. Patient data

10 patients were recruited over 6 months. Mean age was 56 years (range 15-70) and mean BMI of 42.2kg/m^2 (mean 19.2- 30.2). 8 patients had IDC, 5 with concomitant DCIS, 1 had ILC with DCIS, and 1 had invasive mucinous carcinoma. 90% were ER positive, 70% PR positive, and 10% HER2 positive. There were no adverse events.

5.5.2. Image capturing interface

During this trial, the software and hardware were rapidly prototyped throughout (**Figure 21**). The software itself proved unreliable and 4 cases were lost due to the system crashing mid-operation. The interface also included the path for folder where the image would be saved, however the folder and the file path name had to be manually created so that one would know what the image was of (and if *ex-vivo* what side was being imaged). Various imaging settings (e.g. acquisition time, frame rate, gain) would have to be selected and then the image captured by clicking a separate button, thus requiring 2 people for operation.

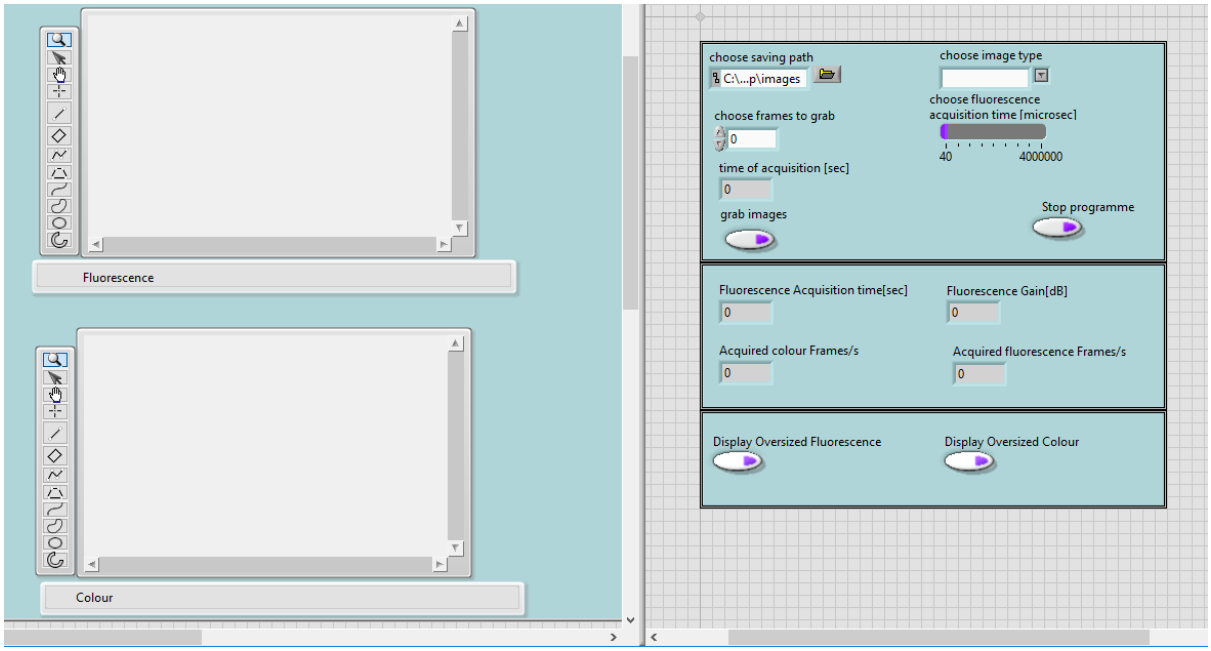


Figure 21: Second **iteration of software interface**.
The left half of the image is the display of the fluorescence (top) and colour (bottom) camera images. The right half, from the top to bottom, includes: the saving path, image type, frame amount, acquisition time, 'get images'(capture), stop programme, fluorescence acquisition time (sec), fluorescence gain (dB), acquired colour frames/s, acquire fluorescence frames/s, and options for the display size for both fluorescence and colour images. The saving path had to be manually created in advance, and then re-entered using the tab on the top left (e.x. images>patient 1> *ex-vivo*>anterior). This was then further reiterated by the 'choose image type' button where the options were tumour *in-vivo*, specimen, and cavity.

Furthermore, it was difficult to position the camera in order to capture the desired image, despite the user interface displaying both colour and infrared images. Additionally, the colour camera defaulted to an oversized image as compared to the infrared, which required an extra step to adjust them to both be the same size. This resulted in the device being cumbersome, not user-friendly, and requiring multiple people for usage. All of these factors contributed to prolonging the operation time by about 15 minutes. Thus, the prototype proved difficult to be integrated into clinical workflow (143).

5.5.3. Image processing

Only anterior and posterior *ex-vivo* specimen images were able to be processed**.** Orientation of the specimen was done as per normal breast surgery proceedings- short stitch superior (1 staple), long stitch lateral (2 staples). These images were marked using GNU Image Manipulation Programme (GIMP) for what constituted true tumour and true normal tissue. True tumour was established using mammography and true normal was based on the histological reports (**Figure 22)**. 20 images were attained from the 10 patients recruited (anterior and posterior views) (143). From those, only 5 image sets were of use as the tumour was potentially superficial enough to be detected (maximum depth of <4mm) (143).

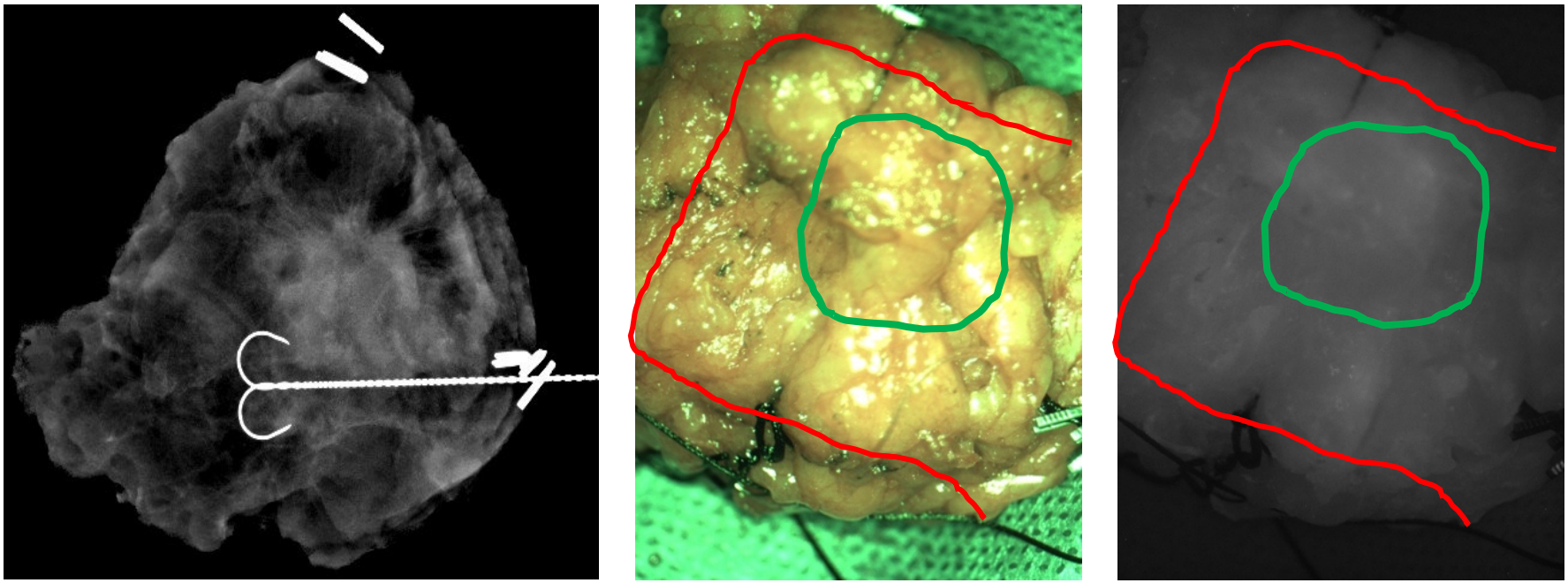


Figure 22: Marking images of the specimen.
Specimen orientation was with sutures and staples (short superior and 2 staples, long lateral and 3 staples). Left image is of the specimen mammography in a patient where wire guidance was used. Middle imaged is the marked colour image. Right is the marked IR image. The mammography was used to mark the colour and IR images for tumour (green circle). Histopathology was used to mark the colour and IR images for normal tissue (everything outside of the red line).

The camera's resolution was able to detect changes at a submillimetre scale, as demonstrated in **Figure 23**.

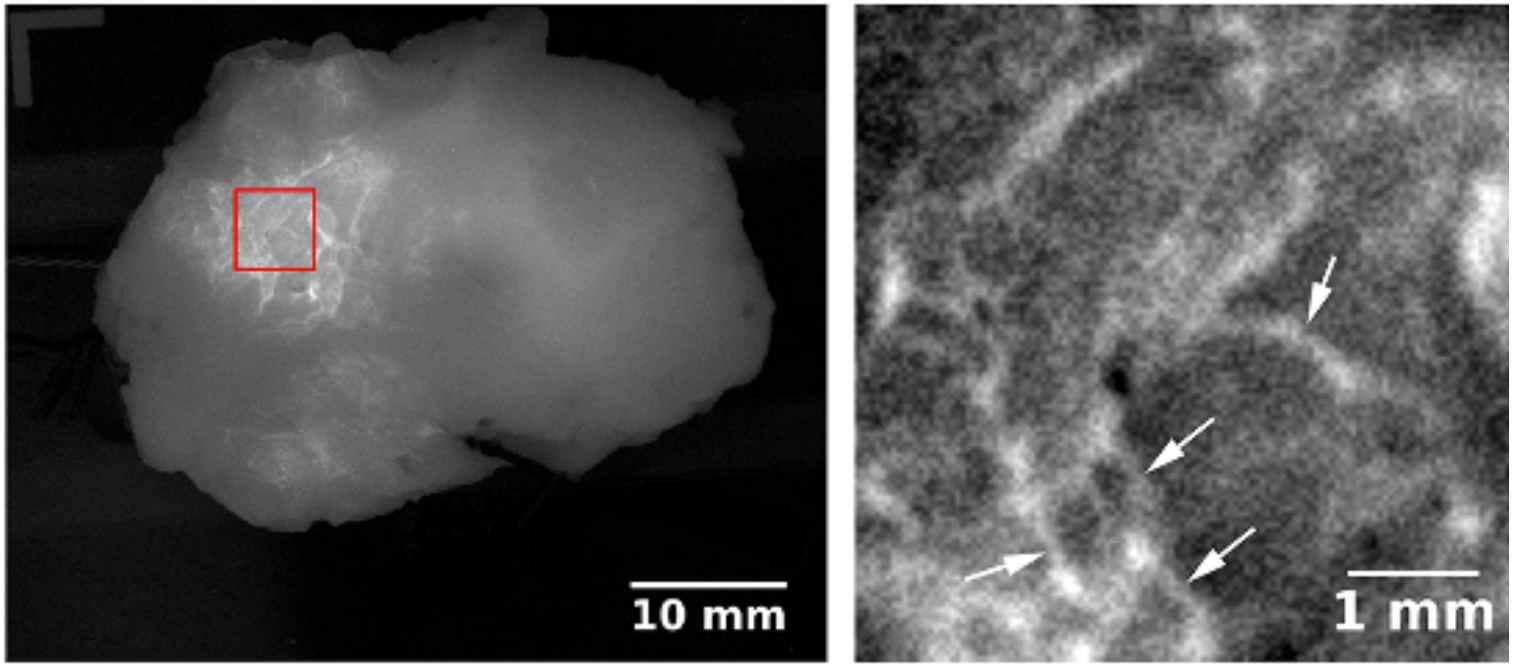


Figure 23: Infrared image of abnormal vasculature in *ex-vivo* specimen.
The right image is a ten-fold enlargement of the red box on the left.
Image reproduced with permission from publisher (143).

TBR was calculated to be 1. However, in 2 patients there was abnormal vascularity in the region of the tumour (**Figure 23**), therefore texture analysis was performed (143). Using texture metrics, an algorithm was created to automatically differentiate between tumour and normal tissue. These images were then segmented into square shaped regions in order to extract texture metrics. Pixel-based processing involved the subdivision of the image into 64x64 pixels marked in true tumour and true normal. As this generated more data points, it was more precise than image-based processing. Pixel-based processing also took into account any particularly bright or dark pixels, so cases in which blue dye was used (for sentinel node navigation) and any paint artefact on histopathology cut-up needed to be excluded.

The results of that were analysed via ROC curve to determine accuracy. The calculation is provided below in **Figure 24**.

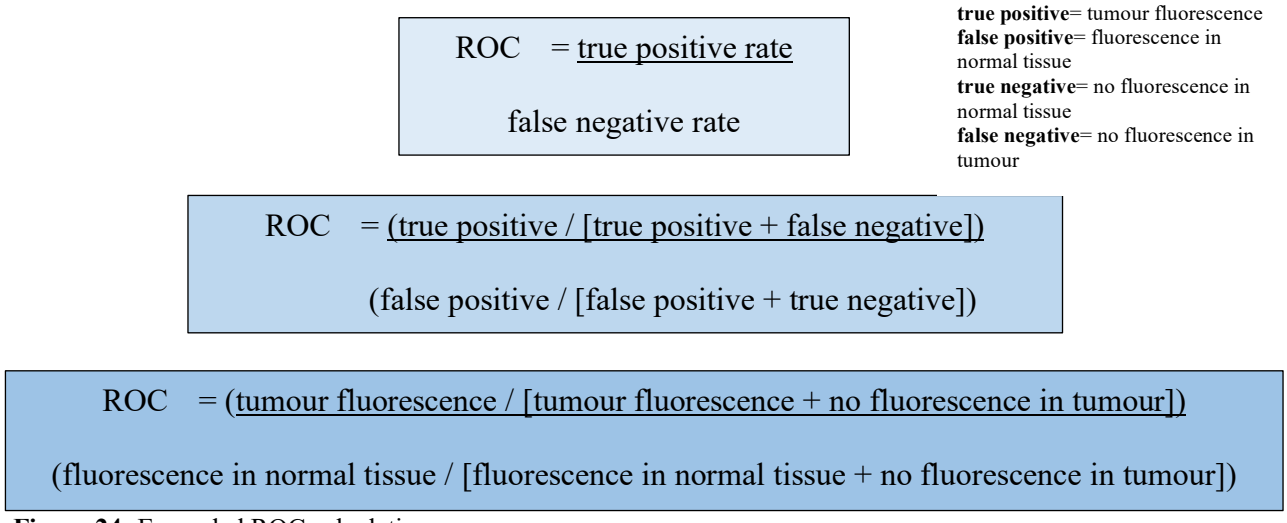


Figure 24: Expanded ROC calculation

The using area under the receiver operating characteristic curve (AUROC) was plotted using logistic regression (LR) and support vector machine learning (SVM). LR was used to identify

a binary outcome for each pixel (either healthy or tumour), whereas SVM identified the decision boundary (with the nearest data points from each class) for optimal classification. Texture metrics including Euler number, fractal dimension, and slope and intercept of the power spectral density curves were extracted (**Figure 25**).

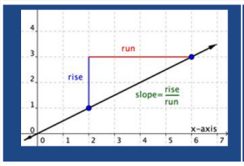
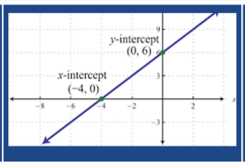
Slope p=0.001	**Intercept** p=0.002	**Euler Number** p<0.001	**Hausdorff box-counting fractal dimension** p=0.38	**Lacunarity** p=0.16
		image connectivity between image features and corresponding holes	change of image pattern detail with scaling	image inhomogeneity

Figure 25: **Texture analysis of images.**
5 texture metrics were applied to our dataset. Only slope, intercept, and Euler number exhibited potentially significant findings (p<0.05).

Therefore, certain texture metrics (slope, intercept, Euler number) could possibly increase sensitivity and specificity of ICG (143).

Using the above 10 patients, a power calculation (next page) was used to determine the number of patients required to correctly reject the nul hypothesis (no difference exists in fluorescence between cancer and normal tissue) when hypothesis is true (there is a difference in fluorescence). This number accounted for data loss from:

- Frequency of positive margins (dependant on successful excision)
- Limited images for analysis (only anterior and posterior aspects of specimen could be used)
- Software/ hardware malfunctions

For the **ratio of sample size ($^{n1}/_{n2}$)**
= 1
(as the number of cancer tissue samples (n1)/ number of healthy tissue samples (n2)) was given all patients had cancer)

-For s**ignificanc**e **(a)** of 0.05
$Z_{1-a/2}$= 1.96 (at a normal distribution of 0.975)
(prevent type 1 error- probability of rejecting difference where one exists)

For **power** (B) of 0.9
Z_{1-B}= 1.28 (at a normal distribution of 0.9)
(prevent type 2 error- probability of correctly rejecting that there is no difference where one exists)

$$\mathbf{n_i} = \frac{(^{n1}/_{n2} + 1)\,(Z_{1-B} + Z_{1-a/2})^2}{^{n/1}/_{n2}(ES^2)}$$

$$= \frac{2 * (Z_{1-b} + Z_{1-a/2})^2}{ES^2}$$

where **ES**= $\frac{\text{(mean fluorescence of healthy tissue- mean fluorescence of cancer)}}{\text{pooled standard deviation}}$

Pooled standard deviation = $\text{Sqrt}\ \frac{(n1-1)s^2/_1 + (n2-1)s^2/_2}{(n1 + n2 - 2)}$

Which was different for each texture metric:
- Euler number ES: 1.65
- Fractal dimension ES: 0.45
- Slope ES: 0.98
- Intercept ES: 0.98

Therefore for final number of samples required:

$$\mathbf{n_i} = \frac{2 * (Z_{1-b} + Z_{1-a/2})^2}{ES^2}$$

- Euler number: 8 samples
- Fractal dimension: 102 samples
- Slope: 22 samples
- Intercept: 21samples

The above power calculation determined that a sample size of 20 patients would be required to assess this theory with statistical significance (with regards to the slope and intercept parameters)(143).

5.6. Spectroscopy with ICG in breast

In 1 of the patients above, ICG fluorescence spectra from the freshly excised specimen were recorded. This comprised 30 spectra of normal tissue and tumor tissue. This was compared with ICG diluted in bovine plasma **(Figure 26**) (143).

In a patient who had not received ICG (the control), breast tissue autofluorescence from 20 spectra were collected from macroscopically normal (connective tissues and fat) and tumour in the freshly excised breast cancer specimen (**Figure 26**) (143).

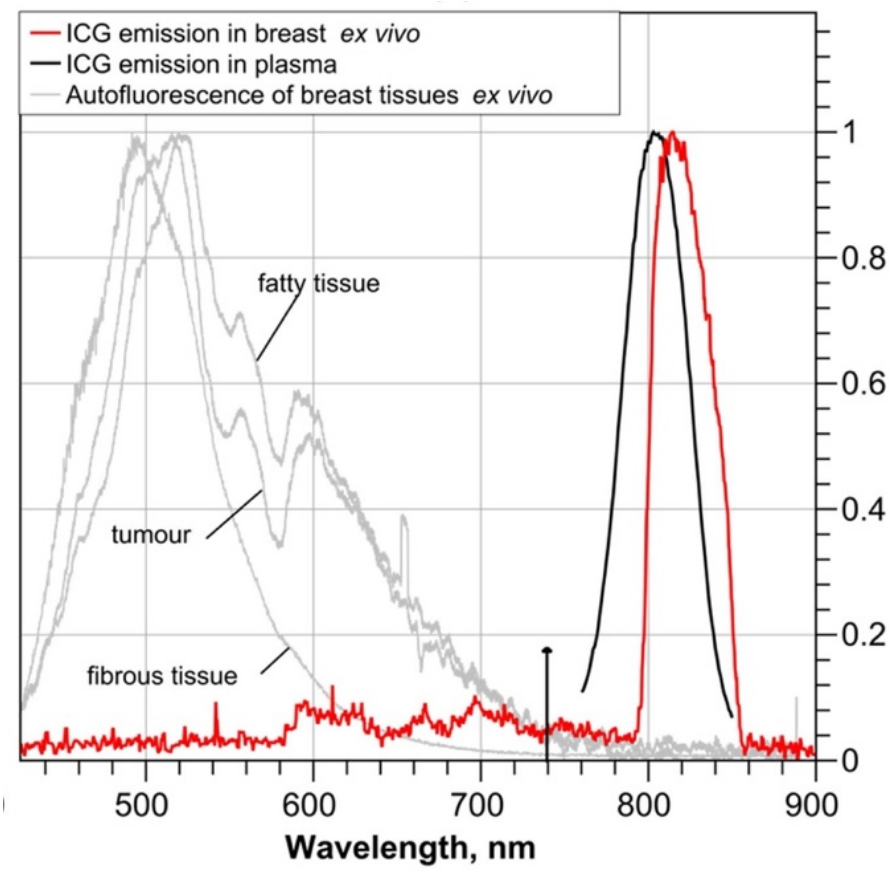


Figure 26: Comparison of ICG fluorescence in breast tissue, bovine plasma, and autofluorescence of the breast.
Breast tissue autofluorescence (grey) exhibits marked differences between tumour/normal/fibrous tissue, in the 550-650nm wavelengths (after the peak). ICG in plasma (black) has a slightly lower emission wavelength than in the *ex-vivo* breast specimen (red).
Note: Image reproduced with permission from the publisher (143).

There was a slight difference in emission wavelengths between plasma and breast tissue (817+/- 1.3nm). This shift of the fluorescence peak could be attributed to multiple factors such as:

- the different concentrations of ICG in plasma and tissue
    - potential self-quenching in plasma if the concentration of ICG too high, or dispersal if it's too low
- dilution of plasma protein binding sites (plasma composes 55% of blood) (149)
- background noise
    - blood has additional cellular components (white and red blood cells)
    - breast tissue has higher scattering/absorption due to different composition (collagen, adipose, and glandular tissue)

However, it is worth noting that the spectral shape (including the peak fluorescence) remained the same. Therefore, serum was used as a proxy measurement for blood. This was important for the analysis of the blood vessels in our ICG trial.

5.7. Conclusion

This chapter has investigated the properties of the GLOW system *in-vivo* primarily with regards to camera useability, but a secondary outcome was determining whether there was any merit to further investigations using ICG. The main conclusions are that there are multiple issues which needed to be addressed prior to clinical adoption, but that ICG warranted further exploration. A summary of the issues and the resulting changes that were made are listed below:

- Limited manoeuvrability of apparatus due to a short (30 cm) light cable. Future studies used a longer (1 m) cable.
- Colour image was oversized with regards to fluorescence image settings. The software was adjusted so that the images were displayed at the same degree of magnification.
- Difficulty determining where the camera was pointing as well as measuring distances for marking. This was resolved in the second study by using two lasers, thereby providing guidance for the camera direction and a fixed distance for image marking.
- Inconsistent orientation of GLOW images as compared to specimen radiography. Future trials ensured that all images were taken in the same orientation as the specimen radiography, with distinguishing features captured in both (i.e. a short stitch superior with 2 staples, and a long lateral stich with 3 staples).
- As the specimen x-ray only provides anteroposterior view, only the anterior and posterior images could be marked. Furthermore, the margin needed to be less than 0.5cm deep (maximum depth limit of camera as per *in-vitro* trial). This limited the images which were able to be included in our analysis and was resolved by recruiting more patients in the subsequent study (as per the power calculation which accounted for this loss).
- There was no dark frame measurement to account for background light before image analysis. This feature was developed for future studies.
- The software was not intuitive and kept crashing. Iterative adjustments were made to:
    - Enable simultaneous capturing of colour, IR, and dark frame images.
    - Develop autoexposure algorithms and create automatic mode (to control shutter speed, acquisition time, etc.).
    - Automate saving images into their own separate folder (i.e. patient 5, *ex-vivo* tumour, anterior).

    - Add a button on the camera so that it automatically acquires images so that the system could be run by a single user (i.e. position the camera, adjust the focus, and push a button to capture the images).
- There was no histopathology analysis, therefore, the next trial included imaging of specimen cut-ups in the pathology laboratory.

Following these changes, a sample size calculation (see section 5.5) determined that 20 women were required in order to obtain statistical significance (143). The following trial was designed to compare 2 different timings of administration (1 immediately prior to resection and 1 when ICG was administered at the beginning of the operation), a total of 40 women would need to be recruited (150).

6. ICG Feasibility Studies using Temporal Variation

Based on the findings from the previous study assessing camera function *in-vivo*, texture metrics could potentially differentiate between tumour and healthy tissue. In this chapter, we perform a feasibility trial assessing the differences between preoperative and intraoperative administration of ICG. The preoperative cohort capitalized on the EPR effect, whereas the intraoperative cohort presented the angiography of the tumour. Each cohort had 20 patients. Images were taken intraoperatively of the tumour *in-situ*, specimen, cavity post resection, and during histopathology cut-up. The images were marked and after pixel-based processing texture metrics were assessed. Our study was different to previous studies with ICG as they were smaller in size, limited in scope (e.g. only patients with NACT (44)), and assessed whole specimen images (rather than pixels with texture metrics) to determine TBR.

I wrote the protocol and gained ethical approval for this study. I recruited and consented the patients and collected metadata. I gained approval from the histopathology department to attend their cutting-up of the specimen, and coordinated with them to be present when they were processing the specimen. Maria Leiloglou and Vadzim Chalau aided in image taking. We co-wrote and co-presented the outputs found below.

The work in this chapter was published in the *Annals of Surgical Oncology* in (2021) ' The impact of temporal variation in indocyanine green administration on tumour identification during fluorescence guided breast surgery' and 'ASO author reflections: Towards fluorescence guided tumour identification for precision breast conserving surgery' as well as in *Sci Rep* (2022) 'Indocyanine Green Fluorescence Image Processing Techniques for Breast Cancer Macroscopic Demarcation'.

It was presented at the *American Association of Breast Surgeons* (2021) ‘Guiding light to optimize wide local excisions: the "GLOW" study’, the *European Molecular Imaging Meeting* (2021) ‘Variability of indocyanine green (ICG) near-infrared maximum emission wavelength in breast tissues’ and the *Imperial Surgery & Cancer Department Afternoon* (2020) ‘Guiding Light Optimising Wide local excisions’.

6.1. Methods

This REC approved trial entitled The Use of Fluorophores for Intraoperative Tumour Detection in Breast Cancer (19/LO/0927, 19/7/2019) was performed in the Charing Cross Hospital site of Imperial College Healthcare NHS Trust. In this study, patients were subdivided into 2 cohorts, each comprising 20 patients (as per the power calculation from the pilot study). The cohorts were defined based on the timing of ICG administration. As in the initial study, the angiography cohort was administered 0.25 mg/kg intravenously (IV) during the operation once skin flaps were raised (images acquired ~5 minutes after). The EPR cohort was instead administered 0.25mg/kg IV preoperatively once they were anesthetised (images acquired ~25 minutes after). The imaging protocol was developed to ensure that fluorescence images and accompanying white light images were acquired of:

- the tumour *in-situ* once skin flaps were raised
- the cavity once the tumour had been excised
- the en-bloc tumour specimen was imaged at the anterior and posterior aspects
- any cavity shave margins in 2 aspects (anterior, posterior)
- any *ex-vivo* sentinel lymph nodes
- the cut-up specimen in histology

Data was collected on patient demographics (age, BMI, ethnicity), clinicopathologic information about the tumour (type, hormonal status, stage, size, etc.), details of the operation and imaging details (type of operation, time of knife to skin, time of injection, time of imaging, etc.), as well as post-operative findings (margin status, reoperation rate, adverse events). For the image analysis, only the anterior and posterior whole specimen images and the histology cut-up images were used. The images obtained were processed (each cohort respectively) to determine the tumour background ratio as well as texture metrics of the image. These values were then used to determine the sensitivity and specificity of each image processing technique, as well as whether there was any correlation between a technique and any of the above listed factors.

6.2. Results

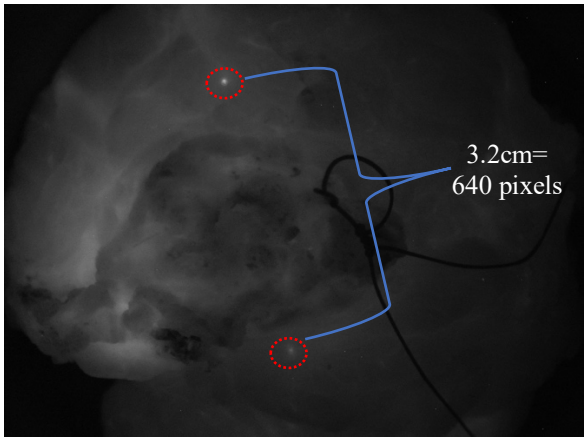
Patient and tumour characteristics were matched between the two cohorts as evidenced in the **Table 6**. Surgeons were blinded to the results of the fluorescent imaging and patients received standard care using conventional localising techniques. There were no adverse events.

Patient Demographics						
	EPR cohort			Angiography cohort		
	Mean	Range (min-max age)	Standard deviation	Mean	Range (min-max age)	Standard deviation
Age (years), p=0.67	57.9	34-78	±11.7	56.5	33-81	±14.7
BMI (kg/m^2), p=0.78	25.63*	20.32-36.51	±3.96	26.57*	19.02-36.6	±4.89
Ethnicity	% (N)			% (N)		
White-British	40% (8/20)			10% (2/20)		
White-Any other white background	10% (2/20)			15% (3/20)		
Black or Black British-African	5% (1/20)			0% (0/20)		
Mixed-Any other mixed background	5% (1/20)			0% (0/20)		
Black or Black British-Caribbean	0% (0/20)			5% (1/20)		
Asian or Asian British-Indian	0% (0/20)			5% (1/20)		
Do not wish to disclose	40% (8/20)			55% (11/20)		
Tumour Characteristics						
	EPR cohort			Angiography cohort		
	Mean	Range (min-max age)	Standard deviation	Mean	Range (min-max age)	Standard deviation
Size (mm)**, p=0.35	13.0	1.7-30	±6.5	15.7	0-34	±9.1
Histological type	% (n/N)			% (n/N)		
IDC	15% (3/20)			15% (3/20)		
IDC + DCIS	70% (14/20)			45% (9/20)		
DCIS	5% (1/20)			15% (3/20)		
ILC +/- ISLN	5% (1/20)			15% (3/20)		
IMC + DCIS	5% (1/20)			0% (0/20)		
IMPC + DCIS	0% (0/20)			5% (1/20)		
Hormone receptor status	% (n/N)			% (n/N)		
ER+, PR+, HER2 -	85% (17/20)			70% (14/20)		
ER+ (DCIS cases)	5 %(1/20)			20% (4/20)		
ER-, HER2 +	0% (0/20)			5% (1/20)		
Triple positive	5% (1/20)			5% (1/20)		
Triple Negative	5% (1/20)			0% (0/20)		
Neoadjuvant treatment	% (n/N)			% (n/N)		
NACT	5% (1/20)			5% (1/20)		
Hormone therapy***	0% (0/20)			5% (1/20)		
Margin status	% (n/N)			% (n/N)		
Positive radial margins	20% (4/20)			45% (9/20)		
Reoperation rate	20% (4/20)			40% (8/20)****		

Table 6. Summary patient demographics and tumour characteristics for ICG.
*2 patients were excluded from BMI calculation as height was not available.
**Only invasive cancer was included in the calculation.
***Hormonal therapy started pre-operatively as per local hospital protocol during the peak of the COVID
****The case which did not have a reoperation was due surgeon discretion for a 1mm margin for DCIS.
IDC= Invasive Ductal Carcinoma, DCIS= Ductal Carcinoma in Situ, ILC= Invasive Lobular Carcinoma, ISLN= In Situ Lobular Neoplasia, IMC= Invasive Mucinous Carcinoma, IMPC= Invasive Micropapillary Carcinoma, FAD= fibroadenoma, ER= estrogen receptor, PR= progesterone receptor, HER2= Human Epidermal Growth Factor Receptor, NACT= Neoadjuvant Chemotherapy.
This data was reproduced with permission of the publisher (150, 151, 152)

6.2.1. Image Processing

In the *ex-vivo* images, true tumour and true healthy tissue was determined as per the previous chapter. In the specimen cut-up, true tumour was based on the accuracy of an experienced histopathologist and true healthy tissue was based on the histological reports. In order to be able to measure out the negative margins (true normal tissue), the laser provided a constant measurement of 3.2cm. Using GIMP software, the lasers helped determine the associated pixel value for 3.2cm. This could then be used to calculate the corresponding pixel value for histopathology margins. An example is provided in **Figure 27**. The 3.2cm is measured as the equivalent of 640 pixels using GIMP software. The histopathology report clear margin of 0.5cm. After cross multiplication, the value of the pixels for the clear margin is 100 pixels. . The 100-pixel value would be used to mark the extent of healthy tissue from the edge of the specimen.



Laser		**Histopathology**
640 pixels	=	x
3.2cm		0.5cm

x = 640 pixels * 0.5cm / 3.2cm

=100 pixels

Figure 27: Explanation of how true normal measurements were calculated from pixel value.
The distance between the 2 laser points, each encircled in a red dotted line, was measured in pixel values (640 pixels). The fixed distance between the lasers was 3.2cm (blue line). Therefore, by using cross-multiplication, one can determine the pixel equivalent for any distance. This was used to mark images for histopathological margins of tumour clearance. In this case, the 0.5cm clearance was equal to 100 pixels.

6.2.2. *Ex-vivo*: Whole specimens

In the en-bloc *ex-vivo* images, 50/80 images (anterior and posterior of 40 patients) were excluded due to the tumour being deeper than the fluorescence imaging system was able to detect (we set a limit of >4mm). From the remaining 30, a further 8 were excluded due to: technical malfunctions, inability to determine tumour ground truth, or histopathological remission. For the remaining 22 *ex-vivo* images, the post-operative specimen x-ray was used to mark the tumour region. Macroscopic delineation of tumour was complemented by the microscopic histopathology reports regarding the distance between tumour and the healthy margin edge (**Figure 28)**. Orientation of the specimen was matched with the images via the standard sutures- short superior with one staple, long lateral with two staples. In cases where it was not possible to image the entire specimen and the associated sutures, in instances where length permitted, the suture was doubled back to the specimen.

6.2.3. *Ex-vivo*: Histology cut-up of specimen

During specimen cut-up, an experienced histopathologist would identify the tumour (true positive). Then based on formal histopathology, after the cut-ups were further sliced with a microtome, stained, and analysed via microscope, the normal (true negative) margins were identified. Samples of images acquired during angiography (**Figure 29**) and enhanced permeability (EPR) phases (**Figure 30**) are demonstrated in the following pages.

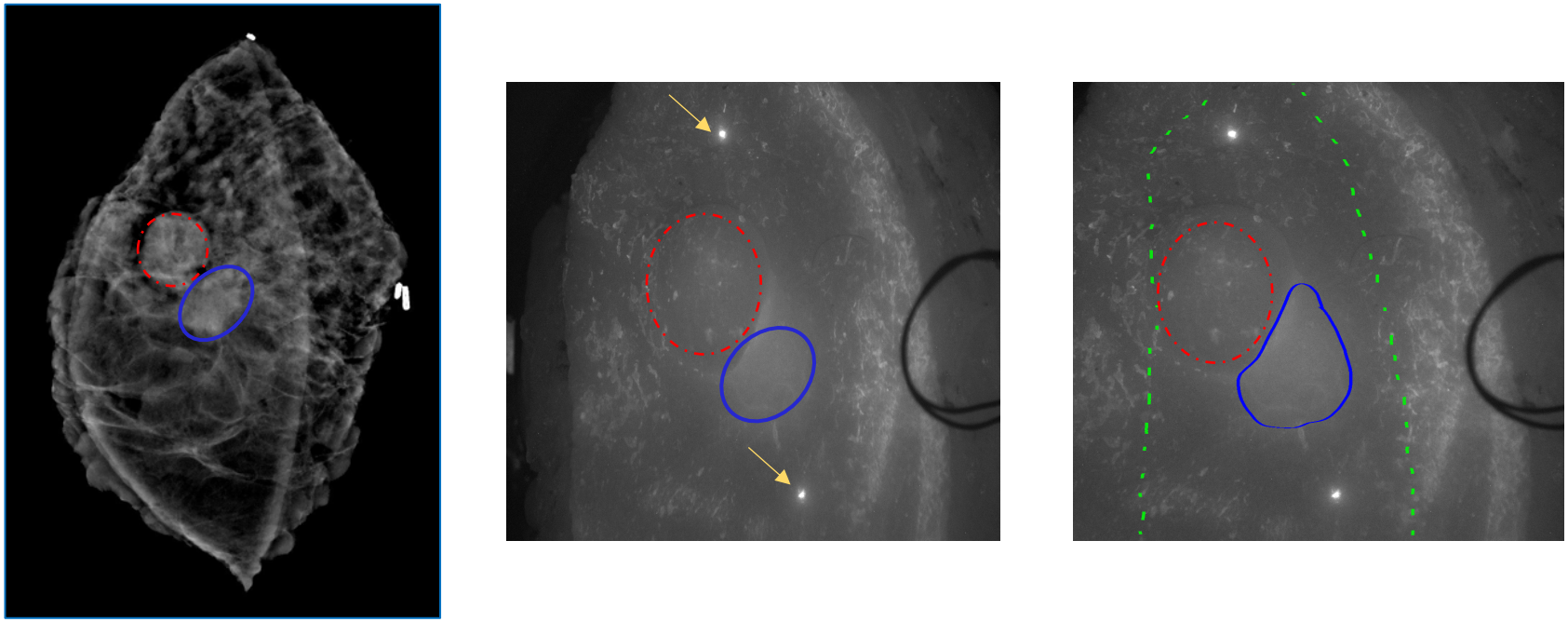


Figure 28: XR, unmarked infrared, and marked infrared images.
A) Specimen radiography, B) IR image in middle, C) marked IR image on right. Orientation of specimen provided by stitches, short superior with 1 staple, and long lateral with 2 staples. Tumour is marked in blue and nipple is marked with a dotted red line. In image B, the yellow arrows point to the 2 laser points used to measure distance for marking. In image C, normal tissue is everything outside the green dotted line. The nipple and tumour are both more radiopaque than the surrounding tissue. The nipple is more circular in shape whereas the tumour appears spiculated. In this case, the tumour (blue circle) is visible just below the nipple (dotted red circle) from the 3 to 6 o'clock position. In this case, the tumour was 1mm deep to the skin surface.

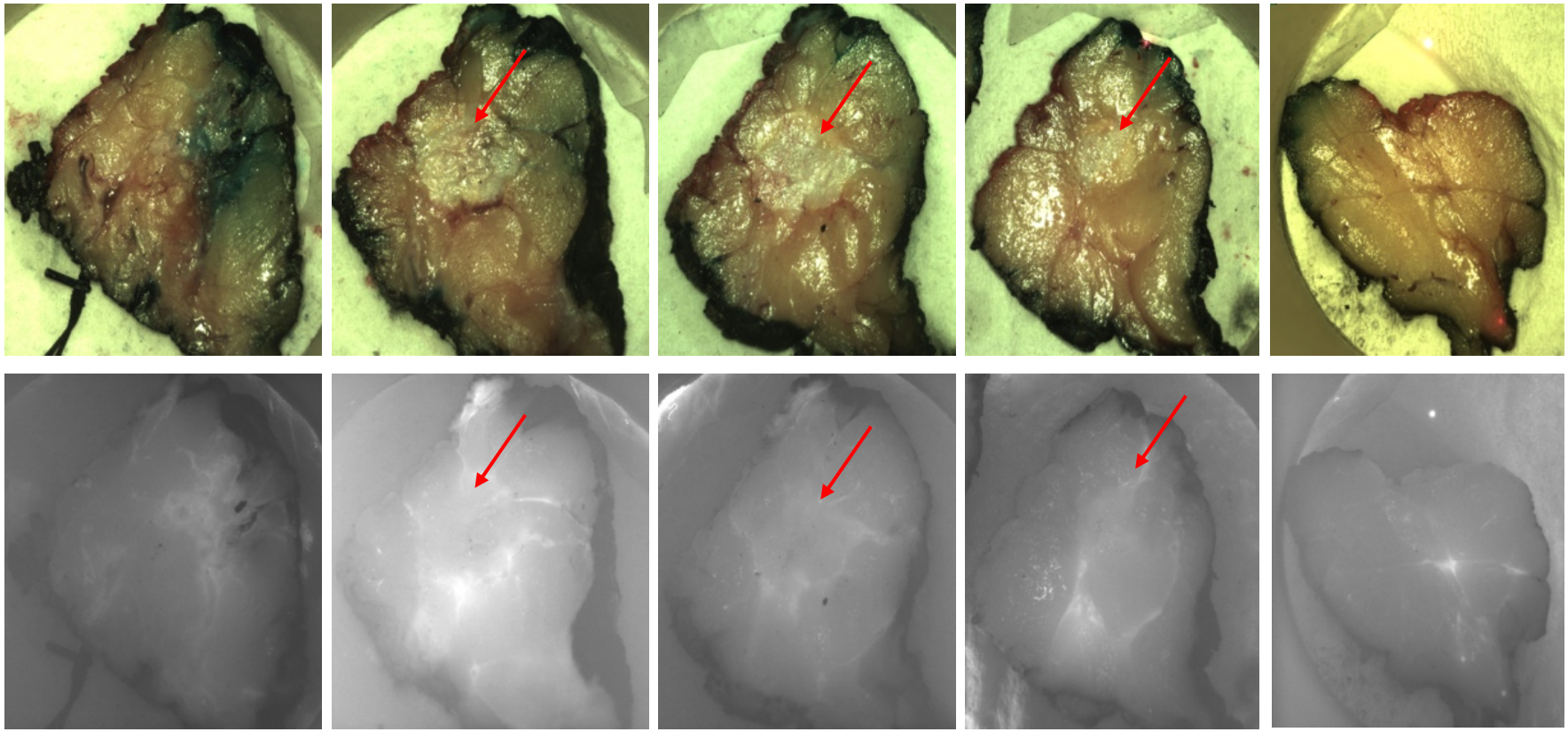


Figure 29: Cut-up of from angiography cohort.
Specimen cut-up in histopathology, from lateral to medial. Top row are the colour images, bottom row are the corresponding infrared images. Tumour outline is visible in slides 2-4 and is marked with red arrows.

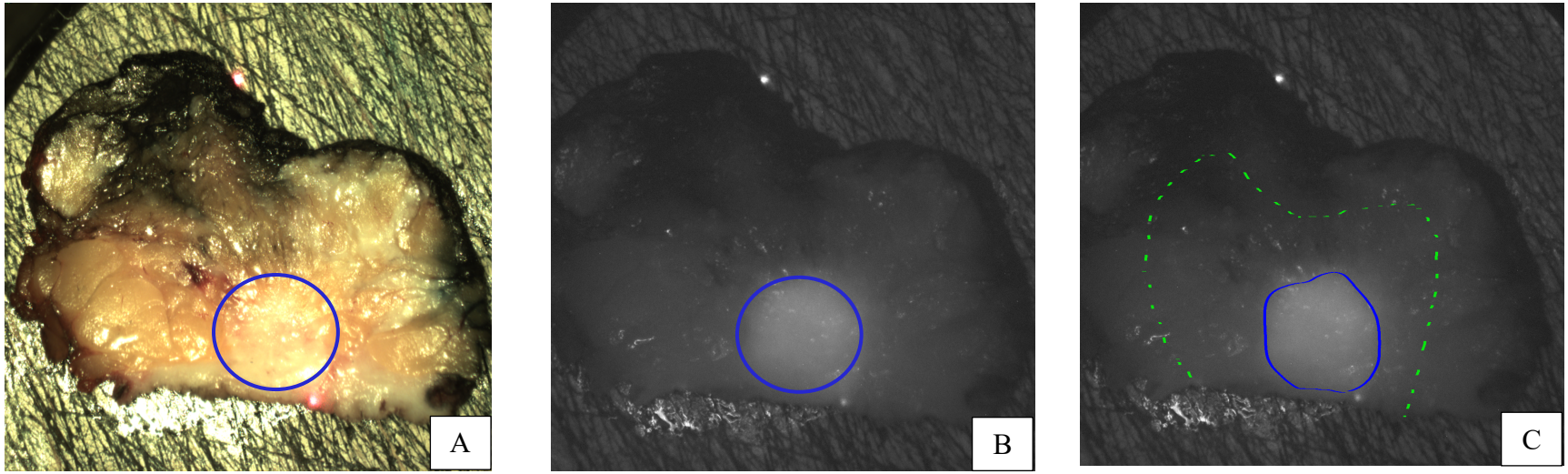


Figure 30: Cut-up from EPR cohort.
A) Colour image on left, B) IR image in middle, C) Marked image on right. A) The tumour has a lighter colour than the surrounding tissue. Tumour is found within the blue circle, anything outside the dotted green is normal tissue, and purple areas are used to exclude paint artefact (which would give a false negative value). The tumour is visible in the middle just above the inferior edge.

6.2.4. Image analysis and application to patient characteristics

Pixel based analysis was used to determine TBR. The mean TBR for all images was 2.60+/-1.48 ($p<0.001$) (150, 151, 152). Regarding variation in TBR across the two cohorts, the TBR in the angiography cohort was higher than in the EPR cohort (3.18+/-1.74, 2.10+/-0.92 respectively), but this was not statistically significant ($p>0.05$) (**Figure 31**) (150, 151, 152).

Sensitivity and specificity of the TBR were, as follows:
Angiography cohort: 0.82+/-0.99 in en-bloc BCS specimen and 0.85+/-0.98 in the cut-ups (150).
EPR cohort: 0.69+/-0.97 in en-bloc BCS specimens and 0.72+/-0.93 in the cut-ups (150).

There was a lack of statistically significant difference in TBR between BMI, tumour subtype, hormonal receptor status, or tumour depth (150). However, this is likely due to a low sample size. The only association was seen in a single age-based subgroup in the angiography cohort during histopathology cut-up (<60years TBR 2.23+/-0.71, >60 TBR 4.77+/-1.84, $p=0.001$) (150). A possible explanation for decreased TBR could be related to looser connective tissue in the breasts of the elderly, however the difference between angiography and EPR has not been explored.

70% of the images marked for true tumour and true healthy were used to train a classification model using logistic regression and support vector machine learning (see section 5.5). The remaining 30% of images were used to validate the model through ROC analysis.
This enabled image processing where a green pseudo-colour map (indicating probability for tumour) was overlaid on the colour image (**Figure 32 and 33)**

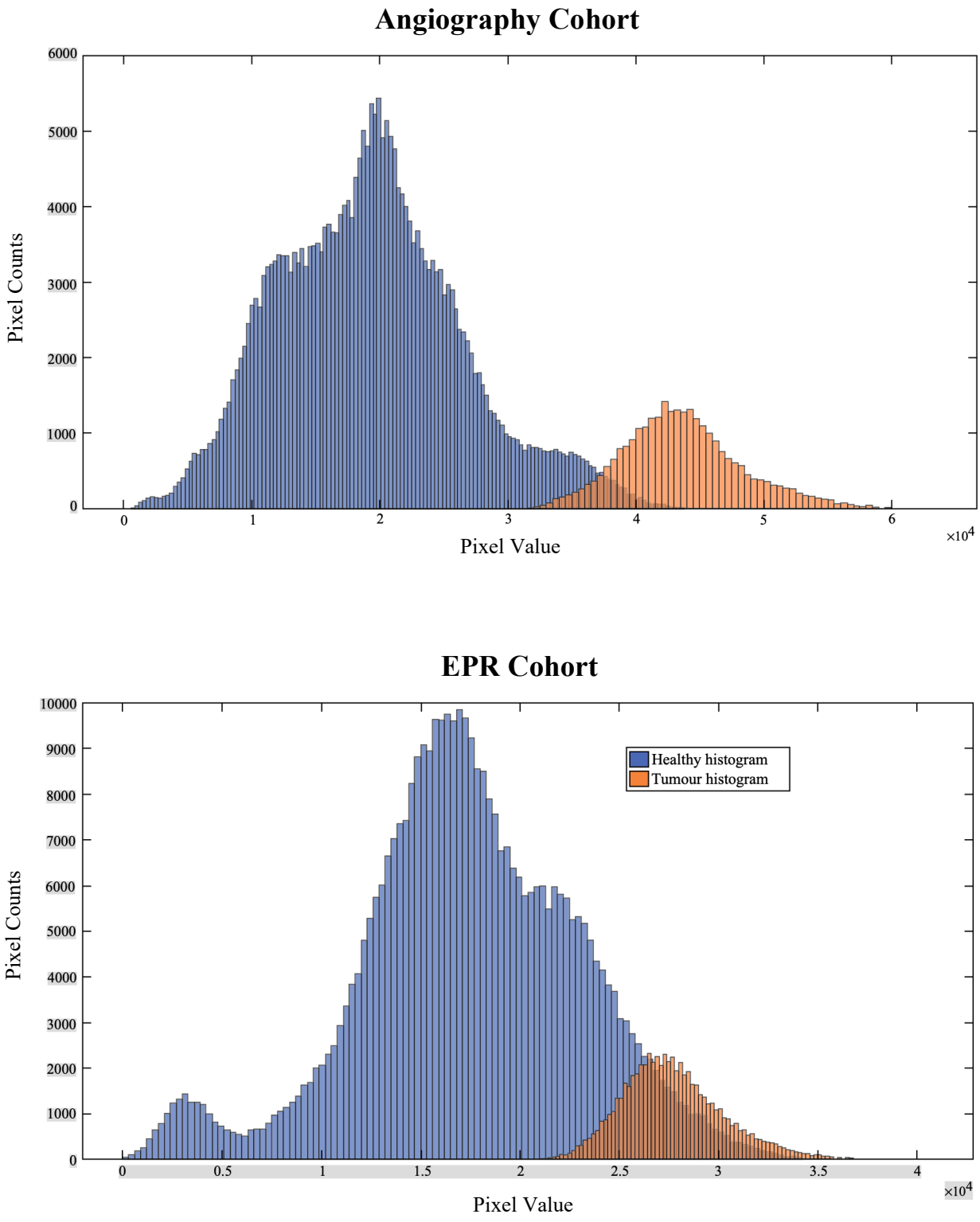


Figure 31: Histograms of pixel values between tumour and healthy tissue.
Top histogram is from the angiography cohort and bottom graph is from the EPR cohort. Orange represents pixel value and counts from tumour tissue. Blue represents the pixel values and counts from healthy tissue.
Image reproduced with permission from the publisher (150).

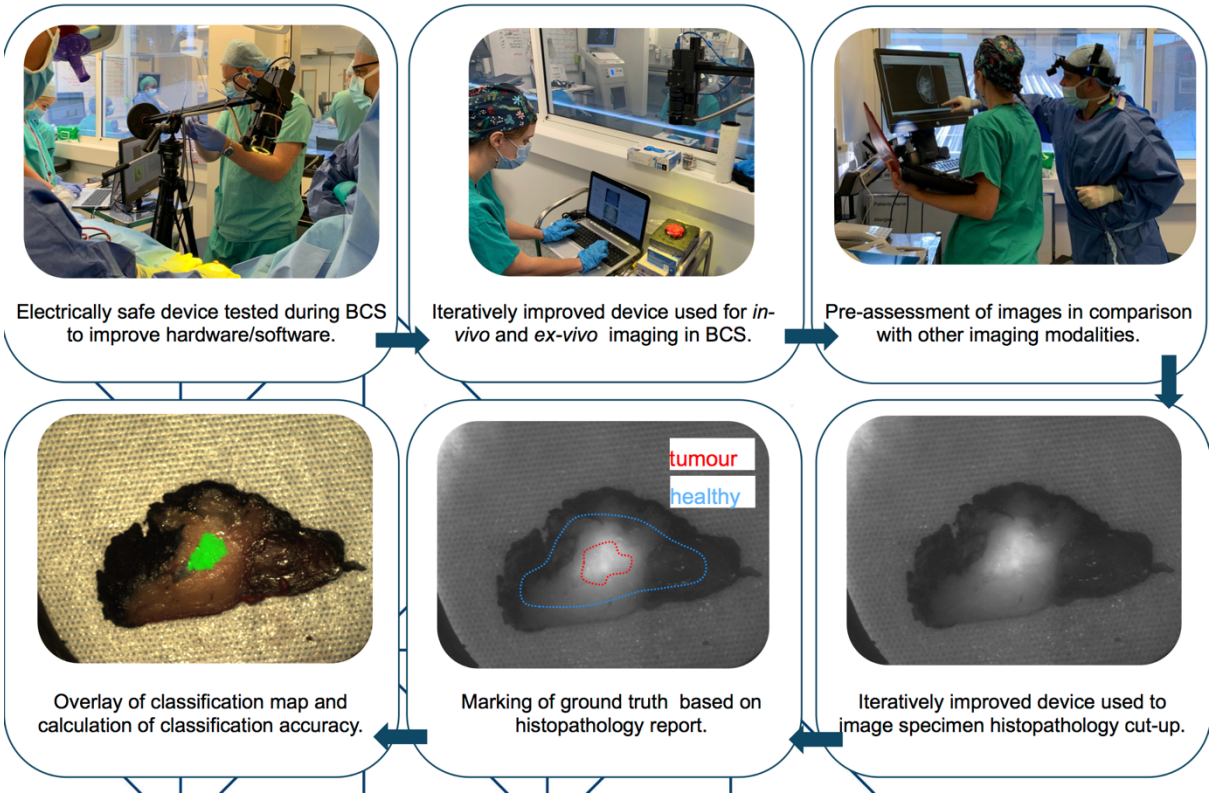


Figure 32: GLOW camera use intraoperatively and during histopathology cut-up.
The top row demonstrates the GLOW camera being used intraoperatively to capture images *in-vivo* (left), *ex-vivo* (middle), and compare it with the standard specimen radiography. Following this, in the bottom row demonstrates the specimen cut-up in histopathology with an IR image (right), the IR image marked for tumour and normal tissue (middle), and a green overlay onto a colour image representing where the tumour is most likely to be based on our trained classification system.

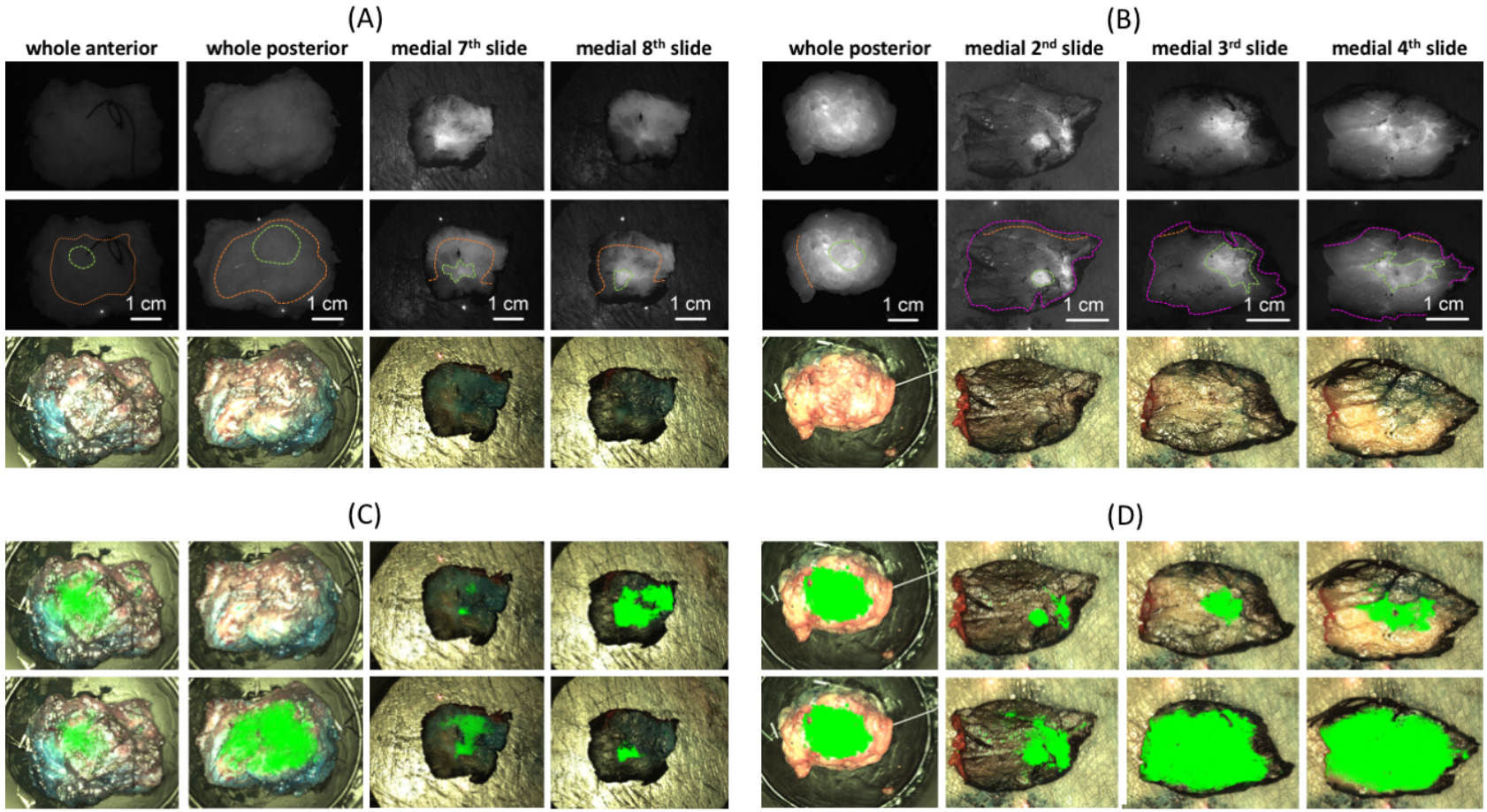


Figure 33: IR images with green overlay predicting tumour site.
A), B) Examples from ex-vivo (after resection) whole specimen and histopathology fluorescence images (first row) which have been marked (second row) for tumour location (green), healthy margin (orange), and corresponding colour images (third row).
C), D) Colour image overlaid with green pseudo-colour map, indicating tumour location based on the results using 2 different AI classification approaches (logistic regression and support vector machine). See section 5.5.3.
A), C) are from a single patient in the EPR cohort B), D) are from a single patient in the angiography cohort.
Image reproduced with permission from the publisher (150).

6.3. Discussion

ICG works within the remit of NIR, thus is outside the realm of tissue autofluorescence. ICG fluorescence was visible up to 4mm below the surface in our trial, which is sufficient to fulfil requirements for BCS according to SSO-ASTRO (no ink on tumour for invasive disease, 2mm for DCIS) and the ABS (1mm for both) (8, 9, 153). Therefore, 4mm is an adequate depth resolution to be confident of a clear resection margin. Furthermore, the combination of fluorescent specimen could be combined with imaging of the surgical cavity post-resection to affirm negative margins. Nevertheless, even with this method the potential of false positives remains an issue if ICG leaks into the cavity intraoperatively, if blood vessels are damaged, or false negatives in the case of microscopic disease (150).

A potential explanation for stronger signal in the angiography cohort may be that the concentration of ICG was higher as the imaging took place before ICG clearance (2-3 minutes) (147). Another possibility is that the abundance of vascular proliferation was better represented through angiography imaging of the vessels than what was leaked/left behind during the EPR phase. However, as both achieved an *in-vivo* TBR greater than 1.5, both signals would be classified as strong enough to differentiate between tumour and normal tissue (69).

It comes as no surprise that during histopathology the angiography phase appears to have a ‘halo’ effect whereas the EPR concentrates in the tumour. This can be explained by the location of the tracer. During angiography, the ICG remained within the blood vessels that were feeding the tumour, thus theoretically did not have the time to permeate into the tumour. Alternately during the EPR phase, enough time had passed for ICG for to be cleared from the bloodstream via excretion from the liver (147).

A significant limitation in histopathology was their use of paint to orient the breast specimen. 6 different paints would be used to mark the specimen as if it were a cube (blue superior, black posterior, etc.). However, yellow and orange paint gave a false positive signal, whereas blue, green, and black gave a false negative signal. Therefore, during image processing those areas were excluded.

It was surprising that there was no association between tumour subtype and TBR, however we did not have sufficient participants to make a valid comparison. That being said, ILC and IMC have been described as less likely to uptake contrast for PET-CT due to their low cellular density (154). The decreased uptake in ILC has also been attributed to a low mitotic rate, diffuse infiltration, as well as low levels of GLUT-1 receptors (154, 155). Additionally, as DCIS is microscopic and FGS works on a macroscopic scale, the current system was unable to identify pure DCIS. However, there was no statistically significant difference in patients that had pure IDC from those that IDC admixed with DCIS.

Pixel-based processing involved the subdivision of the image into 64x64 pixels marked in true tumour and true normal. As this generated more data points, it was more precise than image-based processing where either sensitivity (33%) or specificity (31%) was low (44, 45, 90). In comparison to the other studies, only our study compared different timings of administration of ICG. Intes et al. used continuous wave diffuse optical tomography to assess the inflow and washout of the angiography phase (136), whereas Pop et al. and Veys et al. examined the EPR phase (44, 90). Furthermore, our study had the largest amount of patients included.

It was not feasible to analyse the tumour *in-situ*, radial images of the *ex-vivo* specimen, as well as the cavity. This was because there was no way of determining the ground truth of where

tumour and normal tissue were. In these cases, the algorithm developed using the *ex-vivo* data was used to predict where the tumour is and whether any was left behind during the imaging of the cavity. However, there would be no way to determine accuracy of the signal since full cavity shave margins were not performed as standard in the unit at the time of the study. Furthermore, PMR and re-operative rates were not reflective of fluorescence imaging (as the surgeons were blinded), but rather of the conventional technique being used (wires or seeds).

6.4. Conclusion

In summary, both the angiography and EPR cohorts achieved a TBR which was sufficient to be used *in-vivo*. However, there was an insufficient number of patients with specific cancer subtypes to establish any significant differences amongst them. Furthermore, only our study used pixel-based processing, which was more precise to whole-image processing used in the other studies. However, ICG inherently lacks specificity to breast cancer due to its passive nature.

As a result of this work, we decided to design a second trial using a more breast cancer specific fluorophore. The hypothesis was that the signal would be more specific tumour with a drug that selectively targets breast cancer rather than its vasculature. We chose to pursue aminolevulinic acid, as it demonstrated an accumulation of a fluorescent metabolite in multiple breast cancer cell lines.

7. *In-vivo* pilot trial with ALA

This chapter describes our feasibility trial using ALA. It explains what ALA is, where it exists, and how it is used. It goes into detail about its pharmacokinetics in breast cancer, and how the fluorescent metabolite Protoporphyrin IX (PpIX) accumulates in breast cancer cells. We go on to investigate the use of ALA in breast cancer and whether its improved selectivity affects the strength of the TBR. As PpIX acts within the visible spectrum, we also explore how to overcome the background signals coming from endogenous fluorophores. On the point of multiple excitation peaks, we compare 2 filters targeting different excitation peaks with regards to which provides the best TBR.

I designed and obtained ethical approval for this trial. I procured the ALA, recruited and consented the patients for this trial, and collected the metadata. Maria Leiloglou, Vadzim Chalau, and Dhurka Shanthakumar assisted me with image acquisition. I marked the images and Maria Leiloglou processed them for TBR, sensitivity, and specificity. Maria Leiloglou and I co-wrote the presentations listed below.

This work was presented at the *American Society of Breast Surgeons* (2023) '5-ALA induced fluorescence for tumour visualization in breast-conserving surgery: Part 2 of the "GLOW" study', the *Association of Breast Surgery* (2023) 'Fluorescence and Multispectral Imaging in Breast Conserving Surgery – Proof of Concept Trial', and at the *London Surgical Symposium* (2022) 'Fluorescence Imaging System for Breast Conserving Surgery Guidance- the first in-human trial.'

Publications pending.

7.1. Summary of ALA

ALA is a hydrophilic nonproteinogenic amino acid, and it is a substrate involved in haem metabolism. This pathway is particularly prominent in mitochondria for the development of cytochromes, haemoglobin, and respiratory chain enzymes (55). In the metabolic pathway for the creation of haem, the immediate precursor of haem is Protoporphyrin IX (PpIX) (**Figure 34**), which is an endogenous fluorophore. Upon exogenous administration of ALA, PpIX accumulates due to the rate limiting step which is the conversion of PpIX to haem. The pathological accumulation of PpIX is substantially higher in malignant cells, and thus enables contrast between malignant and non-malignant tissues through fluorescence.

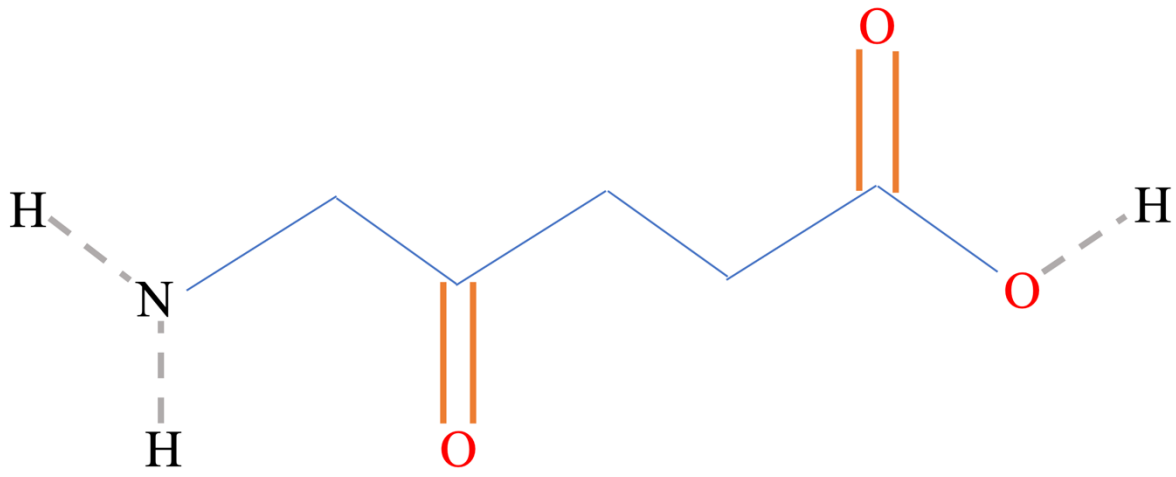


Figure 34: Chemical Structure of ALA.

There have been multiple enzymes implicated in this pathological accumulation in breast cancers, either through increased production of PpIX or through the decreased conversion to haem (**Figure 35)** (72). Overexpression or overactivity of ALA dehydratase, porphobilinogen deaminase (PBGD), uroporphyrinogen decarboxylase (UROD) have been linked to PpIX accumulation in breast cancer through increased production (72, 156, 157). Conversely, the decreased activity of ferrochelatase (FECH)(157) and ABCG2 transporter (the latter only in ER and HER2 positive cancer cell lines) (158) also causes an accumulation of PpIX.

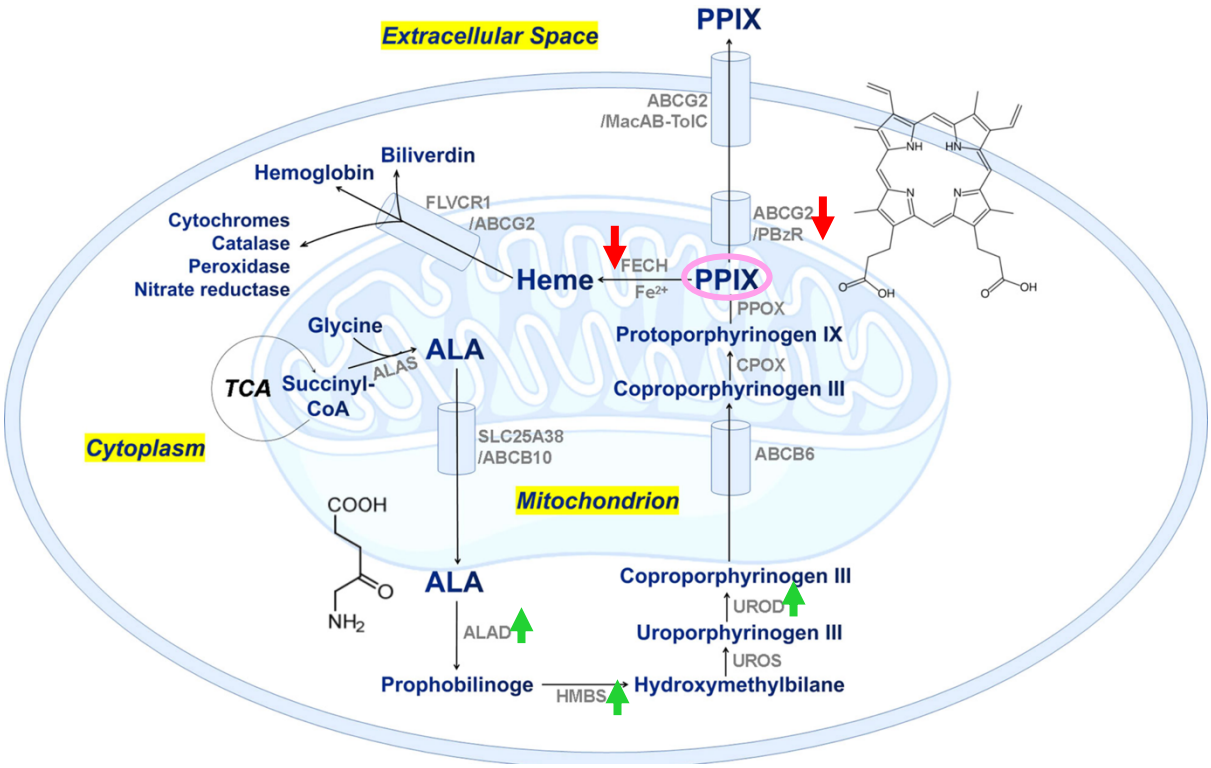


Figure 35: **The metabolism of ALA to PpIX.**
Multiple enzyme derangements have been implicated in the accumulation of PpIX (pink oval outline) in malignant cells through external administration of ALA. Increased activity (green arrows) of ALAD, HMPS, or UROD causes increased production of PPIX. Decreased activity (red arrows) of FECH or ABCG2 causes PpIX to accumulate by limiting conversion to haem.
This image was reproduced and modified with the permission of the author (159).

The European Medicines Agency (EMA) currently approves of the use of ALA in brain, bladder, and skin cancers (160). It has been used in photodynamic therapy as well, as the excitation of PpIX causes the formation of reactive oxygen species, thus leading to cell necrosis. ALA is also being investigated for its potential in diagnosing/treating oral mucosa, oesophageal, vulvar, vaginal, cervical, breast, prostate, lung, liver, pancreaticobiliary, bone, as well as head and neck malignancies (55, 161).

Formulations can be topical or systemic (i.e. oral, intradermal, and intravenous, etc.), and the by-products undergo hepatic and renal clearance (55). Fewer side effects have been reported with oral rather than intravenous formulations, although a longer time is required prior to imaging (162). Side effects are uncommon (1/100- 1/1000) but can include hypotension, ,

photosensitivity reaction, photodermatosis (57). Other reported side effects included nausea, vomiting, tachycardia, derangements in liver function tests (55), nerve problems, and hyperthermia (163).

PpIX has dual excitation wavelengths, 405nm and 635nm, and thus also has 2 respective emission peaks at 635nm and 705nm (144) (**Figure 36**). The excitation wavelength in the violet spectrum offers the highest peak known as the Soret band (400- 450nm) which emits at 635nm (55). This wavelength is highly absorbed by blood (145) and also activates FAD (72). However, there is minimal autofluorescence in breast tissue, as it is composed of mostly fat and connective tissues (71). Conversely, the red wavelength, which is absorbed more, is unable to provide deep penetration.

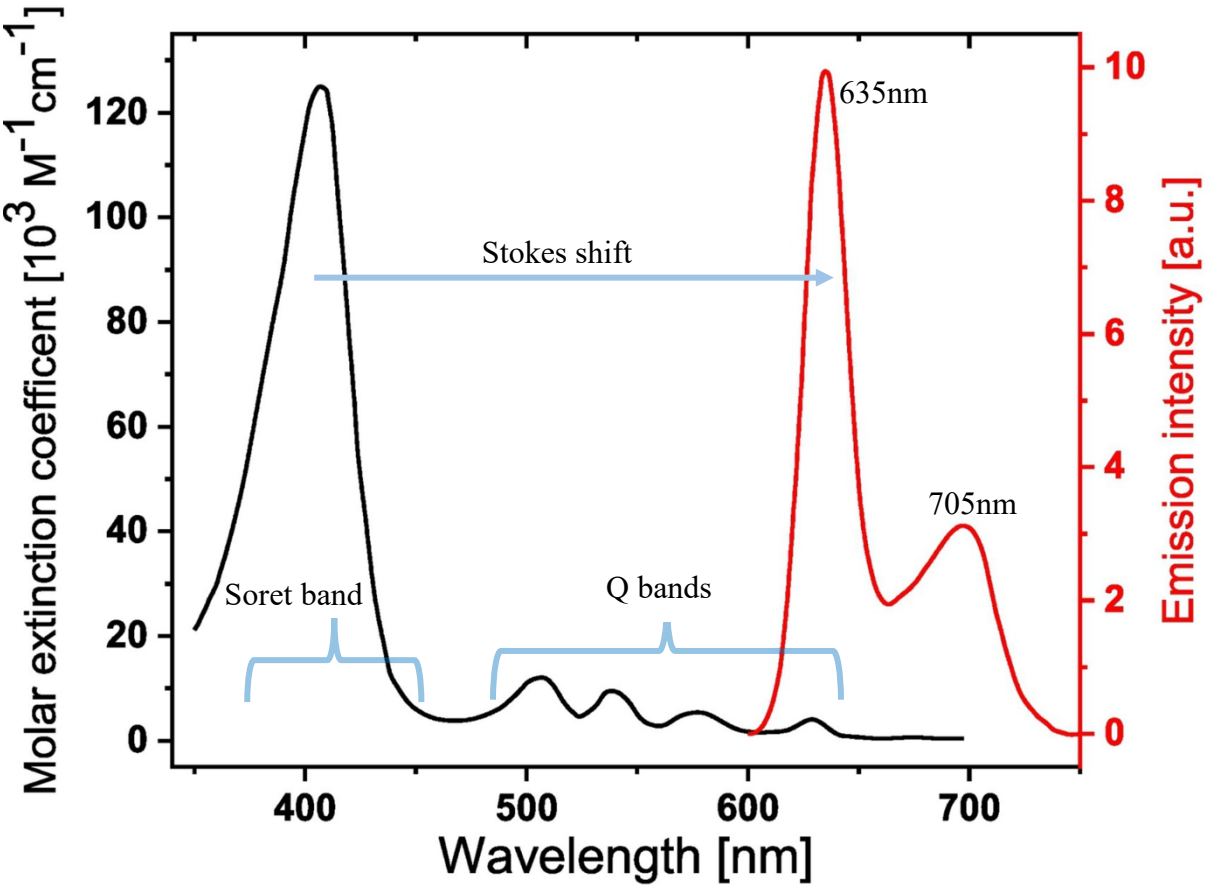


Figure 36: Absorption and Emission Spectra of PpIX.
PpIX has dual excitation wavelengths, 405nm (also known as the Soret band) and 635nm. It therefore also has 2 emission peaks at 635nm and 705nm respectively.
This image was reproduced and modified with the permission of the publisher. (146)

Thus far, two studies have examined the use of ALA in breast tissue (71, 101). The first study examined 13 patients used fluorescence imaging in microscopy (71). It found that 40mg/kg ALA given 40-150 minutes preoperatively caused tumour to have a fluorescence intensity 2.5-5.0 times higher than normal tissue (71). However, this study found that ALA was unable to differentiate between benign fibroadenomas and carcinomas (71). The second study by Ottolino-Perry et al. (101) was an *in-vivo* phase II randomised controlled trial investigating feasibility and safety, as well diagnostic accuracy of ALA on a macroscopic level. Patients were randomly allocated to receive no ALA or either a 15mg/kg or 30mg/kg dose pre-operatively. The findings are reported in **Table 7** below. TBR and identification rate were not reported. Surgeons and pathologists were blinded to the results, therefore positive margin rate and reoperation were reflective of their index technique.

Paper	Method	# pts	camera	dose	target	timing (h)	Sn (%)	Sp (%)	PPV (%)	NPV	DOR
Ottolino-Perry 2021 (59)	RCT	15	custom made (PRODIGI)	0	haem metabolism	N/A	N/A	N/A	N/A	N/A	N/A
		15		15 mg/kg ALA		2-4h pre-op	65	85	100 inside TB, 55.6 outside TB	95 outside TB	26
		15		30 mg/kg ALA		2-4h pre-op	68	80	100% inside TB, 50 outside TB	91 outside TB	10

Table 7: **Accuracy of different doses of 5-ALA as per Ottolino-Perry et al.**
This study compared a 15mg/kg dose of ALA against a 30mg/kg dose using the PRODIGI camera system. The 2doses were assessed for safety and accuracy.
Pts= patients, ex= excitation, em= emission, Sn=sensitivity, Sp= specificity, PPV= positive predictive value, NPV= negative predictive value, TB= tumour border, DOR= diagnostic odds ratio purely based on outside the tumour border.

As per the Gliolan Summary of Product Characteristics, a 20mg/kg dose should be administered to patients 2-4 hours before surgery (57). This time permits the ALA to be metabolised into fluorescent PpIX. (57).

7.2. Method for ALA Pilot trial

We assumed a similar number of patients would be required as for the ALA trial, therefore we obtained ethical approval (REC 19/LO/0927) for 40 patients. However, due to time constraints, only 30 patients were recruited to this blinded prospective single-centre feasibility study (164). In keeping with the current data and guidance on dose as per the Summary of Product Characteristics, 20mg/kg of aminolevulinic acid was provided to drink 2-4 hours preoperatively (57).

Women were included if they were over the age of 18, had a diagnosis of invasive breast cancer or preinvasive disease, and were undergoing BCS. Exclusion criteria included pregnancy, lactation, a history of liver failure and/or photosensivity (including a history of porphyria).

2 bandpass excitation filters were used, one including the Soret band (<600nm, which includes 400- 450nm) and one excluding the Soret band (450-600nm) (164). Emission wavelengths were assessed via a long pass filter 635– 750nm which encompassed both bands (635nm for Soret excitation, 705nm for Q-bands) for ease of use. Fluorescence images were captured of the tumour *in-situ* after skin flaps were raised, the resection cavity, the specimen *ex-vivo*, and cut-up during histology. Surgeons were blinded to the images collected, and gold standard localisation techniques were used intraoperatively. Patients received routine post-operative care.

Data collected included patient demographics (age, weight, height, BMI, ethnicity), tumour characteristics (type, grade, hormonal status, size, location), details about the procedure (time

of ALA administration and imaging, operation performed) and outcomes (margins, PMR, reoperation rates, and significant events).

Routine specimen radiography preceded images of the anterior and posterior aspects of the specimen acquisition. This provided initial guidance on radial margins and was used to guide subsequent cavity shaves.

Afterwards, the specimen was placed into formalin for fixation, and after a minimum of 24h it was inked and cut-up into 2mm slices. A senior histopathologist identified the macroscopic tumour on the cutups, and images were captured of those slices. Subsequently, specimen slices were then embedded in paraffin, and underwent routine processing to obtain H&E images to facilitate conventional reporting of margin status.

Specimen radiography was used to mark tumour presence in anterior/posterior *ex-vivo* images. Using formal histopathological data, the *ex-vivo* images were marked for normal tissue. In the histopathology images, the tumour was identified by a senior histopathologist, and the remaining margins used the histopathology results for normal tissue marking. Images were excluded from processing due to blue dye, paint artefact, or technical difficulties.

Recorded outcomes included patient demographics and clinicopathological data. The images were processed to extract TBR and sensitivity/specificity to tumour with the use of the Receiver Operating Characteristic (ROC) curves using 5-fold cross-validation.

7.3. Results

30 women were enrolled. The median (range) age was 61 years (38-79) and median (range) body mass index was 25kg/m^2 (19.1-42.0) (164). 19 of the patients were Caucasian, 1 was Afro-Caribbean, 1 was Asian, and the remainder did not want to disclose their ethnicity (164). Clinicopathologic results are displayed in **Table 8**. 23 had Invasive Ductal Carcinoma (IDC) (12 of which had concurrent DCIS), 4 Invasive Lobular Cancer (ILC) (2 with in-situ component ISLN), 1 DCIS and ISLN, 1 intrapapillary cancer, and 1 was metastatic (164). 4 were triple negative (and pre-treated with NACT), 2 were triple positive, 3 were ER negative, and the remainder were ER+ and HER 2- (164). Of the 5 patients which received NACT, 2 partially responded to treatment (the remaining 3 fully responded).

Patient Demographics			
	Mean	Range (min-max age)	Standard deviation
Age (years), p=0.67	61	38-79	9.6
BMI (kg/m^2), p=0.78	25	19.1-42.0	5.4
Ethnicity	% (n/N)		
White	63 (19/30)		
Black	3 (1/30)		
Asian	3 (1/30)		
Other	30 (9/30)		
Tumour Characteristics			
Size (mm)	Mean	Range (min-max age)	Standard deviation
	18.7	0.9-39	10.7
Histological type	% (n/N)		
IDC	77 (23/30)		
IDC + DCIS	40 (12/30)		
ILC +/- ISLN	13 (4/30)		
DCIS + ISLN	3 (1/30)		
Intrapapillary	3 (1/30)		
Metastatic	3 (1/30)		
Hormone receptor status	% (n/N)		
ER+, PR+, HER2 -	80 (23/30)		
ER-, HER2 +	10 (3/30)		
Triple positive	7 (2/30)		
Triple Negative**	13 (4/30)		
Neoadjuvant treatment	% (n/N)		
NACT	13 (5/30)		
Margin status	% (N)		
Radial positive margins***	37 (11/30)		
Reoperation rate****	13 (4/30)		

Table 8: Summary patient demographics and tumour characteristics for ALA.
*Two patients were excluded from BMI calculation as height was not available.
**1 of the triple negative cases was a metastases
***Margins of the initial resected specimen were used to mark (prior to cavity shaves).
****The reoperation rate reflects positive margins after cavity shaves.
IDC= Invasive Ductal Carcinoma, DCIS= Ductal Carcinoma in Situ, ILC= Invasive Lobular Carcinoma, ISLN= In Situ Lobular Neoplasia, IMC= Invasive Mucinous Carcinoma, IMPC= Invasive Micropapillary Carcinoma, FAD= fibroadenoma, ER= estrogen receptor, PR= progesterone receptor, HER2= Human Epidermal Growth Factor Receptor, NACT= Neoadjuvant Chemotherapy.

11 had positive primary specimen radial margins (prior to cavity shaves) (164). There were no significant adverse events. There were 4 positive margins according to UK criteria (165), 5 according to the US guidelines (165), and 3 which were both UK and US positive. 4 women required re-operation and 2 underwent completion mastectomies (164).

The image loss rate was 36.6 % (10 out of 30 cases). This was attributed to cases where the tumour was too deep, intralesional blue dye (used to map lymph nodes) or paint (used in histopathology) interfered with fluorescence signal, or the images were unable to be marked (due to microscopic lesions, lack of orientation of the specimen, etc.).

For the filter which included the Soret band, TBR was 1.8 +/- 0.7 in *ex-vivo* imaging and 3.3 +/- 2.0 in histopathology (164). For the other filter which excluded the Soret band, TBR was 1.7 +/- 0.7 in *ex-vivo* and 3.4 +/- 1.8 in histopathology (164). The results are displayed in **Figure 37, 38, 40, 41, 42)** and **Table 9**.

In the comparison between the TBR's of chemo naïve BCS versus NACT-BCS, there were 14 chemo naïve BCS and 5 NACT-BCS cases included (164). For the filter including the Soret band, NACT-BCS cases had a TBR of 2.7 +/- 0.8 whereas chemo naïve BCS had 2.4 +/- 0.8 (164). In the filter excluding the Soret band, NACT had 2.3 +/- 1.0 and tumor had 3.3 +/- 1.1 (**Figure 39,** and **Table 9**) (164).

Comparison of filters between *ex-vivo* and histopathology		
	Soret included	**Soret excluded**
TBR *ex-vivo*	1.8 +/- 0.7	1.7 +/- 0.7
TBR histopathology	3.3 +/- 2.0	3.4 +/- 1.8
Comparison of filters between NACT and primary surgery		
	Soret included	**Soret excluded**
NACT	2.7 +/- 0.8	2.3 +/- 1.0
Primary surgery	2.4 +/- 0.8	3.3 +/- 1.1

Table 9: TBR results between both filters and *ex-vivo* vs histopathology and NACT vs primary surgery. The first column is what specimen type was imaged. The second and third columns are the TBR values if the filter included or excluded the Soret band respectively. For each of the specimen types, there was no significant difference between the filters including/excluding the Soret band.

5-fold cross validation resulted in a sensitivity/specificity of 0.72 ± 0.3/0.76 ± 0.4 in the histopathology sections, and 0.60 ± 0.4/ 0.81 ± 0.2 in the *ex-vivo* data when excluding the Soret band[3] (164).

No statistical significance was found in the TBR values between the two different fluorescence filter modes, primary surgery cases versus patients treated with neoadjuvant chemotherapy, as well as depth of signal (<2mm or 2-3.5mm) (164).

.

[3] As noted above, there was no statistically significant difference between the filters which included/excluded the Soret band.

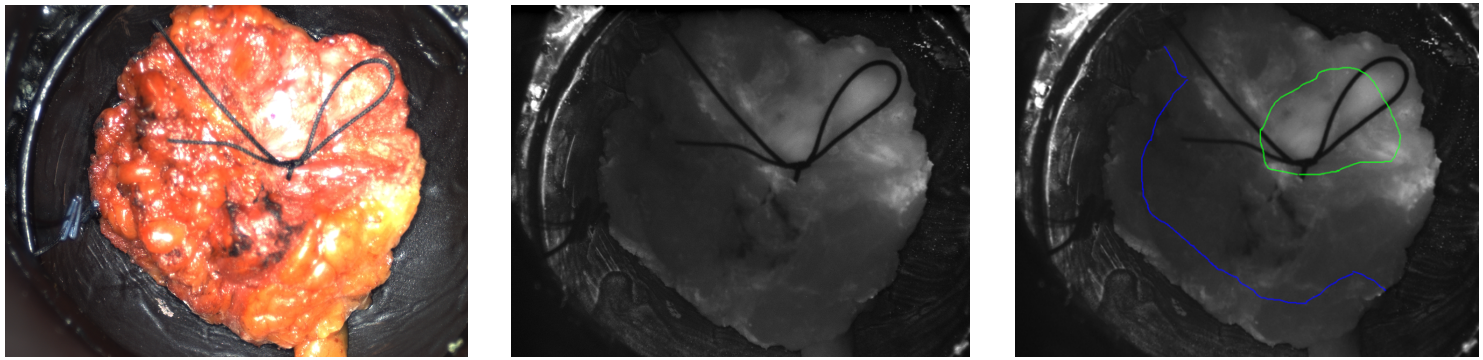


Figure 37: ALA *ex-vivo* specimen images.
Left is colour image, middle is fluorescent image, right is marked fluorescent image. In the marked fluorescent image, tumour is encircled in green and healthy tissue delineated in blue.

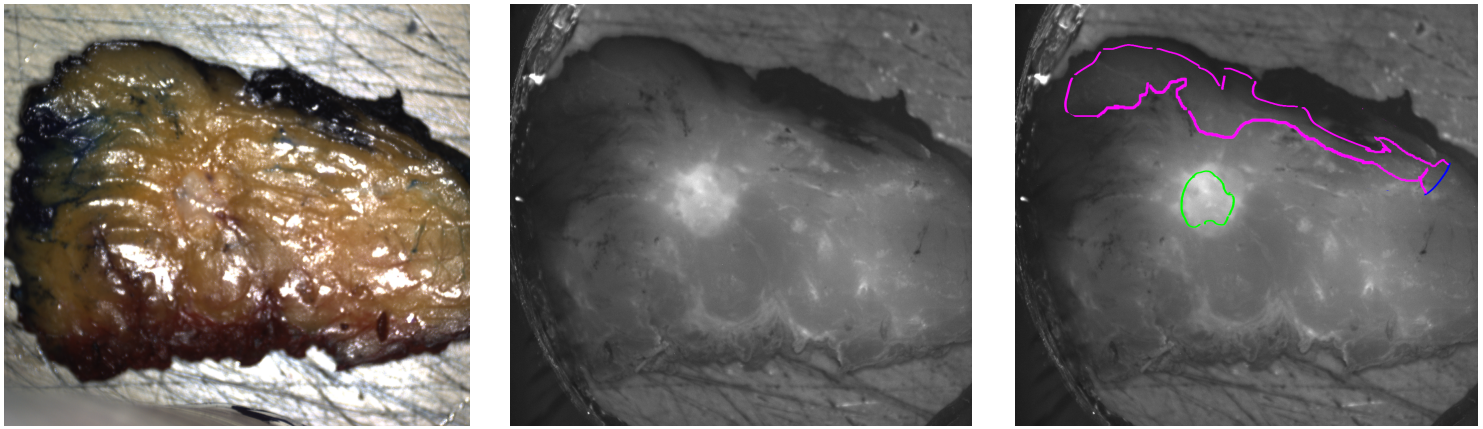


Figure 38: ALA histopathology cut-up images.
Left is colour image, middle is fluorescent image, and right is marked fluorescent image. In the fluorescent image, tumour is encircled in green and healthy tissue is outlined using magenta (marked to exclude paint artefact).

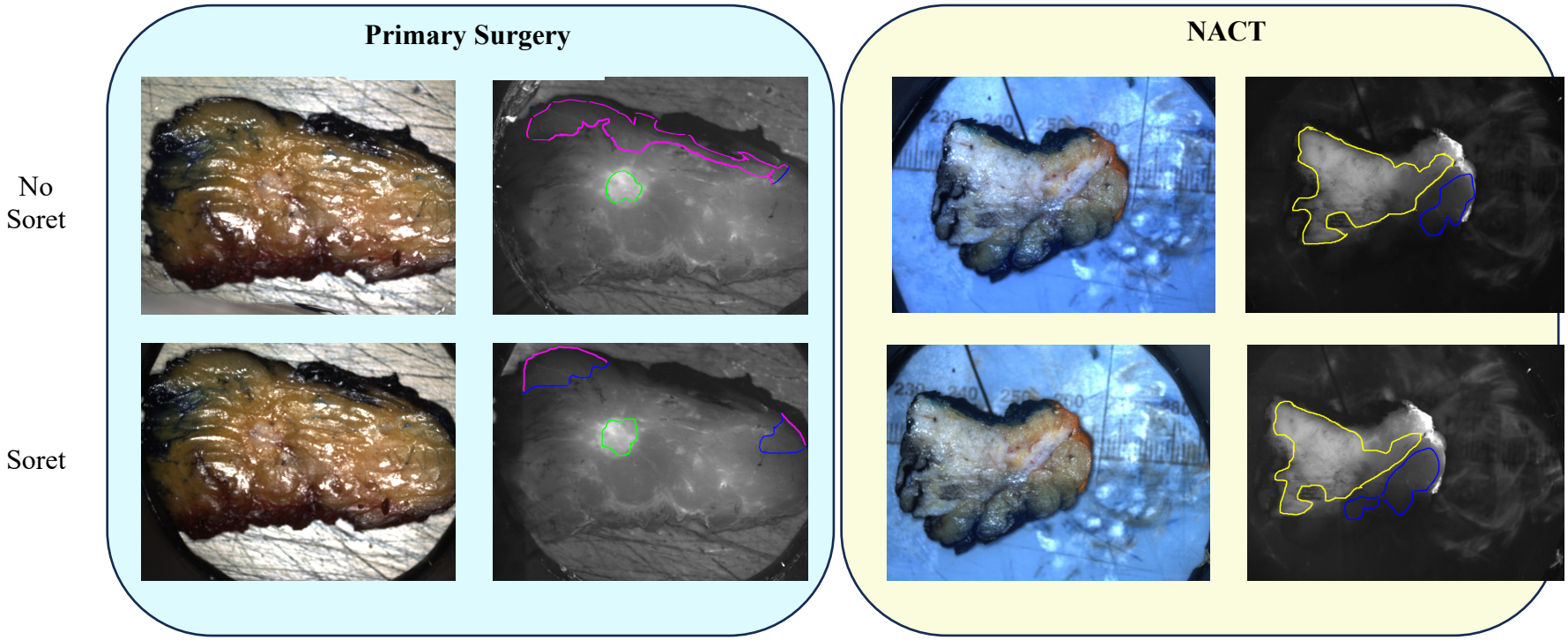
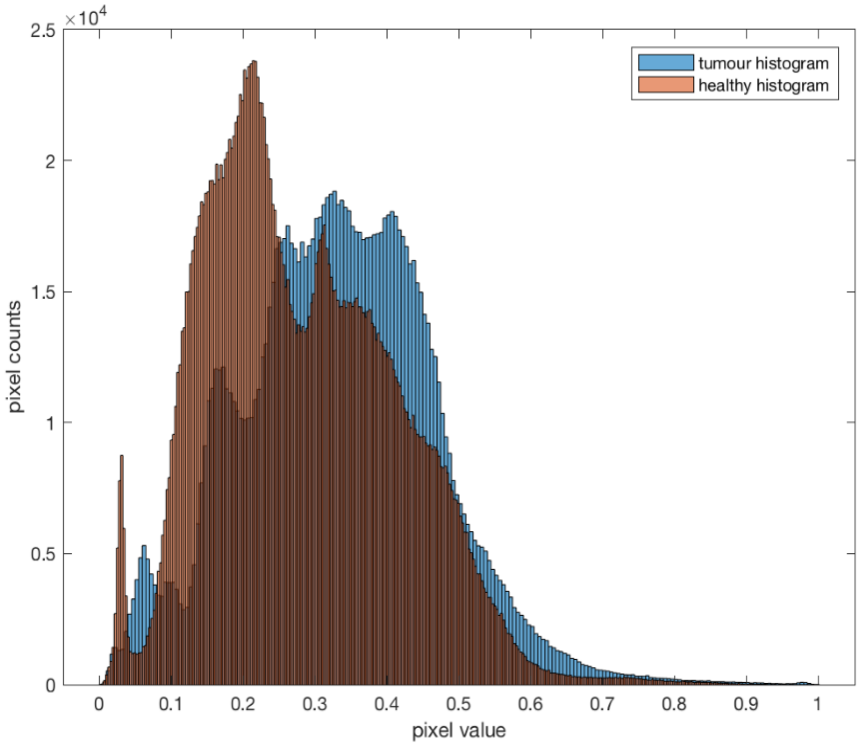


Figure 39: Comparison of primary interventions and filters on histopathology cut-up images.
The images in the blue box are from a patient who underwent primary surgery- colour images are paired with marked IR images where tumour is green and normal is located between blue/magenta. The yellow box is from a patient who had a complete pathological response to NACT -colour images are paired with marked IR images where yellow demarcates fibrosis and blue normal tissue. The top row does not include Soret band (425-625 nm) whereas the bottom row uses Soret band (<625 nm.).

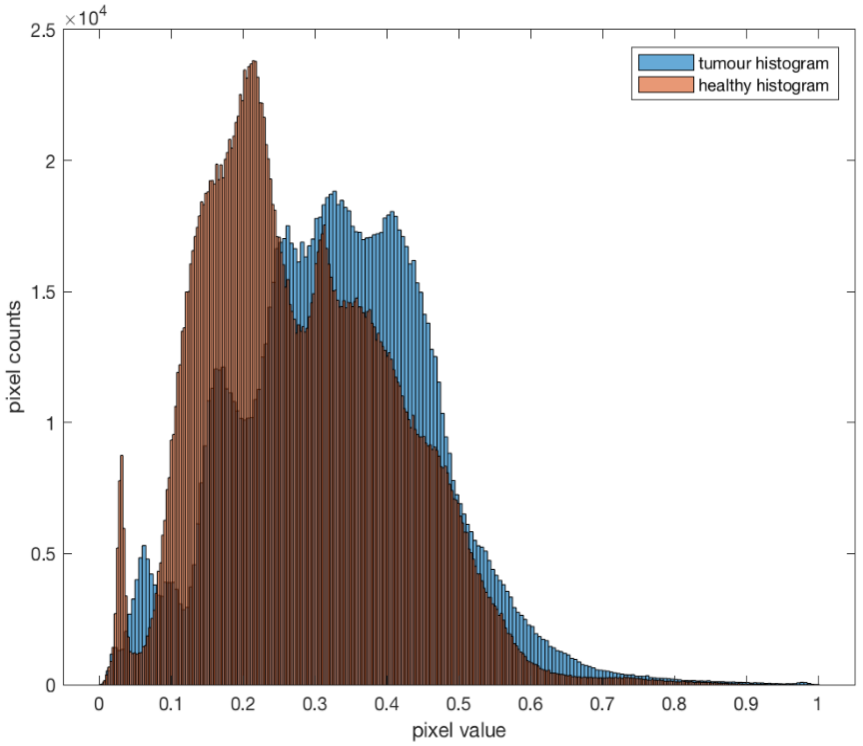
Ex-vivo

Soretincluded



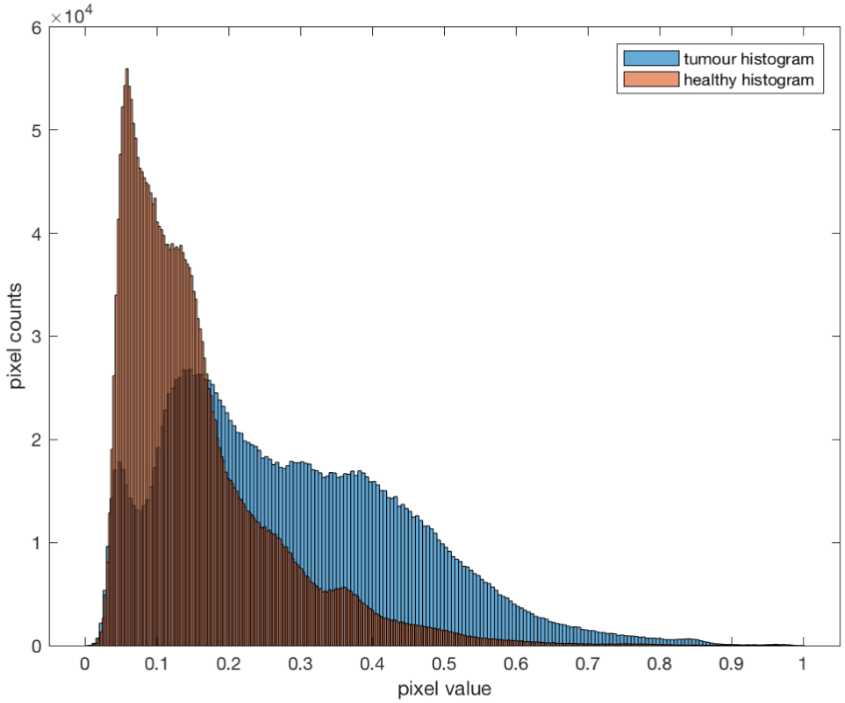
A

Soret excluded

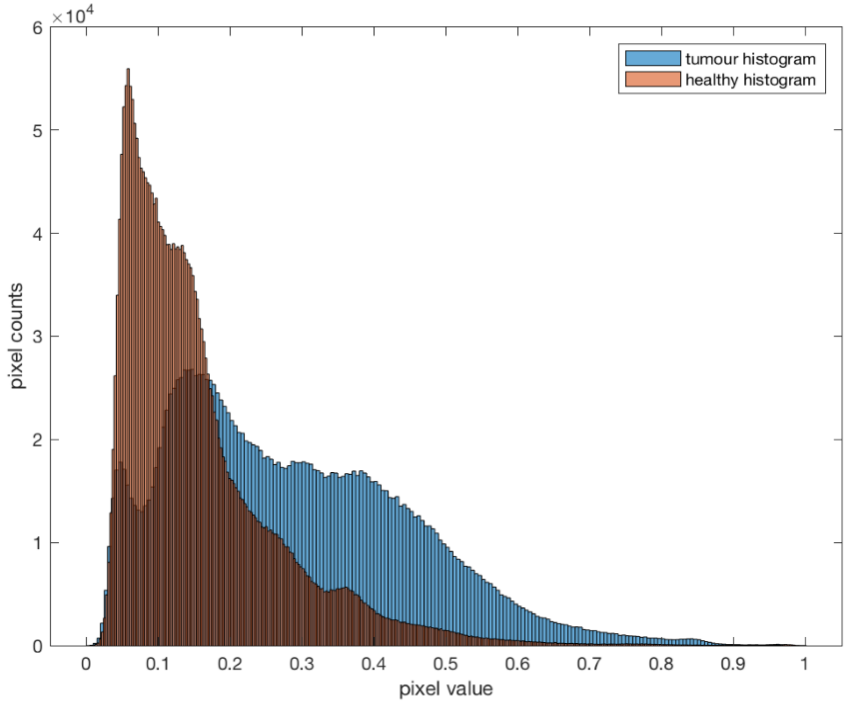


Histopathology

Soret included



Soret excluded



B

Figure 40: Histograms of pixel values between tumour vs healthy tissue
Pixel based processing of difference in fluorescence between healthy (orange) and tumour (blue) tissue using both filters (including/excluding the Soret. band). Figure A is for ex-vivo and Figure B is for histopathology.
*cases with blue dye or NACT were excluded

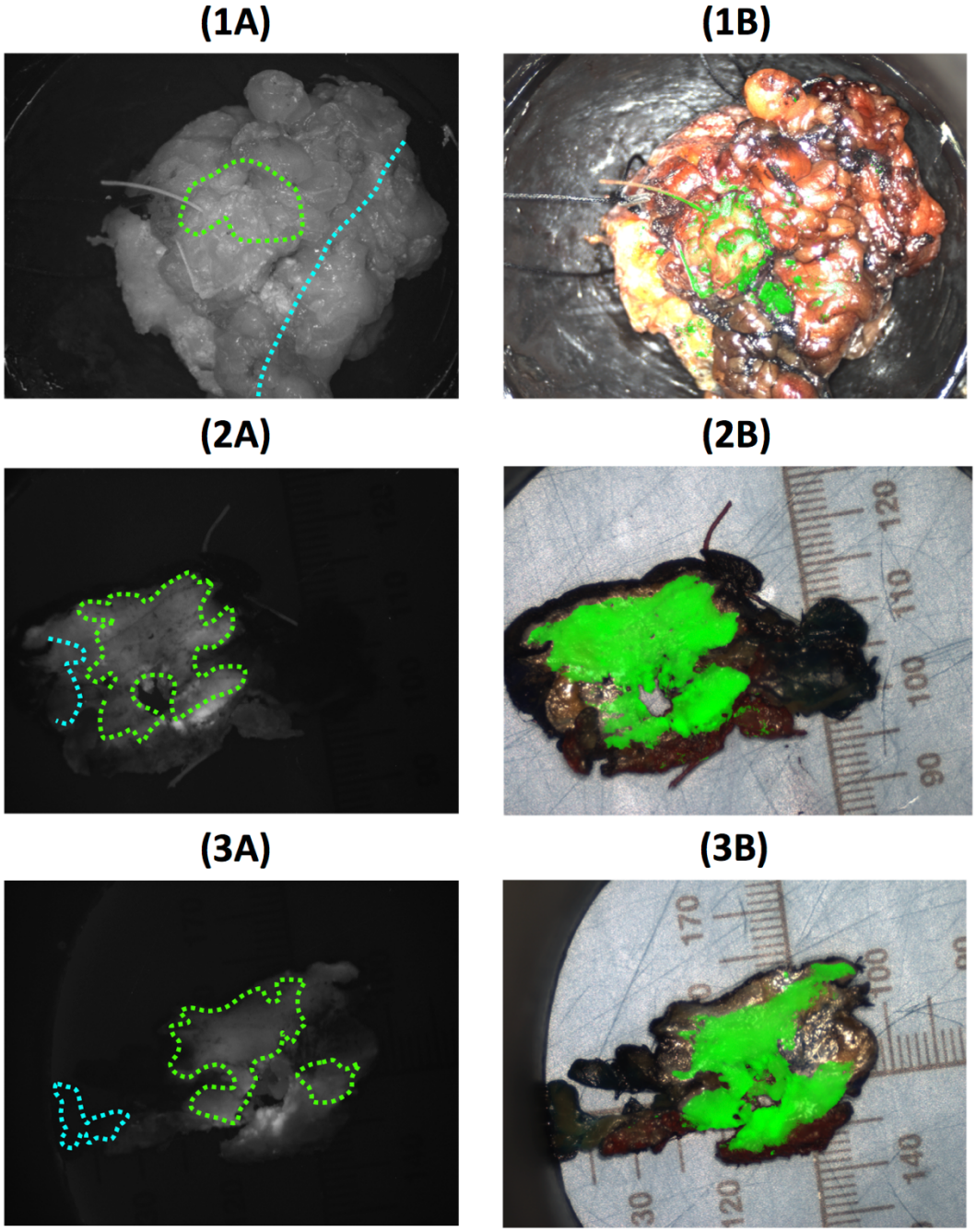


Figure 41: Examples of green overlay on colour images.
Column A are infrared images with tumour encircled in green and histopathologically confirmed normal tissue marked in blue. Column B is the corresponding colour image with a green overlay of the tumour location. Row 1 is the anterior aspect of the *ex-vivo* specimen (the tumour is 1mm deep to the surface). Rows 2 and 3 are the histopathology cut-ups from this specimen.
*Histopathology paint artefacts have been excluded from analysis. The red paint fluoresces in the inferior aspect of both images (false positive). The green/blue/black on the other outer edges dampens the signal (false negative). This image was reproduced with permission from the publisher (166).

7.4. Discussion

ALA administration during BCS can distinguish tumour from normal tissue. The TBR of both the tumour (3.4 ± 1.8) and post NACT fibrosis (2.9 ± 1) were both above the recommended *in-vivo* threshold (≥1.5), thus clinically significant in enabling excision of the tumour in its entirety in both scenarios (69). However, the current analysis indicates that for *ex-vivo* analysis the fluorescence signal is not sensitive to the depth of the tumour which is consistent with the literature (167).

It was interesting to note that both excitation filters (including and excluding the Soret band) provided similar strength in fluorescence signal. One would have expected the filter with the Soret band to be more effective given the higher emission peak. However, as both peaks are found in the >600nm (a long pass 600nm filter was used), perhaps the Soret peak caused oversaturation resulting in similar values.

There were many differences between our trial with ALA and that of Ottolino-Perry et al. We used the food and drug administration approved dose for glioblastoma operations (20 mg/kg) (164), whereas they investigated 2 different doses (15mg/kg and 30 mg/kg) (101). We included tumours of any size (including DCIS), whereas they limited their recruitment to patients with tumours >2cm in size (101). Furthermore, they only captured images of *ex-vivo* bisected specimen using the signal from the middle of the tumour and comparing it to the rim of normal to calculate the TBR (101). Conversely, we captured multiple images including those garnered *in-vivo, ex-vivo* of the whole specimen, and resection cavity to simulate intraoperative guidance through tissue (164). Furthermore, we imaged the histopathology cut-ups to determine whether this technology could also aid histopathologists in their analysis (164). Both of our trials

determined sensitivity and specificity of ALA in breast, however Ottolino-Perry et al. also determined the positive and negative predictive values as well as diagnostic odds ratio (101, 164).

As was the case with the previous study using ICG (and all other breast FGS studies), DCIS could not be identified due to its microscopic nature. A possible explanation for this is that none of the *in-vivo* contrast agents targets DCIS or its calcium deposits. Even if the contrast agent did accumulate, not enough is present for the camera to identify a signal. Furthermore, there are intrinsic camera limitations as FGS is designed to be a macroscopic technique thus cannot detect microscopic changes.

As with the earlier ICG study, positive margin rates were not reflective of FGS (as the surgeons were blinded to our study), but of the gold-standard localisation techniques. Furthermore, our PMR used the margins from the initial specimen removed and did not account for cavity shaves performed afterwards, hence the disparity between the PMR and re-operation rate.

7.5. Conclusion

In summary, ALA achieved a TBR which was sufficient to be used *in-vivo*. However, there was an insufficient number of patients with specific cancer subtypes to establish any significant differences amongst them. Only our study reported on TBR values, compared filters including/excluding the Soret band, as well as compared primary surgery to NACT patients. However, although more specific to breast cancer, there was a high level of background signal

due to endogenous fluorophores. This in turn resulted in impaired signal penetration, in turn limiting the depth at which one can detect tumours.

As a result of this work, we decided to compare the results between our feasibility trials. The aim was to determine the superior method of breast cancer identification. Our hypothesis was that ALA, which was more specific to breast cancer, would be superior to the nonspecific ICG cohorts.

8. Comparison of all modalities

In this chapter, we compared all modalities against one another to identify which performed best. The modifiable dual colour and fluorescence camera system for ICG using both timings (Chapter 5) and ALA using both filters (Chapter 6) were compared with one another. The diagnostic accuracy of these systems in BCS specimens was compared.

I, Maria Leiloglou, and Vadzim Chalau performed the studies with ICG and ALA. Maria Leiloglou analysed the data generated from the above studies. Together we developed the presentations listed below. I presented at ASBRS, Maria Leiloglou at ABS, and Dhurka Shanthakumar at LSS.

The work in this chapter was presented at the *American Society of Breast Surgeons* and published in the *Annals of Surgical Oncology* 'Fluorescence and Multispectral Imaging in Breast Conserving Surgery – Proof of Concept Trial', the *Association of Breast Surgery* and published in the *European Journal of Surgical Oncology* (2023) 'Comparison of Fluorescence and Multispectral Imaging for Margin Status Identification in Breast Conserving Surgery' and 'Intra-operative multispectral imaging for precision in breast conserving surgery', and at the *London Surgical Symposium* (2022) 'Multispectral imaging for intraoperative tumour visualisation in breast conserving surgery'.

8.1. Methods

A total of 70 BCS patients were recruited to a feasibility study after UK Research Ethics Committee (19/LO/0927) approval.:

- 70 patients were allocated to fluorescence imaging sequentially
    - 40 using ICG
    - 30 using ALA

Women undergoing BCS for non-invasive and invasive breast cancer (B5a and B5b) and were over 18 years of age were enrolled. In the fluorescent studies, ICG was injected at a 0.25mg/kg dose pre-operatively (at the time of anaesthetising) or intraoperatively (just before resection), and 20mg/kg ALA was administered 2-4 hours preoperatively and compared with 2 different filter sets. Once the skin flaps were raised, images of the specimen from the ICG angiography cohort were taken just prior to resection, whereas those in the EPR cohort were taken approximately 25 minutes after the patient was anaesthetised. In the ALA cohort, those images were acquired 2-4 hours after ALA ingestion. In both cases, histopathology cut-up images were captured 1-2 days after formalin fixation during specimen bread-loafing.

Outcomes collected included patient demographics, tumour data, reoperation rate, and any adverse events. Images were marked for tumour using the specimen XR (in *ex-vivo* images) and normal tissue using histopathology data.

A TBR threshold was determined to classify tissue as either healthy or tumour. In the case of ICG angiography, texture metrics were also applied (see Chapters 5 and 6).

8.2. Results

Patient and cancer demographics were comparable between studies.

In the *ex-vivo* TBR comparisons, only ICG angiography (2.1, STD 0.6) outperformed ICG EPR (1.7, STD 0.3) ($p<0.05$). The remainder were not different ($p>0.05$). In imaging specimen "cut-ups", the TBR for ICG EPR (2.1, STD 0.9) underperformed when compared to the 5-ALA|Soret (3.5, STD 1.5) and 5-ALA|No Soret (3.1, STD 1.5) ($p=0.02$ and $p<0.01$ respectively) (166). The above results are demonstrated in **Figures 42 and 43**.

ANOVA analysis revealed statistically significant differences in *ex-vivo* accuracy median values, with corresponding interquartile range (IQR), among: a) 5-ALA|No Soret (0.97, IQR:0.04), 5-ALA|Soret (0.88, IQR:0.21), the ICG angiography (0.82, IQR:0.16) and EPR methods (0.69, IQR:0.22) with $p_{Chi\text{-}sq}<0.01$ (**Figure 44**) (166).

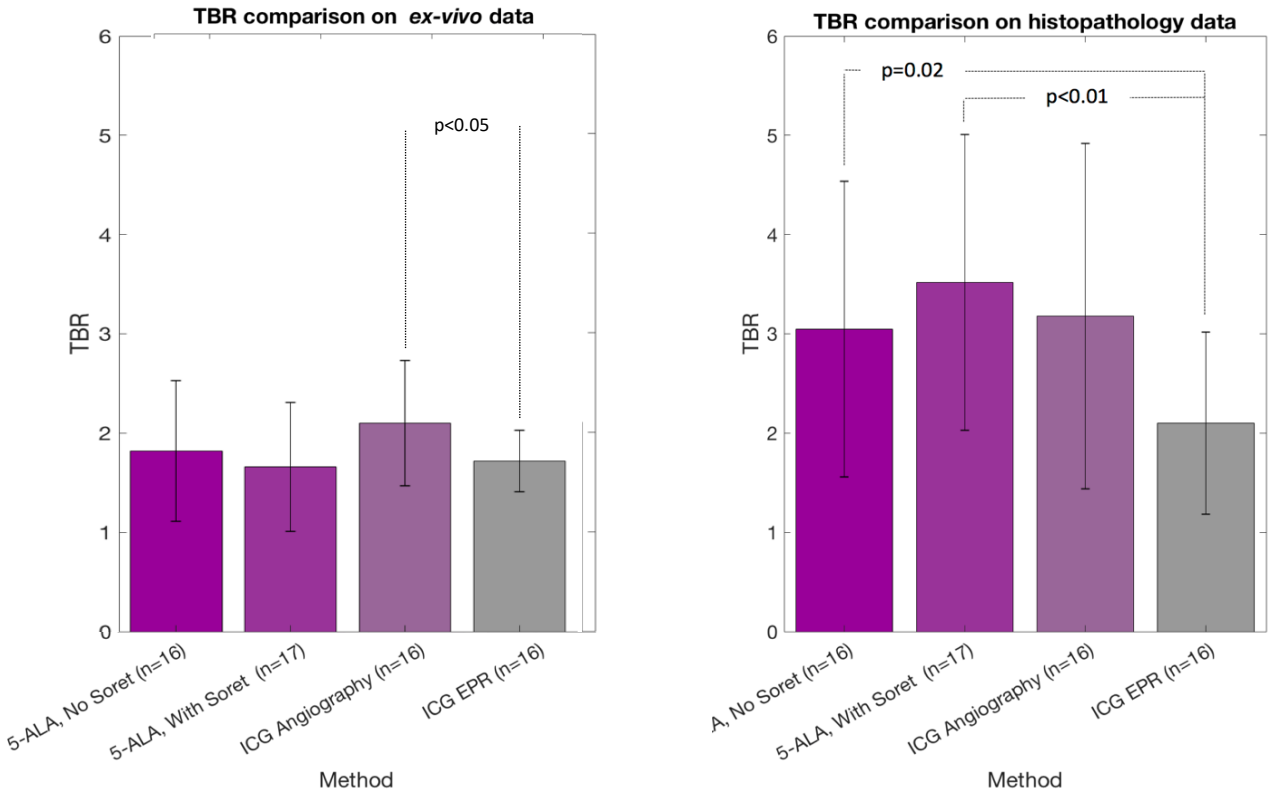


Figure 42: Histogram of TBR values between studies in *ex-vivo* and histopathology results.
Left graph is of the *ex-vivo* pairwise comparison between patients who received 5-ALA or ICG. Right graph compares TBR in *ex-vivo* in histopathology samples. (166)

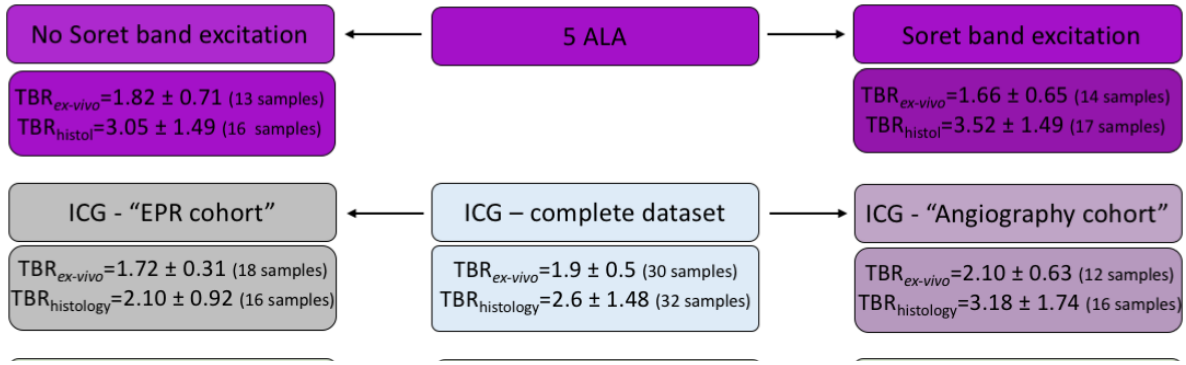


Figure 43: Summary of study results for ALA and ICG trials.
Purple represents the trial with ALA with the left box excluding the Soret band excitation and the right box including it. The central light blue box expresses the results of the trials using ICG, with the left box presenting the EPR cohort and the box on the right demonstrating results from the angiography cohort.

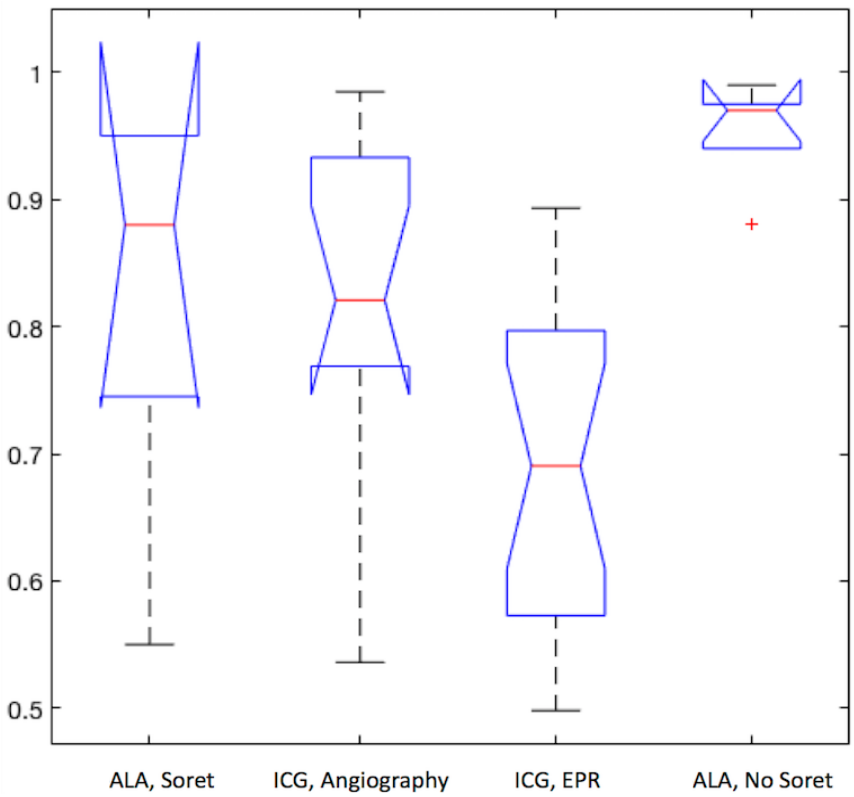


Figure 44: ANOVA analysis on *ex-vivo* TBR.
X- axis is the modalities being compared. Y axis is the average TBR including standard deviations. Only 5-ALA without the Soret band was significantly superior to the ICG EPR cohort.

8.3. Discussion

The first trial with ICG determined that ICG in both the EPR and angiography timings was equivalent in TBR and accuracy (apart from 1 age-based sub-group) (150). The second trial using ALA identified that there was no significant difference between the filters that either included or excluded the Soret band, or in primary surgery vs NACT cases (**Table 9**)(164). Nevertheless, both trials (ICG and ALA) achieved clinically significant TBRs.

9. Conclusion

9.1. Summary

Positive margins following BCS remains a prevalent issue. There have been many attempts to address this, including localising, margin, and imaging techniques. However, they all fail to address this either due to incomplete visualisation, long duration of time required to scan, or dependency on operational skills or patient position. Although imaging techniques have been reported to improve positive margin rates, they do not completely eliminate the problem. We proposed FGS as a potential solution.

FGS enables real-time intraoperative visualisation of tumour without the need for localising probes. The benefit of FGS is that it can be utilised intraoperatively to determine whether tumour-associated fluorescence is seen at the edge of the resection specimen or within the resection cavity. Light properties in tissue have been explored including inherently fluorescent molecules which exist in the body.

FGS in breast was investigated with its usage in identification of cancer, sentinel nodes, and the lymphatic system. Although its use in the identification of breast cancer is still in its early phase, my systematic review identified multiple fluorescent agents which are already undergoing clinical trials, some with promising results. My meta-analysis identified that ICG is not inferior to the gold standard of RI and BD in SLN mapping. As a result, hospitals that are unable to source, store, eliminate radioactive waste, or change the hospital's infrastructure to use RI would benefit. Furthermore, it is already in experimental use for identifying damaged

lymphatics and reconstructing them after SLN resection. Thus, FGS in breast cancer is a potential solution.

Our GLOW camera system was trialed *in-vitro* and was found to be sensitive to levels as low as 1/100th of the expected concentration in blood in various media. We also trialled ICG *ex-vivo* in porcine tissue and found the maximum depth at which ICG could be detected is 5mm (38). Lastly, we concluded that the GLOW camera was not inferior in sensitivity to the commercial SPY, but as a prototype it was less user-friendly.

In our feasibility studies, we used ICG (Chapters 5 and 6) and ALA (Chapter 7). The benefits and disadvantages of each fluorophore are summarised in **Table 10**, with our contribution listed below.

	Advantages	**Disadvantages**
ICG	• acts in NIRF (800nm) therefore not impacted by tissue autofluorescence (147) • short half-life (147) therefore no risk of toxicity • can combine with other imaging modalities • penetrates up to few mm (and higher concentrations increase this depth) (150)	• binds to plasma proteins therefore during angiography phase sometimes difficult to tell healthy/tumour vessels apart (147) • invasive as ICG requires intravenous injection (147) • multiple drug reactions (including 1/10 000 risk of anaphylaxis) (147) • unable to detect small tumours or low concentrations
	Our contribution: • we recruited more patients in our trials as compared to other trials • we compared two different timings of administration • angiography provided a higher TBR than with EPR timing, however both were clinically significant • there was one statistically significantly difference in TBR in the angiography cohort between women over / under 60 years of age • we identified texture metrics using pixel-based processing as a superior method as compared to whole-image processing (as done in previous trials)	

ALA	• deranged metabolism specific to breast cancer cells (72) • less invasive as administered orally or topically (168) • can combine with other imaging modalities	• acts in visible spectrum therefore clashes with other endogenous fluorophores • longer half-life than ICG thus can accumulate in healthy tissues too • photosensitivity • unable to detect small tumours or low concentrations
	Our contribution: • trialled breast cancer specific fluorophore not yet explored • compared filters including and excluding the Soret band and determined they were similar in efficacy	

Table 10: Advantages and Disadvantages of Various Imaging Modalities, and the contribution of this thesis.
The above table describes the benefits and disadvantages of ICG and ALA. Each section is followed by the contribution our novel findings provide.

However, in order for any technology to be brought into clinical use, it has to be fast, easy to use, affordable, and accurate. According to Maloney et al., the recommended sensitivity is 95% with a specificity of 85% (17).

In our ICG studies, we were able to achieve this with the histopathology for the angiography phase (150). For the remainder of cases, only the recommended specificity was achieved. However, the sensitivity was insufficient, with it ranging from 69% and 82% in both *ex-vivo* images (in EPR and angiography cohorts respectively) and 72% sensitivity in the EPR histopathology cohort (150). However, this was superior to all previous ICG studies, which used whole-image processing (instead of pixel-based) in a smaller subset of patients.

In our ALA studies, we were the first to have explored this fluorescent agent with regards to:

- signal strength for healthy vs tumour tissues in primary surgery cases
- signal from primary surgery vs NACT cases
- signal difference between including/excluding the Soret band in emission filters

We were successful in differentiating between tumour and normal tissue using TBR. Furthermore, we established that there was no difference in signal between patients pre-treated with NACT or those receiving primary surgery. Additionally, we determined that there was no difference between including/excluding the Soret band in our filter. Using these results, we were able to power future studies to determine sensitivity and specificity. (164)

9.2. Limitations

The GLOW camera was unable to detect DCIS, the most common culprit for close or positive margins. The camera's inherent limitation for resolution (reported to be at submillimeter scale) (143) is unable to detect microscopic DCIS (reported to be <0.5mm in size) (169). A potential solution would be through combining FGS with a margin modality so that the former can guide the resection and the latter would ensure adequate clearance.

Many images were lost due to either a technical error, the injection intratumorally of blue dye (false negative in both *ex-vivo* and histopathology cut-ups), or paint artefact during histopathology (wherein the orange/yellow dyes gave a false positive, and blue/green/black dyes gave false negatives). We mitigated for the paint artefact by excluding the painted areas from our image analysis.

Furthermore, we were unable to mark radial images of *ex-vivo* specimens as only AP XR were available to provide information on the tumour location. As the anterior margin (skin) and posterior margin (pectoralis muscle) reach the surgical limits of resection, it is the radial margins which cause the need for reoperations. In order to achieve intraoperative feedback, our

2D system would need to be adjusted to enable simultaneous analysis of multiple depths for a 3D image of the cavity to detect any remaining fluorescent tissue requiring further excision.

Although we did image the specimen in all views (superior, lateral, inferior, medial) and cavity shaves, we were unable to mark those images for true tumour and true healthy tissue. Post-operative histopathology only stated that the specimen had positive margins along a border but did not specify where or how much of the border was involved. This was the same in the case of shaves, where they simply stated that it contained cancer cells or was healthy. However, after we trained the algorithm to differentiate tumour from healthy tissue using our anterior/posterior specimen and histopathology images, we applied it to the remaining images (but were unable to confirm successful identification).

Lastly, insufficient accumulation of dye due to low uptake in the tissues (such as in necrotic tissue or tumours with a low mitotic rate such as IMC) would be unable to provide a distinct signal between tumour and background tissue (170).

9.3. Future work

Optimising accuracy in differentiating cancer from normal tissue via intraoperative real-time visual feedback during BCS has the potential to improve positive margin rates. However, there remain many areas which can be explored in future work with regards to fluorophores, camera development, or combining FGS with another system.

Given that there is a considerable amount of genotypic and phenotypic variety between breast cancer, it is difficult to identify one target that encompasses this range. Ideally, a more accurate probe should be developed, but this may prove difficult given the above. Alternately, one could

combine multiple fluorophores, however there is no guarantee of it being able to target all cancer types and exposes the patient to the side effects of the drugs administered. Furthermore, fluorophore development is not being led by the pharmaceutical industry, but by start-ups. This results in a lack of resources to push large enough clinical trials for fluorophores. Future work should subcontract start-ups in research and development, thereby granting them the funding required to develop a new agent, afterwards jointly running clinical trials.[4]

The same can be said of commercial systems in med-tech companies when it comes to partnering with start-ups in developing new camera systems or improving current ones. Moreover, when it comes to the commercial systems available, most are designed to work in the NIR and are often tested using ICG. Camera systems should be developed to target each fluorophore individually so that the lowest amount of drug can be used, resulting in decreased costs as well as dose-dependent side effects. Our GLOW camera system has modifiable filters which have enabled the camera to be used in both the NIR (ICG) and visible spectrum (ALA), but this exciting development needs to continue progressing more to promote higher sensitivity.

Current camera systems produce 2D images, but they cannot account for depth of the cavity. One way of tackling this problem is through flattening out the cavity (thereby creating a 2D image) which would enable the surgeon to know whether the cavity was free of tumour or if they need to take further cavity shaves. However, upon release when the cavity returns to its normal depth, it may lose the orientation it had before so that focused cavity shaves would not be possible and instead cavity shaves from all sides would have to be taken. Cameras should

[4] See appendix 1 for our work with Professor Tate's biomedical team in developing a fluorophore.

be developed so that these images can be displayed in 3D, ideally integrated into a hands-free wearable camera system such as the Hololens.

Furthermore, future work will combine the macroscopic information garnered from an NIR camera system with another microscopic margin modality (margin probe, i-knife, etc.). This multimodal approach would enable further demarcation of the border between healthy tissue and tumour. However, validation of these trials would necessitate comparisons with immediate histological analysis using frozen section.

Although FGS in BCS is in its infancy, the rapid evolution of this technology is imminent. Whether it is by developing a more sensitive camera, more accurate probe, combining it with another system, or all of the above, it will be at the forefront of BCS.

The future is bright, the future is GLOWing!

References

1. Breast Cancer Statistics [Available from: https://www.cancerresearchuk.org/health-professional/cancer-statistics/statistics-by-cancer-type/breast-cancer.
2. Sung H, Ferlay J, Siegel RL, Laversanne M, Soerjomataram I, Jemal A, et al. Global Cancer Statistics 2020: GLOBOCAN Estimates of Incidence and Mortality Worldwide for 36 Cancers in 185 Countries. CA Cancer J Clin. 2021;71(3):209-49.
3. De Boniface J, Szulkin J, Johansson ALV. Survival After Breast Conservation vs Mastectomy Adjusted for Comorbidity and Socioeconomic StatusA Swedish National 6-Year Follow-up of 48 986 Women. JAMA Surg. 2021;156(7):628-37.
4. Corradini S, Reitz D, Pazos M, Schönecker S, Braun M, Harbeck N, et al. Mastectomy or Breast-Conserving Therapy for Early Breast Cancer in Real-Life Clinical Practice: Outcome Comparison of 7565 Cases. Cancers. 2019;11(2).
5. Mastectomy or lumpectomy? The choice of operation for clinical stages I and II breast cancer. The Steering Committee on Clinical Practice Guidelines for the Care and Treatment of Breast Cancer. Canadian Association of Radiation Oncologists. CMAJ. 1998;158:15-21.
6. breastcancer.org. Research Suggests Lumpectomy Plus Radiation Leads to Better Survival for Early-Stage Breast Cancer but There Are Questions About Study 2014 [Available from: https://www.breastcancer.org/research-news/20140220-3.
7. Breast cancer molecular types: Cancer Treatment Centers of America; 2022 [cited 2022 23 November]. Available from: https://www.cancercenter.com/cancer-types/breast-cancer/types/breast-cancer-molecular-types.
8. Tang SS, Kaptanis S, Haddow JB, Mondani G, Elsberger B, Tasoulis MK, et al. Current margin practice and effect on re-excision rates following the publication of the SSO-ASTRO consensus and ABS consensus guidelines: a national prospective study of 2858 women undergoing breast-conserving therapy in the UK and Ireland. Eur J Cancer. 2017;84:315-24.
9. Moran MS, Schnitt SJ, Giuliano AE, Harris JR, Khan SA, Horton J, et al. Society of Surgical Oncology-American Society for Radiation Oncology consensus guideline on margins for breast-conserving surgery with whole-breast irradiation in stages I and II invasive breast cancer. Ann Surg Oncol. 2014;21(3):704-16.
10. Jeevan R, Cromwell DA, Trivella M, Lawrence G, Kearins O, Pereira J, et al. Reoperation rates after breast conserving surgery for breast cancer among women in England: retrospective study of hospital episode statistics. BMJ. 2012;345:e4505.
11. Chauhan H, Jiwa N, Raj NV, Thiruchelvam PTR, Hogben K, Al-Mufti R, et al. Clinicopathological Predictors of Positive Resection Margins in Breast Conserving Surgery. Manuscript submitted for publication,. 2024.
12. McCahill LE, Single, R. M., Aiello Bowles, E. J., Feigelson, H. S., James, T. A., Barney, T., Engel, J. M., Onitilo, A. A. Variability in reexcision following breast conservation surgery. JAMA. 2012;307(5):467-75.
13. Munshi A, Kakkar, S., Bhutani, R., Jalali, R., Budrukkar, A., Dinshaw, K. A. Factors influencing cosmetic outcome in breast conservation. . Clin Oncol (R Coll Radiol). 2009;21(4):285-93.
14. Grant Y, Al-Khudairi R, St John E, Barschkett M, Cunningham D, Al-Mufti R, et al. Patient-level costs in margin re-excision for breast-conserving surgery. Br J Surg. 2019;106(4):384-94.
15. Vettoretto N, Foglia E, Ferrario L, Gerardi C, Molteni B, Nocco U, et al. Could fluorescence-guided surgery be an efficient and sustainable option? A SICE (Italian Society of Endoscopic Surgery) health technology assessment summary. Surgical Endosc. 2020;34(7):3270-84.
16. Fisher B, Redmond C, Poisson R, Margolese R, Wolmark N, Wickerham L, et al. Eight-Year Results of a Randomized Clinical Trial Comparing Total Mastectomy and Lumpectomy with or without Irradiation in the Treatment of Breast Cancer. N Engl J Med. 1989;320(13):822-8.

17. Maloney BW, McClatchy DM, Pogue BW, Paulsen KD, Wells WA, Barth RJ. Review of methods for intraoperative margin detection for breast conserving surgery. J Biomed Opt. 2018;23(10):1-19.
18. Chagpar AB, Killelea BK, Tsangaris TN, Butler M, Stavris K, Li F, et al. A Randomized, Controlled Trial of Cavity Shave Margins in Breast Cancer. N Engl J Med. 2015;373(6):503-10.
19. Leff DR, St John ER, Takats Z. Reducing the Margins of Error During Breast-Conserving Surgery: Disruptive Technologies or Traditional Disruptions? JAMA Surg. 2017;152(6):517-8.
20. Davis KM, Raybon CP, Monga N, Waheed U, Michaels A, Henry C, et al. Image-guided Localization Techniques for Nonpalpable Breast Lesions: An Opportunity for Multidisciplinary Patient-centered Care. Journal of Breast Imaging. 2021;3(5):13.
21. Chan BK, Wiseberg-Firtell JA, Jois RH, Jensen K, Audisio RA. Localization techniques for guided surgical excision of non-palpable breast lesions. Cochrane Database Syst Rev. 2015(12):CD009206.
22. Davey MG, O'Donnell JPM, Boland MR, Ryan ÉJ, Walsh SR, Kerin MJ, et al. Optimal localization strategies for non-palpable breast cancers –A network meta-analysis of randomized controlled trials. Breast. 2022;62:103-13.
23. Kedrzycki MS, Elson DS, Leff DR. Guidance in breast-conserving surgery: tumour localization versus identification. Br J Surg. 2022.
24. St John ER, Al-Khudairi R, Ashrafian H, Athanasiou T, Takats Z, Hadjiminas DJ, et al. Diagnostic Accuracy of Intraoperative Techniques for Margin Assessment in Breast Cancer Surgery: A Meta-analysis. Ann Surg. 2017;265(2):300-10.
25. Tang R, Coopey SB, Buckley JM, Aftreth OP, Fernandez LJ, Brachtel EF, et al. A Pilot Study Evaluating Shaved Cavity Margins with Micro-Computed Tomography: A Novel Method for Predicting Lumpectomy Margin Status Intraoperatively. The Breast Journal. 2013;19(5):485-9.
26. Chang TP, Leff, D. R., Shousha, S., Hadjiminas, D. J., Ramakrishnan, R., Hughes, M. R., Yang, G. Z., & Darzi, A. Imaging breast cancer morphology using probe-based confocal laser endomicroscopy: towards a real-time intraoperative imaging tool for cavity scanning. Breast cancer research and treatment. 2015;153(2):299- 310.
27. Nguyen FT, Zysk, A. M., Chaney, E. J., Kotynek, J. G., Oliphant, U. J., Bellafiore, F. J., Rowland, K. M., Johnson, P. A., & Boppart, S. A. . Intraoperative evaluation of breast tumor margins with optical coherence tomography. Cancer research. 2009;69(22):8790- 6.
28. Mohs A, Mancini MC, Singhal S, Provenzale JM, Leyland-Jones B, Wang MD, et al. Hand-held spectroscopic device for in vivo and intraoperative tumor detection: contrast enhancement, detection sensitivity, and tissue penetration. . Analytical Chemistry. 2021;82(21):9058-65.
29. Schnabel F, Boolbol SK, Gittleman M, Karni T, Tafra L, Feldman S, et al. A randomized prospective study of lumpectomy margin assessment with use of MarginProbe in patients with nonpalpable breast malignancies. Ann Surg Oncol. 2014;21(5):1589-95.
30. Vidya R, Leff DR, Green M, McIntosh, S. A., St John, E., Kirwan, C. C., Romics, L., Cutress, R. I., Potter, S., Carmichael, A., Subramanian, A., O'Connell, R., Fairbrother, P., Fenlon, D., Benson, J., Holcombe, C. Innovations for the future of breast surgery. Br J Surg. 2021;108(8):908-16.
31. Dixon JM, Renshaw, L., Young, O., Kulkarni, D., Saleem, T., Sarfaty, M., Sreenivasan, R., Kusnick, C., Thomas, J., & Williams, L. J. Intra-operative assessment of excised breast tumour margins using ClearEdge imaging device. European journal of surgical oncology. 2016;42(12):1834–40.
32. Kong K, Zaabar, F., Rakha, E., Ellis, I., Koloydenko, A., & Notingher, I. . Towards intra-operative diagnosis of tumours during breast conserving surgery by selective-sampling Raman micro-spectroscopy. Physics in medicine and biology. 2014;59(20):6141- 52.
33. St John ER, Balog J, McKenzie JS, Rossi M, Covington A, Muirhead L, et al. Rapid evaporative ionisation mass spectrometry of electrosurgical vapours for the identification of breast pathology: towards an intelligent knife for breast cancer surgery. Breast Cancer Research. 2017;19(1).

34. Krekel NMA, Haloua MH, Lopes Cardozo AMF, de Wit RH, Bosch AM, de Widt-Levert LM, et al. Intraoperative ultrasound guidance for palpable breast cancer excision (COBALT trial): a multicentre, randomised controlled trial. Lancet Oncol. 2013;14:7.
35. Mallory M, Sagara Y, Aydogan F, DeSantis S, Jayender J, Caragacianu D, et al. Feasibility of Intraoperative Breast MRI and the Role of Prone Versus Supine Positioning in Surgical Planning for Breast Conserving Surgery. The breast journal. 2017;232(6):713-7.
36. Grootendorst MR, Cariati M, Kothari A, Tuch DS, Purushotham A. Cerenkov luminescence imaging (CLI) for image-guided cancer surgery. Clin Transl Imaging. 2016;4(5):353-66.
37. Nagaya T, Nakamura YA, Choyke PL, Kobayashi H. Fluorescence-Guided Surgery. Front Oncol. 2017;7:314.
38. Leiloglou M, Kedrzycki MS, Chalau V, Thiruchelvam PTR, Darzi A, Elson DS, et al. Versatility in Fluorescence Guided Surgery with the GLOW Camera System. Surgical Life: The Journal of the Association of Surgeons of Great Britain and Ireland. 2021;59:32-9.
39. Croce AC, Bottiroli G. Autofluorescence spectroscopy and imaging: a tool for biomedical research and diagnosis. Eur J Histochem. 2014;58(4):2461.
40. Nagaya T, Nakamura, Y. A., Choyke, P. L., & Kobayashi, H. . Fluorescence-Guided Surgery. Frontiers in oncology. 2017;7(314).
41. Kedrzycki MS, Elson DS, Leff DR. Guidance in breast-conserving surgery: tumour localization versus identification. British Journal of Surgery. 2023;110(8):920-2.
42. Smith BL, Lanahan CR, Specht MC, Kelly BN, Brown CL, Strasfeld D, et al. Feasibility Study of a Novel Protease-Activated Fluorescent Imaging System for Real-Time, Intraoperative Detection of Residual Breast Cancer in Breast Conserving Surgery. Ann Surg Oncol 2020;27:7.
43. Tong M, Guo W. Indocyanine green fluorescence-guided lumpectomy of nonpalpable breast cancer versus wire-guided excision: A randomized clinical trial. . Breast J. 2019;25:3.
44. Veys I, Pop CF, Barbieux R, Moreau M, Noterman D, De Neubourg F, et al. ICG fluorescence imaging as a new tool for optimization of pathological evaluation in breast cancer tumors after neoadjuvant chemotherapy. PLoS One. 2018;13(5):e0197857.
45. Keating J, Tchou J, Okusanya O, Fisher C, Batiste R, Jiang J, et al. Identification of breast cancer margins using intraoperative near-infrared imaging. J Surg Oncol. 2016;113(5):508-14.
46. Tummers QRJG, Hoogstins CES, Gaarenstroom KN, de Kroon CD, van Poelgeest MIE, Vuyk J, et al. Intraoperative imaging of folate receptor alpha positive ovarian and breast cancer using the tumor specific agent EC17. Oncotarget. 2016;7(22):32144-55.
47. Park MH, Lim W, Jo D, Jung JS, Kim S, Kim J, et al. Rapid Differential Diagnosis of Breast Microcalcification Using Targeted Near-Infrared Fluorophores. Adv Healthc Mater. 2018;7(7).
48. Tummers QRJG, Verbeek FPR, Schaafsma BE, Boonstra MC, Van Der Vorst JR, Liefers GJ, et al. Real-time intraoperative detection of breast cancer using near-infrared fluorescence imaging and Methylene Blue. Eur J Surg Oncol. 2014;40(7):850-8.
49. Lee EG, Kim SK, Han JH, Lee DE, Jung SY, S L. Surgical outcomes of localization using indocyanine green fluorescence in breast conserving surgery: a prospective study. Sci Rep. 2021;11(9997).
50. Leiloglou M. Fluorescence for Image and Spectrum Guided Breast-Conserving Surgery: Imperial College London; 2022.
51. Dramićanin T, Dramićanin M. Using Fluorescence Spectroscopy to Diagnose Breast Cancer. In: Stauffer MT, editor. Applications of Molecular Spectroscopy to Current Research in the Chemical and Biological Sciences: IntechOpen; 2016.
52. Lammers T, Kiessling, F., Hennink, W. E., & Storm, G. Drug targeting to tumors: principles, pitfalls and (pre-) clinical progress. J Control Release 2012;161(2):175-87.
53. Morshed M, Chowdhury EH. Gene Delivery and Clinical Applications. Encyclopedia of Biomedical Engineering: Elsevier; 2019. p. 345-51.
54. Bamrungsap S, Zhao Z, Chen T, Wang L, Li C, Fu T, et al. A Focus on Nanoparticles as a Drug Delivery System. Nanomedicine. 2012;7:1253-71.

55. Pottier R, Krammer B, Stepp H, Baumgartner R. Photodynamic Therapy with ALA: A Clinical Handbook. Hader D, Jori G, editors. Cambridge, UK: RSC Publishing; 2006. 276 p.
56. Stummer W, Pichlmeier U, Meinel T, Wiestler OD, Zanella F, Reulen H-J. Fluorescence-guided surgery with 5-aminolevulinic acid for resection of malignant glioma: a randomised controlled multicentre phase III trial. The Lancet Oncology. 2006;7(5):392-401.
57. Gliolan 30mg/ml powder for oral solution. 2018 [Available from: https://www.medicines.org.uk/emc/product/4638/smpc.
58. Sachar M, Anderson KE, Ma X. Protoporphyrin IX: the Good, the Bad, and the Ugly. J Pharmacol Exp Ther. 2016;356(2):267-75.
59. Ottolino-Perry K, Shahid A, DeLuca S, Son V, Sukhram M, Meng F, et al. Intraoperative fluorescence imaging with aminolevulinic acid detects grossly occult breast cancer: a phase II randomized controlled trial. Breast Cancer Res 2021;23(72).
60. Marshall MV, Rasmussen JC, Tan IC, Aldrich MB, Adams KE, Wang X, et al. Near-Infrared Fluorescence Imaging in Humans with Indocyanine Green: A Review and Update. Open Surg Oncol J. 2010;2(2):12-25.
61. Ginimuge P, Jyothi S. Methylene Blue: Revisited. J Anaesthesiol Clin Pharmacol. 2010;26(4):517-20.
62. Klijn J, Berns P, Schmitz P, Foekens J. The Clinical Significance of Epidermal Growth Factor Receptor (EGF-R) in Human Breast Cancer: A Review on 5232 Patients. Endocr Rev. 1992;13.
63. Samkoe KS, Shahzad Sardar H, Gunn JR, Feldwisch J, Linos K, Henderson E, et al. Measuring microdose ABY-029 fluorescence signal in a primary human soft-tissue sarcoma resection. SPIE2019.
64. Hekman MC, Rijpkema M, Muselaers CH, Oosterwijk E, Hulsbergen-Van de Kaa CA, Boerman OC, et al. Tumor-targeted dual-modality imaging to improve intraoperative visualization of clear cell renal cell carcinoma: A first in man study. Theranostics. 2018;8(8):2161-70.
65. Boogerd LSF, Hoogstins CES, Schaap DP, Kusters M, Handgraaf HJM, van der Valk MJM, et al. Safety and effectiveness of SGM-101, a fluorescent antibody targeting carcinoembryonic antigen, for intraoperative detection of colorectal cancer: a dose-escalation pilot study. Lancet Gastroenterol Hepatol. 2018;3(3):181-91.
66. Hoogstins CES, Boogerd LSF, Mulder BGS, Mieog JSD, Swijnenburg RJ, van de Velde CJH, et al. Image-Guided Surgery in Patients with Pancreatic Cancer: First Results of a Clinical Trial Using SGM-101, a Novel Carcinoembryonic Antigen-Targeting, Near-Infrared Fluorescent Agent. Ann Surg Oncol. 2018;25(11):3350-7.
67. Pansare V, Hejazi S, Faenza W, Prud'homme RK. Review of Long-Wavelength Optical and NIR Imaging Materials: Contrast Agents, Fluorophores and Multifunctional Nano Carriers. Chem Mater. 2012;24(5):812-27.
68. Kamath SD, Bhat RA, Ray S, Mahato KK. Autofluorescence of normal, benign, and malignant ovarian tissues: a pilot study. Photomedicine and laser surgery. 2009;27(2):325–35.
69. Tummers WS, Warram JM, van den Berg NS, Miller SE, Swijnenburg RJ, Vahrmeijer AL, et al. Recommendations for reporting on emerging optical imaging agents to promote clinical approval. Theranostics. 2018;8(19):5336-47.
70. Li D, Zhang J, Chi C, Xiao X, Wang J, Lang L, et al. First-in-human study of PET and optical dual-modality image-guided surgery in glioblastoma using (68)Ga-IRDye800CW-BBN. Theranostics. 2018;8(9):2508-20.
71. Ladner D, Steiner R, Allemann J, Haller U, Walt H. Photodynamic diagnosis of breast tumors after oral application of aminolevulinic acid. . Br J Cancer. 2001;84:33-7.
72. Millon SR, Ostrander JH, Yazdanfar S, Brown JQ, Bender JE, Rajeha A, et al. Preferential accumulation of 5-aminolevulinic acid-induced protoporphyrin IX in breast cancer: a comprehensive study on six breast cell lines with varying phenotypes. J Biomed Opt. 2010;15(1):018002.
73. Sturm MB, Joshi BP, Lu S, Piraka C, Khondee S, Elmunzer BJ, et al. Targeted Imaging of Esophageal Neoplasia with a Fluorescently Labeled Peptide: First-in-Human Results. Science Translational Medicine. 2013;5(184):184ra61-ra61.

74. Miampamba M, Liu J, Harootunian A, Gale AJ, Baird S, Chen SL, et al. Sensitive in vivo Visualization of Breast Cancer Using Ratiometric Protease-activatable Fluorescent Imaging Agent, AVB-620. Theranostics. 2017;7(13):3369-86.
75. Unkart JT, Chen SL, Gonzalez JE, Harootunian A, Wallace AM. Intraoperative tumor detection using a ratiometric activatable fluorescent peptide: A first-in human phase i study allows tumors to be visualized in the operating room. Cancer Research Conference: 39th Annual CTRC AACR San Antonio Breast Cancer Symposium United States. 2017;77(4 Supplement 1).
76. Unkart JT, Chen SL, Wapnir IL, Gonzalez JE, Harootunian A, Wallace AM. Intraoperative Tumor Detection Using a Ratiometric Activatable Fluorescent Peptide: A First-in-Human Phase 1 Study. Ann Surg Oncol. 2017;24(11):3167-73.
77. McCannel T. Two Year Results of a Phase 1/2 Open-Label Clinical Trial of AU-011 for the Treatment of Small to Medium Choroidal Melanoma Aura Biosciences: Aura Biosciences Inc; 2019 [Available from: http://www.aurabiosciences.com/news-archive/2019/4/22/aura-biosciences-to-present-two-year-phase-1b2-clinical-data-for-au-011-at-the-association-for-research-in-vision-and-ophthalmology-arvo-2019-annual-meeting.
78. Koch M, De Jong JS, Glatz J, Symvoulidis P, Lamberts LE, Adams ALL, et al. Threshold Analysis and Biodistribution of Fluorescently Labeled Bevacizumab in Human Breast Cancer. Cancer Res. 2017;77(3):623-31.
79. Koller M, Qiu SQ, Linssen MD, Jansen L, Kelder W, de Vries J, et al. Implementation and benchmarking of a novel analytical framework to clinically evaluate tumor-specific fluorescent tracers. Nat Commun. 2018;9(1):3739.
80. Lamberts LE, Koch M, de Jong JS, Adams ALL, Glatz J, Kranendonk MEG, et al. Tumor-Specific Uptake of Fluorescent Bevacizumab-IRDye800CW Microdosing in Patients with Primary Breast Cancer: A Phase I Feasibility Study. Clin Cancer Res. 2016;23(11):2730-41.
81. Patil CG, Walker DG, Miller DM, Butte P, Morrison B, Kittle DS, et al. Phase 1 Safety, Pharmacokinetics, and Fluorescence Imaging Study of Tozuleristide (BLZ-100) in Adults With Newly Diagnosed or Recurrent Gliomas. Neurosurgery. 2019;85(4):E641-E9.
82. Dintzis SM, Hansen S, Harrington KM, Tan LC, Miller DM, Ishak L, et al. Real-time Visualization of Breast Carcinoma in Pathology Specimens From Patients Receiving Fluorescent Tumor-Marking Agent Tozuleristide. Arch Pathol Lab Med. 2018.
83. Baik FM, Hansen S, Knoblaugh SE, Sahetya D, Mitchell RM, Xu C, et al. Fluorescence Identification of Head and Neck Squamous Cell Carcinoma and High-Risk Oral Dysplasia With BLZ-100, a Chlorotoxin-Indocyanine Green Conjugate. JAMA Otolaryngol Head Neck Surg. 2016;142(4):330-8.
84. Nakopoulou L, Tsirmpa I, Alexandrou P, Louvrou A, Ampela C, Markaki S, et al. MMP-2 protein in invasive breast cancer and the impact of MMP-2/TIMP-2 phenotype on overall survival. Breast Cancer Res Treat. 2003;77:145-55.
85. Tummers WS, Miller SE, Teraphongphom NT, Gomez A, Steinberg I, Huland DM, et al. Intraoperative Pancreatic Cancer Detection using Tumor-Specific Multimodality Molecular Imaging. Ann Surg Oncol. 2018;25(7):1880-8.
86. Warram JM, de Boer E, van Dam GM, Moore LS, Bevans SL, Walsh EM, et al. Fluorescence imaging to localize head and neck squamous cell carcinoma for enhanced pathological assessment. J Pathol Clin Res. 2016;2(2):104-12.
87. O'Shannessy D, Somers E, Maltzman J, Smale R, Fu Y. Folate receptor alpha (FRA) expression in breast cancer- identification of a new molecular subtype and assication with triple negative disease. Springerplus. 2012;1.
88. Esfahani SA, Heidari P, Kim SA, Ogino S, Mahmood U. Optical Imaging of Mesenchymal Epithelial Transition Factor (MET) for Enhanced Detection and Characterization of Primary and Metastatic Hepatic Tumors. Theranostics. 2016;6(12):2028-38.
89. EMI-137 Injection: Investigators Brochure [unpublished Brochure]. Edinburgh Molecular Imaging Ltd. 2018.

90. Pop C, Veys I, Vankerckhove S, Barbieux R, Chintinne M, Moreau M, et al. Absence of residual fluorescence in the surgical bed at near-infrared fluorescence imaging predicts negative margins at final pathology in patients treated with breast-conserving surgery for breast cancer. Eur J Surg Oncol. 2021;47(2):269-75.
91. Mito JK, Ferrer JM, Brigman BE, Lee CL, Dodd RD, Eward WC, et al. Intraoperative detection and removal of microscopic residual sarcoma using wide-field imaging. Cancer. 2012;118(21):5320-30.
92. Whitley MJ, Weissleder R, Kirsch DG. Tailoring Adjuvant Radiation Therapy by Intraoperative Imaging to Detect Residual Cancer. Semin Radiat Oncol. 2015;25(4):313-21.
93. Smith BL, Gadd MA, Lanahan CR, Rai U, Tang R, Rice-Stitt T, et al. Real-time, intraoperative detection of residual breast cancer in lumpectomy cavity walls using a novel cathepsin-activated fluorescent imaging system. Breast Cancer Res Treat. 2018;171(2):413-20.
94. Whitley MJ, Cardona DM, Lazarides AL, Spasojevic I, Ferrer JM, Cahill J, et al. A mouse-human phase 1 co-clinical trial of a protease-activated fluorescent probe for imaging cancer. Sci Transl Med. 2016;8(320):320ra4.
95. Hoogstins CES, Tummers Q, Gaarenstroom KN, de Kroon CD, Trimbos J, Bosse T, et al. A Novel Tumor-Specific Agent for Intraoperative Near-Infrared Fluorescence Imaging: A Translational Study in Healthy Volunteers and Patients with Ovarian Cancer. Clin Cancer Res. 2016;22(12):2929-38.
96. Okusanya O, DeJesus E, Jiang J, Judy R, Venegas OG, Deshpande G, et al. Intraoperative Molecular Imaging Can Identify Lung Adenocarcinomas during Pulmonary Resection. J Thorac Cardiovasc Surg 2015;150:28-35.
97. Boogerd LSF, Hoogstins CES, Gaarenstroom KN, de Kroon CD, Beltman JJ, Bosse T, et al. Folate receptor-α targeted near-infrared fluorescence imaging in high-risk endometrial cancer patients: A tissue microarray and clinical feasibility study. Oncotarget. 2018;9(1):791-801.
98. Hoogstins CE, Tummers QR, Cohen AF, Van De Velde CJ, Low PS, Vahrmeijer AL, et al. A first in human study with the first tumor-specific agent with fluorescence in the NIR spectrum for image guided surgery: A translational study. Molecular Imag Biol. 2016;1:S169.
99. Gao RW, Teraphongphom N, de Boer E, van den Berg NS, Divi V, Kaplan MJ, et al. Safety of panitumumab-IRDye800CW and cetuximab-IRDye800CW for fluorescence-guided surgical navigation in head and neck cancers. Theranostics. 2018;8(9):2488-95.
100. Vuijk FA, Hilling DE, Mieog JSD, Vahrmeijer AL. Fluorescent-guided surgery for sentinel lymph node detection in gastric cancer and carcinoembryonic antigen targeted fluorescent-guided surgery in colorectal and pancreatic cancer. J Surg Oncol. 2018;118(2):315-23.
101. Ottolino-Perry K, Shahid A, DeLuca S, Son V, Sukhram M, Meng F, et al. Intraoperative fluorescence imaging with aminolevulinic acid detects grossly occult breast cancer: a phase II randomized controlled trial. Breast Cancer Res. 2021;23(1):72.
102. Ballardini B, Santoro L, Sangalli C, Gentilini O, Renne G, Lissidini G, et al. The indocyanine green method is equivalent to the (9)(9)mTc-labeled radiotracer method for identifying the sentinel node in breast cancer: a concordance and validation study. Eur J Surg Oncol. 2013;39(12):1332-6.
103. Guo J, Yang H, Wang S, Cao Y, Liu M, Xie F, et al. Comparison of sentinel lymph node biopsy guided by indocyanine green, blue dye, and their combination in breast cancer patients: a prospective cohort study. World J Surg Oncol. 2017;15(1):196.
104. Griffiths M, Chae M, Rozen W. Indocyanine green-based fluorescent angiography in breast reconstruction. Gland Surg. 2016;5(2).
105. Grosenick D, Rinneberg H, Cubbedo R, Taroni P. Review of optical breast imaging and spectroscopy. J Biomed Opt. 2016;21.
106. Chorfi H, Ayadi K, Bouamama L, Boufendi L. Contribution to the study of cancer tissues by light scattering. Optik. 2020;221.

107. Yhee JY, Son S, Son S, Joo MK, Kwon IC. The EPR Effect in Cancer Therapy. In: In: Bae Y. MR, Park K. (eds), editor. Cancer Targeted Drug Delivery New York: Springer; 2013.
108. Pu Y, Wang W, Yang Y, Alfano RR. Native fluorescence spectra of human cancerous and normal breast tissues analyzed with non-negative constraint methods. Appl Opt. 2013;52(6):1293-301.
109. Chen Y, Cairns, R., Papandreou, I., Koong, A., Denko, N. C. . Oxygen consumption can regulate the growth of tumors, a new perspective on the Warburg effect. . PLoS One. 2009;4(9).
110. Vaupel P, Schlenger K, Knoop C, Höckel M. Oxygenation of human tumors: evaluation of tissue oxygen distribution in breast cancers by computerized O2 tension measurements. Cancer Res. 1991;51:3316-22.
111. Kedrzycki MS, Leiloglou M, Ashrafian H, Jiwa N, Thiruchelvam PTR, Elson DS, et al. Meta-analysis Comparing Fluorescence Imaging with Radioisotope and Blue Dye-Guided Sentinel Node Identification for Breast Cancer Surgery. Ann Surg Oncol. 2020.
112. He K, Chi C, Kou D, Huang W, Wu J, Wang Y, et al. Comparison between the indocyanine green fluorescence and blue dye methods for sentinel lymph node biopsy using novel fluorescence image-guided resection equipment in different types of hospitals. Transl Res. 2016;178:74-80.
113. Mieog JS, Troyan SL, Hutteman M, Donohoe KJ, van der Vorst JR, Stockdale A, et al. Toward optimization of imaging system and lymphatic tracer for near-infrared fluorescent sentinel lymph node mapping in breast cancer. Ann Surg Oncol. 2011;18(9):2483-91.
114. Pitsinis V, Provenzano E, Kaklamanis L, Wishart GC, Benson JR. Indocyanine green fluorescence mapping for sentinel lymph node biopsy in early breast cancer. Surg Oncol. 2015;24(4):375-9.
115. Polom K, Murawa D, Nowaczyk P, Rho YS, Murawa P. Breast cancer sentinel lymph node mapping using near infrared guided indocyanine green and indocyanine green human serum albumin in comparison with gamma emitting radioactive colloid tracer. Eur J Surg Oncol. 2012;38(2):137-42.
116. Samorani D, Fogacci T, Panzini I, Frisoni G, Accardi FG, Ricci M, et al. The use of indocyanine green to detect sentinel nodes in breast cancer: a prospective study. Eur J Surg Oncol. 2015;41(1):64-70.
117. Schaafsma BE, Verbeek FPR, Rietbergen DDD, Van Der Hiel B, Van Der Vorst JR, Liefers GJ, et al. Clinical trial of combined radio- and fluorescence-guided sentinel lymph node biopsy in breast cancer. Br J Surg. 2013;100(8):1037-44.
118. Somashekhar SP, Kumar CR, Ashwin KR, Zaveri SS, Jampani A, Ramya Y, et al. Can Low-cost Indo Cyanine Green Florescence Technique for Sentinel Lymph Node Biopsy Replace Dual Dye (Radio-colloid and Blue Dye) Technique in Early Breast Cancer: A Prospective Two-arm Comparative Study. Clin Breast Cancer. 2020.
119. Sorrentino L, Sartani A, Pietropaolo G, Bossi D, Mazzucchelli S, Truffi M, et al. A Novel Indocyanine Green Fluorescence-Guided Video-Assisted Technique for Sentinel Node Biopsy in Breast Cancer. World J Surg. 2018;42(9):2815-24.
120. Valente SA, Al-Hilli Z, Radford DM, Yanda C, Tu C, Grobmyer SR. Near Infrared Fluorescent Lymph Node Mapping with Indocyanine Green in Breast Cancer Patients: A Prospective Trial. J Am Coll Surg. 2019;228(4):672-8.
121. van der Vorst JR, Schaafsma BE, Verbeek FP, Hutteman M, Mieog JS, Lowik CW, et al. Randomized comparison of near-infrared fluorescence imaging using indocyanine green and 99(m) technetium with or without patent blue for the sentinel lymph node procedure in breast cancer patients. Ann Surg Oncol. 2012;19(13):4104-11.
122. Meric-Bernstam F, Rasmussen JC, Krishnamurthy S, Tan IC, Zhu B, Wagner JL, et al. Toward nodal staging of axillary lymph node basins through intradermal administration of fluorescent imaging agents. Biomed Opt Express. 2013;13(5):183-96.
123. Bunn S, Graham M. Supply of Medical Radioisotopes: UK Parliament; 2017 [Available from: https://post.parliament.uk/research-briefings/post-pn-0558/.

124. Sanidas EE, de Bree E, Tsiftsis DD. How many cases are enough for accreditation in sentinel lymph node biopsy in breast cancer? Am J Surg. 2003;185(3):202-10.
125. Papathemelis T, Jablonski E, Scharl A, Hauzenberger T, Gerken M, Klinkhammer-Schalke M, et al. Sentinel Lymph Node Biopsy in Breast Cancer Patients by Means of Indocyanine Green Using the Karl Storz VITOM(R) Fluorescence Camera. Biomed Res Int. 2018;2018:6251468.
126. Hara Y, Otsubo, R., Shinohara, S., Morita, M., Kuba, S., Matsumoto, M., Yamanouchi, K., Yano, H., Eguchi, S., Nagayasu, T. Lymphedema After Axillary Lymph Node Dissection in Breast Cancer: Prevalence and Risk Factors-A Single-Center Retrospective Study. Lymphat Res Bio. 2022;20(6):600-6.
127. DiSipio T, Rye S, Newman B, Hayes S. Incidence of unilateral arm lymphoedema after breast cancer: a systematic review and meta-analysis. Lancet Oncol. 2013;14(6):500-15.
128. Auba C, Marre D, Rodríguez-Losada G. Lymphaticovenular anastomoses for lymphedema treatment: 18 months postoperative outcomes Microsurgery. 2012;32(4):261-8.
129. Levy AS, Murphy, A. I., Ishtihar, S., Peysakhovich, A., Taback, B., Grant, R. T., Ascherman, J. A., Feldman, S., Rohde, C. H. Lymphatic Microsurgical Preventive Healing Approach for the Primary Prevention of Lymphedema: A 4-Year Follow-Up. Plast Reconstructr Surg. 2023;151(2):413-20.
130. Hirche C, Mohr Z, Kneif S, Murawa D, Hunerbein M. High rate of solitary sentinel node metastases identification by fluorescence-guided lymphatic imaging in breast cancer. Journal of Surgical Oncology. 2012;105(2):162-4.
131. Guo W, Zhang L, Ji J, Gao W, Liu J, Tong M. Breast cancer sentinel lymph node mapping using near-infrared guided indocyanine green in comparison with blue dye. Tumour Biol. 2014;35(4):3073-8.
132. Hojo T, Nagao T, Kikuyama M, Akashi S, Kinoshita T. Evaluation of sentinel node biopsy by combined fluorescent and dye method and lymph flow for breast cancer. Breast. 2010;19(3):210-3.
133. Ogasawara Y, Ikeda H, Takahashi M, Kawasaki K, Doihara H. Evaluation of breast lymphatic pathways with indocyanine green fluorescence imaging in patients with breast cancer. World J Surg. 2008;32(9):1924-9.
134. Hirche C, Engel H, Hirche Z, Doniga S, Herold T, Kneser U, et al. Real-time lymphography by indocyanine green fluorescence: improved navigation for regional lymph node staging. Ann Plast Surg. 2014;73(6):701-5.
135. Breslin TM, Xu F, Palmer GM, Zhu C, Gilchrist KW, Ramanujam N. Autofluorescence and diffuse reflectance properties of malignant and benign breast tissues. Ann Surg Oncol. 2004;11(1):65-70.
136. Intes X, Ripoll J, Chen Y, Nioka S, Yodh AG, Chance B. In vivo continuous-wave optical breast imaging enhanced with Indocyanine Green. Med Phys. 2003;30(6):1039-47.
137. Zhang C, Mao Y, Wang K, Tian J. Methylene Blue-Based Near-Infrared Fluorescence Imaging for Breast Cancer Visualization in Resected Human Tissues. Technol Cancer Res Treat. 2019;36(15).
138. Smith BL, Hunt KK, Carr D, Blumencranz P, Hwang E, Gadd MA, et al., editors. Intraoperative Pegulicianine Fluorescence Guidance for Tumor Detection During Lumpectomy Surgery for Stage 0-III Breast Cancer. American Society of Breast Surgeons; 2023; Boston Massachusetts.
139. Norton N, Youssef B, Hillman DW, Nassar A, Geiger XJ, Necela BM, et al. Folate receptor alpha expression associates with improved disease-free survival in triple negative breast cancer patients. NPJ Breast Cancer. 2020;6(4).
140. Masuda H, Zhang D, Bartholomeusz C, Doihara H, Hortobagyi GN, Ueno NT. Role of Epidermal Growth Factor Receptor in Breast Cancer. Breast Cancer Res Treat. 2012;136.
141. Kedrzycki MS, Leiloglou M, Thiruchelvam PTR, Elson DS, Leff DR. Fluorescence guided surgery in breast cancer: A systematic review of the literature. Eur J Surg Oncol. 2021;47(5).
142. Schaafsma BE, Mieog JSD, Hutteman M, Van der Vorst JR, Kuppen PJK, Lowik C, et al. The Clinical Use of Indocyanine Green as a Near-Infrared Fluorescent Contrast Agent for Image-Guided Oncologic Surgery. J Surg Oncol. 2011;104(3):323-32.

143. Leiloglou M, Kedrzycki MS, Chalau V, Thiruchelvam PTR, Darzi AW, Leff DR, et al. Tissue texture extraction in indocyanine green fluorescence imaging for breast-conserving surgery. J Phys D: Appl Phys. 2021;54(19).
144. Rollakanti K, Kanick S, Davis S, Pogue BW, Maytin E. Techniques for fluorescence detection of protoporphyrin IX in skin cancers associated with photodynamic therapy. Photonics Lasers Med. 2013;2:287-303.
145. Markwardt NA, Haj-Hosseini N, Hollnburger B, Stepp H, Zelenkov P, Ruhm A. 405 nm versus 633 nm for protoporphyrin IX excitation in fluorescence-guided stereotactic biopsy of brain tumors. J Biophotonics. 2016;9(9):901-12.
146. Croizat G, Gregor A, Joniova J, Gerelli E, Wagnières G. Identification of excimer delayed fluorescence by Protoporphyrin IX: A novel access to local chromophore concentration? Journal of photochemistry and photobiology B, Biology. 2022;229(112408).
147. Summary of Product Characteristics- Verdye. In: GmbH DG, editor. 2007.
148. Poellinger A, Burock, S., Grosenick, D., Hagen, A., Lüdemann, L., Diekmann, F., Engelken, F., Macdonald, R., Rinneberg, H., & Schlag, P. M. Breast cancer: early- and late-fluorescence near-infrared imaging with indocyanine green--a preliminary study. Radiology. 2011;258(2):409-16.
149. InformedHealth.org. In brief: What does blood do? Internet: Institute for Quality and Efficiency in Health Care (IQWiG); 2006 [cited 2024 May 9]. Available from: https://www.ncbi.nlm.nih.gov/books/NBK279392/.
150. Kedrzycki MS, Leiloglou M, Chalau V, Chiarini N, Thiruchelvam PTR, Hadjiminas DJ, et al. The Impact of Temporal Variation in Indocyanine Green Administration on Tumor Identification During Fluorescence Guided Breast Surgery. Ann Surg Oncol. 2021;28:5617-25.
151. Kedrzycki MS, Leiloglou M, Chalau V, Lin J, Thiruchelvam PTR, Elson DS, et al., editors. Guiding Light to Optimize Wide Local Excisions: The "GLOW" Study. The American Society of Breast Surgeons Official Proceedings, Volume XXII 2021 Annual Meeting Scientific Session Abstracts; 2021: Ann Surg Oncol.
152. Leiloglou M, Kedrzycki MS, Chalau V, Chiarini N, Thiruchelvam PTR, Hadjiminas DJ, et al. Indocyanine green fluorescence image processing techniques for breast cancer macroscopic demarcation. Sci Rep. 2022;12
153. Surgery TTotAoB. Margin Width in Breast Conservation Surgery. In: Surgery AoB, editor. online: Association of Breast Surgery; 2015. p. 1-2.
154. Bos R, van Der Hoeven JJ, van Der Wall E, van Der Groep P, van Diest PJ, Comans EF, et al. Biologic correlates of (18)fluorodeoxyglucose uptake in human breast cancer measured by positron emission tomography. J Clin Oncol. 2002;20(2):379-87.
155. Baba S, Isoda T, Maruoka Y, Kitamura Y, Sasaki M, Yoshida T, et al. Diagnostic and prognostic value of pretreatment SUV in 18 F-FDG/PET in breast cancer: comparison with apparent diffusion coefficient from diffusion-weighted MR imaging J Nucl Med. 2014;55(5):736-42.
156. Navone N, Polo C, Firsardi A, Andrade N, Battle A. Heme Biosynthesis in Human Breast Cancer- Mimetic 'in Vitro' studies and some heme enzymic activity levels. Int J Biochem. 1990;22:1407-11.
157. Yang X, Li W, Palasuberniam P, Myers KA, Wang C, Chen B. Effects of Silencing Heme Biosynthesis Enzymes on 5-Aminolevulinic Acid-mediated Protoporphyrin IX Fluorescence and Photodynamic Therapy. Photochem Photobiol. 2015;91(4):923-30.
158. Palasuberniam P, Yang X, Kraus D, Jones P, Myers KA, Chen B. ABCG2 transporter inhibitor restores the sensitivity of triple negative breast cancer cells to aminolevulinic acid-mediated photodynamic therapy. Sci Rep. 2015;5:13298.
159. Gu L, Yue X, Zhong HZ, Mei K, Wang D. A new technique of quantifying protoporphyrin IX in microbial cells in seawater. Front Mar Sci. 2022;9.
160. Krammer B, Plaetzer K. ALA and its clinical impact from benchside to bedside. Photochem Photobiol Sci. 2008;7:283-9.

161. Nokes B, Apel M, Jones C, Brown G, Lang JE. Aminolevulinic acid (ALA): photodynamic detection and potential therapeutic applications. J Surg Res. 2013;181(2):262-71.
162. Loh C, MacRobert A, Bedwell J, Regulal J, Krasner N, Bown S. Oral versus intravenous administration of 5-aminolaevulinic acid for photodynamic therapy. Br J Cancer. 1993;68:41-51.
163. Qumseya B, Wolfsen D. Photodynamic Therapy for Barrett's Esophagus and Esophageal Carcinoma. Clin Endosc. 2013;46:30-7.
164. Kedrzycki MS, Leiloglou M, Chalau V, Shanthakumar D, Thiruchelvam PTR, Elson DS, et al. 5-ALA induced fluorescence for tumor visualization in breast-conserving surgery: Part 2 of the "GLOW" study. American Association of Breast Surgeons. The American Society of Breast Surgeons Official Proceedings, Volume XXIV 2023 Annual Meeting Scientific Session Abstracts Ann Surg Oncol; 2023. p. 259-664.
165. Tang SS, Kaptanis S, Haddow JB, Mondani G, Elsberger B, Tasoulis MK, et al. Current margin practice and effect on re-excision rates following the publication of the SSO-ASTRO consensus and ABS consensus guidelines: a national prospective study of 2858 women undergoing breast-conserving therapy in the UK and Ireland. Eur J Cancer. 2017;84:9.
166. Kedrzycki MS, Leiloglou M, Chalau V, Shanthakumar D, Thiruchelvam PTR, Elson DS, et al. Fluorescence and Multispectral Imaging in Breast Conserving Surgery – Proof of Concept Trial. The American Society of Breast Surgeons. The American Society of Breast Surgeons Official Proceedings, Volume XXIV 2023 Annual Meeting Scientific Session Abstracts: Ann Surg Oncol; 2023. p. 529-664.
167. Wang K, Ke Q, Lin L, Han L, Wang X, Li B, et al. Depth-dependent fluorescence properties of protoporphyrin IX in epithelial tissue. J Biomed Opt.21(10).
168. Aminolevulinic acid, CID=137 [cited 2019 June 12]. Available from: https://pubchem.ncbi.nlm.nih.gov/compound/Aminolevulinic-acid.
169. Evans AJ, James J. Overview of Radiologic Aspects of Breast Disease: Elsevier; 2011.
170. Bitencourt AG, Graziano L, Osório CA, Guatelli CS, Souza JA, Mendonça MH, et al. MRI Features of Mucinous Cancer of the Breast: Correlation With Pathologic Findings and Other Imaging Methods. American Journal of Roentgenology. 2016;206(2):238–46.

Appendix 1: Developing a Fluorophore

Nonspecific agents such as ICG lack in sensitivity and specificity, it is not sufficiently accurate as to be adopted into clinical practice for BCS. Therefore, the need to identify a specific target in breast cancer and develop a probe to facilitate FGS is clearly necessary. However, identifying a target which addresses the heterogeneity of breast cancer remains unsolved.

This work is done in collaboration with Professor Tate and his team at the biomedical science department. The team have developed potent and selective probes for several members of the kallikrein family of serine proteases that are involved in many cancers and have successfully converted some into quenched fluorescence probes that could be employed in FGS.

Given this work is exploratory in enzymatic overexpression in breast cancer, 100 paired (tumour and normal) samples were used to:

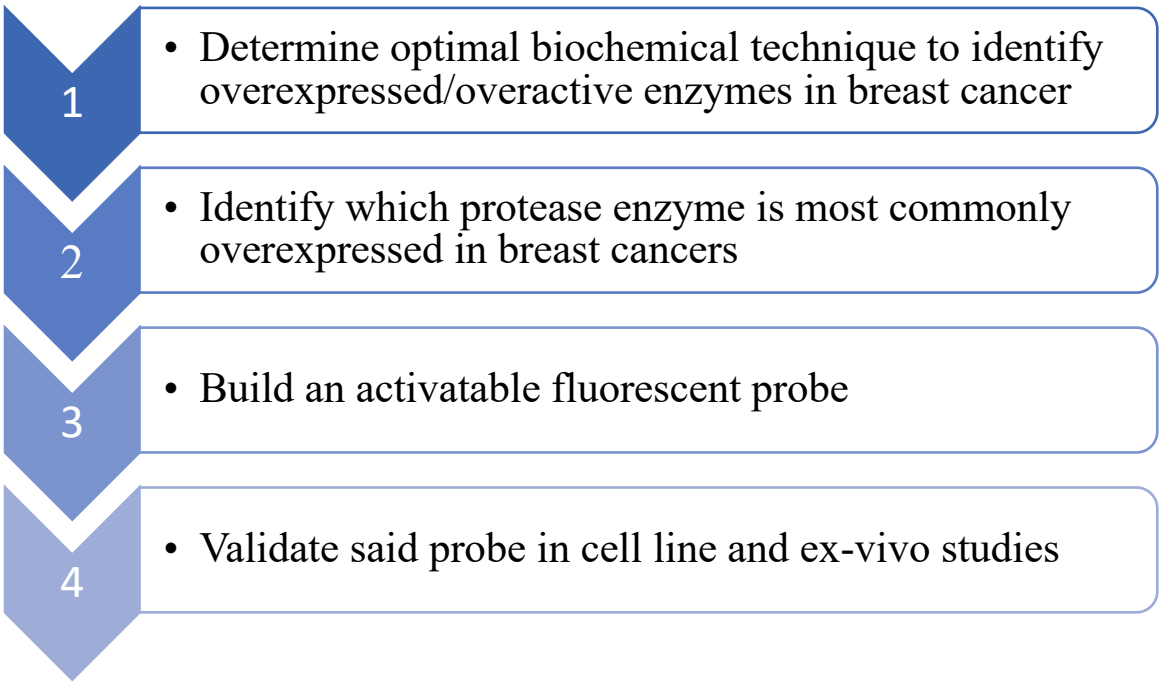


Figure 45: Flowchart of enzyme activated probe development process

With regards to step 1, the 3 biochemical techniques which were evaluated for identification of overexpressed/overactive enzymes were:

- Western blot (gel electrophoresis followed by antibody probing)
- Mass spectrometry (measuring the mass-to-charge ratio (m/z) of 1 or more molecules)
- Hybrid Combinatorial Substrate Library (HyCoSuL) to screen supernatant against a library of tetrapeptides which release fluorescence upon cleavage.

The above analysis determined that the HyCoSuL technique is optimal.

The team identified 2 enzymes present within breast cancer cells. The enzyme cathepsin is already known and has been undergoing clinical trials for FGS in BCS (93). The second enzyme will be revealed in a future publication.

Prof Tate's team are currently in stage 3, building an activatable probe (**Figure 45**). To achieve a high level of specificity, the probe will require both enzymes to be present. This will enable cleavage of their respective connections to quenchers (molecules that suppress fluorescence). Once the probe has both bonds cleaved it will be activated and fluoresce.

Appendix 2: Our Patient and Public Involvement Journey

Our patient and public involvement journey was recently published on the Imperial College London blog for the Patient Experience Research Centre. It highlights the insight we gained through our many interactions and fuelled our efforts to address this prevalent issue that affects so many women.

https://blogs.imperial.ac.uk/perc/2023/07/14/lighting-the-way-with-fluorescence-guided-surgery-patient-and-public-involvement-in-our-phds/

Lighting the way with fluorescence guided surgery Patient and Public Involvemend in our PhDs

Naomi Asantewa-Sechereh
14 July 2023

In conversation with: Maria Leiloglou, Research Associate in the Hamlyn Centre, Imperial College London; and Martha Kedrzycki, Academic Surgical Registrar within the Imperial College Healthcare NHS Trust.

What is GLOW?
GLOW stands for 'Guiding Light Optimising Wide local excisions'. It describes the fluorescence imaging empowering surgeons to provide accurate breast-conserving surgery to their patients.

1 in 7 women will be diagnosed with breast cancer during their lifetime. Most of these women will have early-stage breast cancer, and as such their treatment will be breast-conserving surgery. In breast-conserving surgery only the tumour and a small amount of normal breast tissue (margin) surrounding the tumour is removed, allowing women to keep as much of the remaining normal breast tissue as possible. However, approximately 1 in 5 women undergoing breast-conserving surgery will have a positive margin (i.e. cancer cells are detected) meaning some cancer cells may have been left behind, which increases the risk of the cancer coming back. To reduce this risk, they will need a second surgery to remove further tissue.

Our research team has been exploring the use of fluorescent guidance during breast-conserving surgery. By using fluorescent dyes that target cancer cells, we can essentially 'light up the tumour' in the infrared (not visible) spectrum. This helps surgeons to identify and remove all cancerous tissue in real-time during the first operation. This technique has the potential to significantly reduce the need for second surgeries and improve outcomes for women undergoing breast-conserving surgery.

Who are we?



Maria Leiloglou and Martha Kedrzycki

Maria Leiloglou is currently a Research Associate in the Hamlyn Centre for Robotic Surgery committed to clinical translation of smart devices to positively transform the future of healthcare. During her PhD (2018-2022) she developed and translated three smart cameras that could be used in real-time to assist surgeons in identifying and removing cancer during breast-conserving surgery.

Martha Kedrzycki is an Academic Surgical Registrar at Imperial College Healthcare NHS Trust. Her PhD focused on using fluorescent guidance during breast conserving surgery in women through pioneering a clinical trial.

Maria and Martha worked together in an effort to improve outcomes for those 1 in 7 women who may one day be diagnosed with breast cancer.

Our patient and public involvement journey

Below is our patient and public involvement journey, highlighting the key lessons we learned from each activity.

Meetings with the Imperial Cancer Research UK Public Involvement Group for Cancer
During our PhD we worked alongside a patient group who met regularly at Maggie's West London centre (a cancer support charity). The group was a team of cancer survivors, dedicated to influencing local cancer-related research. We wanted to hear their perspective on the need for improved breast-conserving surgery and to get their feedback on our research design and methodology. We wanted to ensure that the risks would be minimised and that the benefits of the research would outweigh any potential harm.


A patient group at Maggie's West London.

The group helped us understand what level of risk patients would find acceptable in order to participate in our study. They strongly recommended to approach and explain the risks to the prospective patients well in advance to give them time to think and discuss with their family. They also helped us to tailor the wording of our trial documents so that it could be understandable for everyone. Through our interactions, we gained a valuable understanding of their perspective which allowed us to effectively communicate our research and make improvements to our methodology. We reviewed and updated the inclusion/exclusion criteria to minimise the risk of an agent-induced allergic reaction.

Research as Art

During the Imperial PhD Summer Showcase, an annual event open to the public which celebrates research being carried out by Imperial's PhD students, we opted for an interactive exhibit. We asked members of the public to operate on 'breast' cupcakes to remove a tumour (an area coloured green) found in the middle of the cupcake. They were then free to devour the cupcakes after!


A visitor participating in the exhibit.

There was an overwhelming positive reaction from the public for our research and our presentation was awarded with the people's choice prize and the first prize from the judge's panel. It was a fun and interactive way for the public to engage and understand our technology through an all-senses/ hands-on experience. We again practiced and developed science communication skills with the public.

Podcast
As part of the Institute of Global Health and Innovation podcast series, we were invited to discuss our research on their podcast platform. As well as fostering new partnerships with other Imperial College London teams, this podcast served as a means of effectively introducing our study when inviting members of the public to our public involvement activities.

Presentation at the Imperial Science Café
We promised the women who participated in our trial that we would share how they contributed to the advancement in the treatment of breast cancer. In addition to our participants, we invited their friends, families, and multiple charities to our presentation 'Imperial Science Café: Lighting the way to better breast cancer surgery?'. Due to the pandemic, we were forced to move this event online, which helped us stay connected during those difficult times.

Everyone who attended was receptive and engaged in our presentation and asked us many thought-provoking questions throughout. Additionally, the women who took part in our research were proud to have contributed to the advancement of breast cancer surgery. We

were inspired by their joy at having participated, as we would not have been able to do our research without them. We worked together to offer hope for future women who would be diagnosed with breast cancer.

Imperial at the Science Museum Lates

In May 2022 we were honoured to participate in Science Museums Lates – an after-hours opportunity for adults interested in science to engage with leading researchers on a given theme. Over 1,500 visitors attended the cancer-themes Lates entitled "Cancer Revolution: Science, Innovation and Hope". Visitors were encouraged to pop by our booth for an informal 1-2-1 chat about our work and they could also see some of our surgical systems. Their overwhelming support during our interactions was essential in motivating us to continue our research endeavours. Visitors shared their personal stories about breast cancer, treatment, and the impact of re-operation on their experiences. We came to understand the potential value of our research in improving the lives of breast cancer survivors.



Maria with a visitor at Science Museums Lates, May 2022.

Interview with Fiona

Fiona is one of the many women who needed a second operation due to some cancer cells being left behind after her first operation.


Image from Fiona's interview.

Fiona shared her experience on the impact of having a failed breast conserving surgery. Her story was inspiring for us as women and as researchers, as she expressed her hopes of improving outcomes for future patients so that nobody would have to go through what she did. On a personal level, we admire her for her generosity and dedication to the cause.

Multiple women who participated in the trial asked for us to use this technology on them during their surgery and were disappointed when we explained that project was still research and not yet available. Despite this having no impact on what their own outcomes would be, they still wanted to participate so that future women would be able to benefit from this research.

Promoting public involvement in Health Research

During our PhD, we participated in the collective effort of Imperial College London and Cancer Research UK in promoting public involvement in health research. As part of the campaign, a video was created to showcase the testimonials of patients and researchers, detailing their personal experiences and how their perspectives were transformed through their public involvement journey. We couldn't be prouder to have had the opportunity to impact the research community by encouraging them to engage with patients and the public in their work.

What advice would you give other researchers?

- Focus on early engagement to ensure that your research is relevant and appropriate.
- Invest in relationships to seek feedback during the research from groups you have formed trust and a collaborative environment with.
- Acknowledge patients' and the public's contributions and remind them how important and unique their input is. This will help maintain motivation and engagement. Acknowledgment can be expressed verbally or through rewards and official publication acknowledgments.

So, what's next?
Having completed the second half of our trial, we invited all trial participants, public involvement representatives, their family and charities (Breast Cancer Now, Open Age, and Cancer Research UK), and members of the public to join us on Thursday 11 May 2023 at Imperial College London for an update on the progress of our research. The women who have supported us have been instrumental in shaping and guiding our research. They have also motivated and inspired us to keep going. We have learned that that public involvement is an essential part of delivering excellence in research. We have shared our talk online for the participants that could not attend on the day.

By Naomi Asantewa-Sechereh

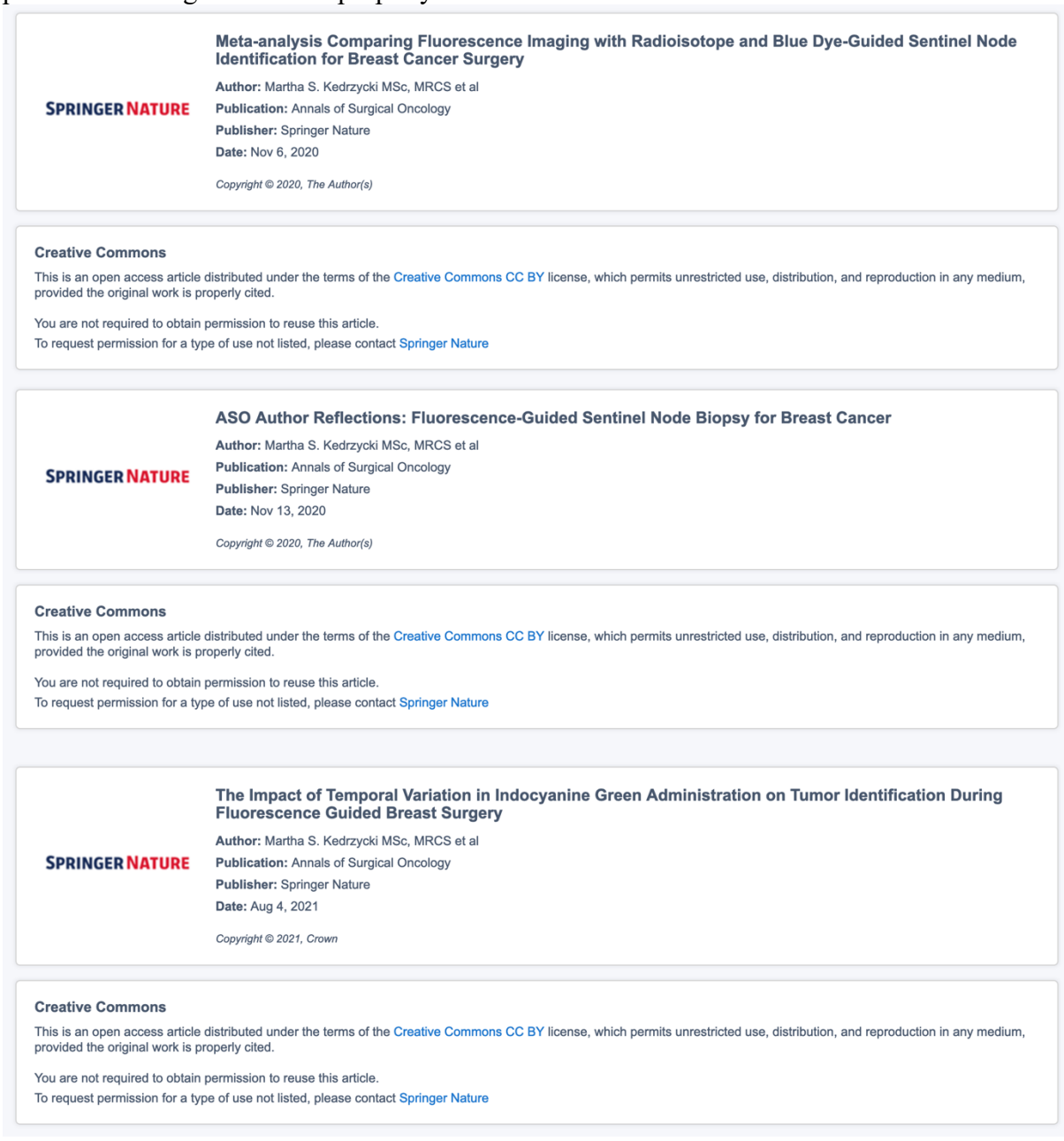
Categorised under Reflections

Tagged Public Engagement, Patient & Public Involvement, Advisory Group, Feedback, Cancer, Workshops

Appendix 3: Permissions for Reproduction of Articles

Springer

All articles are licensed under the Creative Commons Attribution 4.0 International License, which permits unrestricted use, distribution, modification, and reproduction in any medium, provided the original work is properly cited.



Meta-analysis Comparing Fluorescence Imaging with Radioisotope and Blue Dye-Guided Sentinel Node Identification for Breast Cancer Surgery

Author: Martha S. Kedrzycki MSc, MRCS et al
Publication: Annals of Surgical Oncology
Publisher: Springer Nature
Date: Nov 6, 2020

Copyright © 2020, The Author(s)

Creative Commons

This is an open access article distributed under the terms of the Creative Commons CC BY license, which permits unrestricted use, distribution, and reproduction in any medium, provided the original work is properly cited.

You are not required to obtain permission to reuse this article.
To request permission for a type of use not listed, please contact Springer Nature

ASO Author Reflections: Fluorescence-Guided Sentinel Node Biopsy for Breast Cancer

Author: Martha S. Kedrzycki MSc, MRCS et al
Publication: Annals of Surgical Oncology
Publisher: Springer Nature
Date: Nov 13, 2020

Copyright © 2020, The Author(s)

Creative Commons

This is an open access article distributed under the terms of the Creative Commons CC BY license, which permits unrestricted use, distribution, and reproduction in any medium, provided the original work is properly cited.

You are not required to obtain permission to reuse this article.
To request permission for a type of use not listed, please contact Springer Nature

The Impact of Temporal Variation in Indocyanine Green Administration on Tumor Identification During Fluorescence Guided Breast Surgery

Author: Martha S. Kedrzycki MSc, MRCS et al
Publication: Annals of Surgical Oncology
Publisher: Springer Nature
Date: Aug 4, 2021

Copyright © 2021, Crown

Creative Commons

This is an open access article distributed under the terms of the Creative Commons CC BY license, which permits unrestricted use, distribution, and reproduction in any medium, provided the original work is properly cited.

You are not required to obtain permission to reuse this article.
To request permission for a type of use not listed, please contact Springer Nature

SPRINGER NATURE

ASO Author Reflections: Towards Fluorescence Guided Tumor Identification for Precision Breast Conserving Surgery

Author: Maria Leiloglou MSc et al
Publication: Annals of Surgical Oncology
Publisher: Springer Nature
Date: Aug 18, 2021

Copyright © 2021, The Author(s)

Creative Commons

This is an open access article distributed under the terms of the Creative Commons CC BY license, which permits unrestricted use, distribution, and reproduction in any medium, provided the original work is properly cited.

You are not required to obtain permission to reuse this article.
To request permission for a type of use not listed, please contact Springer Nature

SPRINGER NATURE

Indocyanine green fluorescence image processing techniques for breast cancer macroscopic demarcation

Author: Maria Leiloglou et al
Publication: Scientific Reports
Publisher: Springer Nature
Date: May 21, 2022

Copyright © 2022, The Author(s)

Creative Commons

This is an open access article distributed under the terms of the Creative Commons CC BY license, which permits unrestricted use, distribution, and reproduction in any medium, provided the original work is properly cited.

You are not required to obtain permission to reuse this article.
To request permission for a type of use not listed, please contact Springer Nature

ASBRS Conference Posters/Presentations

ASBrS Official Proceedings Citation

LR

Laura Randel <lrandel@breastsurgeons.org>

To: Laura Randel <lrandel@breastsurgeons.org>

Tue 06/06/2023 16:09

This email from lrandel@breastsurgeons.org originates from outside Imperial. Do not click on links and attachments unless you recognise the sender. If you trust the sender, add them to your safe senders list to disable email stamping for this address.

To: 2023 Oral, Quickshot, and Poster Presenters

The citation for the ASBrS Official Proceedings containing your abstract is below. Thanks again for submitting your research to ASBrS. The next call for abstracts deadline will be 11/8. The submission site will open in August.

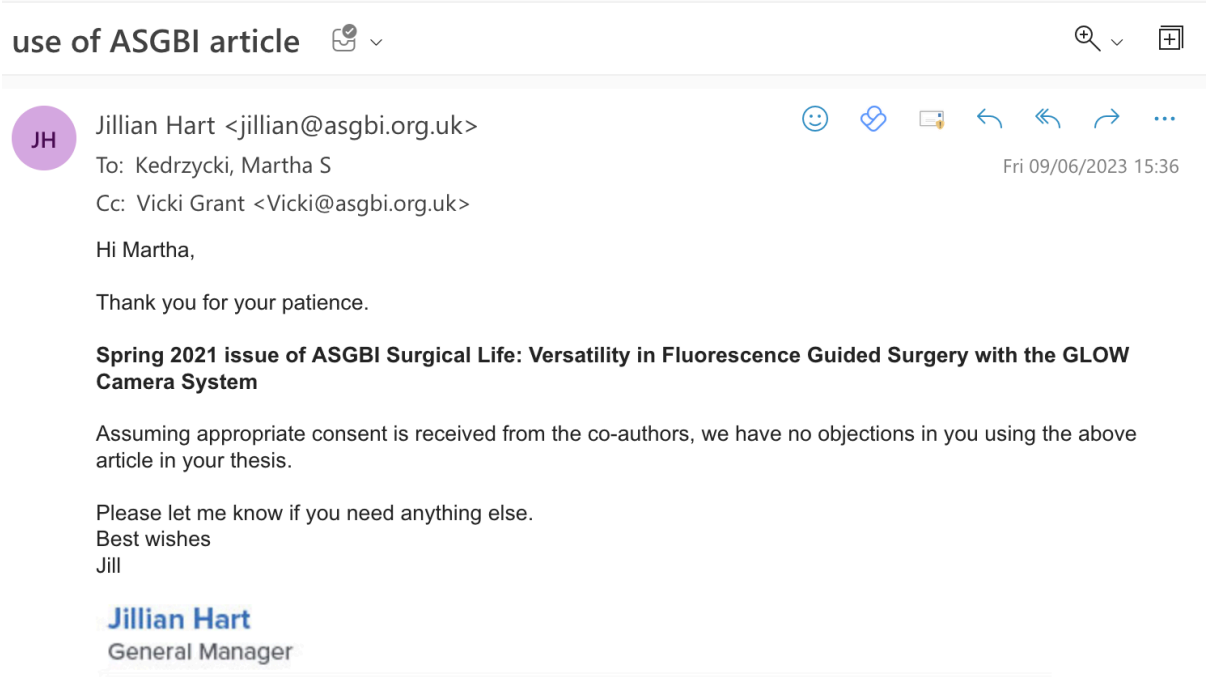
Citation: The American Society of Breast Surgeons Official Proceedings, Volume XXIV 2023 Annual Meeting Scientific Session Abstracts. Ann Surg Oncol 30 (Suppl 2), 259–664 (2023). https://doi.org/10.1245/s10434-023-13650-w

Shareable Link: https://rdcu.be/ddSY9

Regards,

Laura Randel
Associate Executive Director
The American Society of Breast Surgeons

Association of Surgeons of Great Britain and Ireland (Surgical Life)



use of ASGBI article

JH

Jillian Hart <jillian@asgbi.org.uk>

To: Kedrzycki, Martha S

Fri 09/06/2023 15:36

Cc: Vicki Grant <Vicki@asgbi.org.uk>

Hi Martha,

Thank you for your patience.

Spring 2021 issue of ASGBI Surgical Life: Versatility in Fluorescence Guided Surgery with the GLOW Camera System

Assuming appropriate consent is received from the co-authors, we have no objections in you using the above article in your thesis.

Please let me know if you need anything else.
Best wishes
Jill

Jillian Hart
General Manager

Oxford University Press (publisher of BMJ)

If you are an OUP Author: Following publication, except for medical society guidelines, OUP authors may reuse their own articles in full or part in other works without direct permission from OUP, providing that the article is not reused under any form of Open Access, full credit is given to the original publication and the reuse is not commercially sponsored. A full outline of re-use as well as our archiving policies can be found on the Oxford Permissions page: https://academic.oup.com/pages/standard-publication-reuse-rights. Please note that each individual journal may have additional reuse rights/restrictions and so please do consult the OUP Journal's webpage to ensure you have a full overview. Should your re-use go outside of what is outlined and you require a formal letter of permission, this can be obtained through our RightsLink service available by clicking on the "Permissions" option located under the article title on our website.

Maria Leiloglou's Thesis

The copyright of this thesis rests with the author. Unless otherwise indicated, its contents are licensed under a Creative Commons Attribution Non-Commercial 4.0 International Licence (CC BY-NC). Under this licence, you may copy and redistribute the material in any medium or format. You may also create and distribute modified versions of the work. This is on the condition that: you credit the author and do not use it, or any derivative works, for a commercial purpose. When reusing or sharing this work, ensure you make the licence terms clear to others by naming the licence and linking to the licence text. Where a work has been adapted, you should indicate that the work has been changed and describe those changes. Please seek permission from the copyright holder for uses of this work that are not included in this licence or permitted under UK Copyright Law.

IntechOpen

We are an Open Access publisher that applies Creative Commons (CC) licenses to our works, meaning that you may freely use and adapt our materials as long as you cite the source

chapter of the original material. You can use our materials even for commercial purposes without specific permission from our side. The only obligation is to properly reference the work (according to the terms of the CC licenses).

Journal of Physics D

use of article image for thesis

This email from permissions@ioppublishing.org originates from outside Imperial. Do not click on links and attachments unless you recognise the sender. If you trust the sender, add them to your safe senders list to disable email stamping for this address.

Dear Martha Kedrzycki,

Thank you for your request to reproduce content from Journal of Physics D: Applied Physics.

The content you have requested was published under a CC BY licence which permits reuse for any purposes, even commercial, provided the licence terms are adhered to.

Therefore you may reuse the content without permission, so long as you reference it adequately and adhere to the terms of the CC BY licence.

Please note this does not apply to any content/figure which is credited to another source in our publication or has been obtained from a third party, which is not available under a suitable open access licence. Express permission for such content/figures must be obtained from the copyright owner.

Kind regards,

Sophie
Copyright & Permissions Team
Sophie Brittain - Rights & Permissions Assistant
Cameron Wood - Legal & Rights Adviser
Contact Details
E-mail: permissions@ioppublishing.org

Frontiers (for figure 32)

Copyright © 2022 Gu, Yue, Zhong, Mei and Wang. This is an open-access article distributed under the terms of the Creative Commons Attribution License (CC BY). The use, distribution or reproduction in other forums is permitted, provided the original author(s) and the copyright owner(s) are credited and that the original publication in this journal is cited, in accordance with accepted academic practice. No use, distribution or reproduction is permitted which does not comply with these terms.

Elsevier



Identification of excimer delayed fluorescence by Protoporphyrin IX: A novel access to local chromophore concentration?

Author: Gauthier Croizat,Aurélien Gregor,Jaroslava Joniova,Emmanuel Gerelli,Georges Wagnières
Publication: Journal of Photochemistry and Photobiology B: Biology
Publisher: Elsevier
Date: April 2022

© 2022 The Authors. Published by Elsevier B.V.

Frontiers in Oncology

Fluorescence-Guided Surgery

Copyright: © 2017 Nagaya, Nakamura, Choyke and Kobayashi. This is an open-access article distributed under the terms of the Creative Commons Attribution License (CC BY). The use, distribution or reproduction in other forums is permitted, provided the original

author(s) or licensor are credited and that the original publication in this journal is cited, in accordance with accepted academic practice. No use, distribution or reproduction is permitted which does not comply with these terms.